Stony Brook University

Theoretical Characterization of Water/Surfaces Interactions

A Dissertation Presented by

Adrien Poissier

to
The Graduate School

in Partial Fulfillment of the
Requirements
For the Degree of

Doctor of Philosophy
in
Physics

Stony Brook University
December 2011

Stony Brook University
The Graduate School

Adrien Poissier

We, the dissertation committee for the above candidate for the
Doctor of Philosophy degree, hereby recommend
acceptance of this dissertation.

Maria Victoria Fernandez-Serra - Dissertation Advisor
Assistant Professor of Physics

Matthew Dawber - Chairperson of Defense
Assistant Professor of Physics

Philip B. Allen - Committee Member
Professor of Physics

Alan Calder - Committee Member
Assistant Professor of Physics

Dario Stacchiola - Outside Member
Assistant Chemist - Brookhaven National Laboratory

This dissertation is accepted by the Graduate School
Lawrence Martin
Dean of the Graduate School

Abstract of the Dissertation

Theoretical Characterization of Water/Surfaces Interactions

BY

Adrien Poissier

Doctor of Philosophy

IN

Physics

Stony Brook University

2011

Much effort is being devoted to the understanding of water-substrate interactions at metallic or semiconducting surfaces with catalytic properties. Confined water represents a great interest for physicists and chemists interested in state-of-the-art technologies such as, fuel cells where the rates of proton have to be controlled, nano-sensors, heterogeneous catalysis, or nano-fluids. Creation of hydrogen gas from water dissociation, also remains an important challenge in order to complete the cycle of CO2 free green energies production. Photocatalytic processes, with semiconducting substrates such as GaN 10$\underline{1}$0 seem to represent strong candidates towards this achievement.

This work focuses on the investigation of water-substrate interactions. It is mainly directed from first-principle calculations with molecular dynamics simulations. The nature of the hydrogen bond is broadly discussed and comparisons between water-water and water-substrate are proposed. Interesting features of spontaneous metal polarization are also put in evidence

and electrochemical mechanisms are explained.

To Jenny

«Il faut être très patient [...]

Tu t'assoiras d'abord un peu loin de moi, comme ça, dans l'herbe. Je te regarderai du coin de l'oeil et tu ne diras rien. Le langage est source de malentendus. Mais, chaque jour, tu pourras t'asseoir un peu plus près...»

Le Petit Prince

Antoine de Saint-Exupéry

Contents

List of Figures

Acknowledgments

The very first acknowledgment has to go to Pr. Nicolás Lorente who has been the very first one to teach me how exciting physics is. He is one of the brightest scientists I ever got the chance to meet, and I could never be thankful enough for the tremendous amount of time and energy he devoted for me in my early student years.

I would like to sincerely acknowledge my dissertation committee who accepted to evaluate this work. I would like especially to deeply thank Pr. Alan Calder and Pr. Philip B. Allen for the revisions and comments they made about the manuscript.

I am really grateful to all my windowless-office colleagues: Li, Jue and Betül. They made those dark days sunnier. A special thanks has to go to Sriram with whom I shared March Meeting hotel rooms for two years, and who tried to explain to me cricket's rules (but still... a five-day game? seriously??)

I would like to thank my friends in Stony Brook, Mike, Sarah and Savannah for the awesome boat trips and Knoll Top parties. A very special and sincere thanks goes to my two best housemates ever: Tess and Alex (aka Shed and Pinocchio). We shared our lives in Knoll Top and those moments will certainly remain the best memories I have during my Stony Brook years.

I am sincerely grateful to Alain, Brigitte, Marie and Joelle who made the graduation such an emotional moment. I appreciated their discretion and the way have been with me during the whole week.

I want to profoundly thank two great physicists and friends. Matt “the chef”, best cook ever (he could perfectly be french!) and Marivi, without whom I wouldn’t be writing this now. I had the immense pleasure to have been supervised by such a talented scientist and generous person. I would like to thank both of you for making me feel like I was a part of the family. I also have to thank my brothers Tag and Skylar for the fruitful discussions we had together.
I want to thank Julie for having been so supportive during the graduation day and for having made me part of what I am today.
I would like to thank my parents for all they did for me. They have always been there since the very beginning. They gave me the taste of discovery and knowledge, and taught me values that I entirely rely on. I am so proud of being their son.

Finally, I would like to thank Jenny for being such a prodigious person. I admire the ability she has to understand things, to understand me, to understand everything about everything. Because you always have been with me during this entire journey, this work is dedicated to you.

Chapter 1

The intriguing element

Introduction

Several excellent books, textbooks or articles [2, 10, 23] already dealt with the exhilarating story of the most famous liquid on Earth. My goal in this chapter is not to make an exhaustive review on water. Rather, I would like to point out some of the most intriguing properties that make water being an extraordinary liquid. But what does make water so special? Is that because it is proved to be an essential condition for earth-like living? Is it because water covers more than 70% of the surface of the planet? Or maybe because we are able to observe in everyday life the three water states; solid, liquid and gas? Perhaps also because of its many anomalies that make it such an atypical and exotic liquid? Certainly a bit of all of those reasons together, are making H_2O one of the sexiest molecule of the globe.

1.1 The beginning

In the beginning there was water[1]. Water on Earth is believed to be as old as the blue planet.

Some 4.5 billion years ago, the Earth started its formation, that resulted from many planetesimals and asteroids collisions. It started slowly to aggregate and become denser, under the action of the gravitational force. Collisions delivered all of the Earth elements. Within 50 million years, heavy elements, such as iron, sank into the core, while lighter elements such as silicon, aluminum, potassium, magnesium or oxygen, formed a rocky crust at the surface.

Figure 1.1: Okavango Delta, Botswana. Photo: N. Poissier.

Among the rocky part, were the volatile compounds, delivered by collisions with comets, meteorites and protoplanets, in the beginning of the Earth formation. Those volatile compounds were mostly hydrogen, nitrogen, carbon oxides and water. As the molten rock cooled down and solidified, vapors were released in a process called *outgassing*. While very

[1] H_2O a biography of water, Philip Ball, Orion Books, 1999.

different from today, atmosphere was being created. Slowly, lighter elements in the atmosphere, such as hydrogen were lost, but water, heavy enough, remained in the Earth atmosphere under the gravitational force. One day, between 4.4 and 4.0 billion years ago, temperature on Earth had cooled enough to allow water to condense and eventually rain down to start forming the oceans.

1.2 From *hudor* to H_2O

From the very first time our ancestors started to try understanding the world around them, water played a central role and was a steady pillar of most theories. One of the major quest, was the reduction of all surrounding matter to a finite number of elements. Around the seventh century BC, Thales imagined that all matter could derive from Water only. The three observable forms of water: solid, liquid and gas, probably reinforced Thales' convictions. Also, it seemed possible to form solid rock from water (water leaves a residue of salt after evaporation that looks like rock grains). Once evaporated, water looked very much like air. Those observations made Thales believe that water was the only necessary substance and therefore, the only real Earth element. Later, around the fifth century BC, other ideas emerged, and Empedocles formulated the first four-element matter description. All the matter was formed from either of the four : Fire, Air, Earth or Water. At about the same time, Chinese sages established a concept with five elements, being Earth, Metal, Wood, Fire and Water. The number "five" was a central element of the Taoist philosophy. It was also related to the five primary colors (Yellow, Blue, Red, White and Black), to the five directions (South,North,West,East and Central), or the five fingers of the hand. All theoretical framework built by Greeks and Chinese

remained the foundation of primitive science for twenty centuries.

In the sixteenth and seventeenth centuries other systems of elements appeared. A three-element system was established by dropping the Fire element. Two-element system was also proposed where all matter could be described in terms of "heat" and "cold" only. Johann Baptist van Helmont, a Belgian chemist, even formulated a one-element system, with Water being the unique element. He performed a five years experiment where he grew a young willow tree in soil by administrating water only. He, first, weighted the tree and the dry soil, then he covered the soil with a metallic plate to avoid any dust to deposit onto it. After five years, he dried the soil and weighted both the tree and the soil. The soil was about the same weight while the tree's weight increased. Since the only substance the tree received was water, he concluded that water had transformed into wood and based his theory on the fact that Water was the only necessary substance and then, the only real element.

Scientists started to perform more experiments as laboratory equipment was becoming more and more precise. In 1667, Johann Joachim Becher established the "phlogiston theory" to explain metal combustion. He noticed that metals transformed when heated in air, and could be transformed back when heated with charcoal. He believed that metals contained phlogiston, a substance that was liberated when heated. Once heated, the metal was "dephlogisticated" and appeared under its real aspect. Air was saturated in phlogiston and could not carry any more substance, combustion was then impossible. Pure air was seen as dephlogisticated air, since it could make the combustion with the metal. Animals and plants were also releasing phlogiston by breathing dephlogisticated air. He explained the fact that combustion requires air by the need for phlogiston to travel in a media. In fact phlogiston can be seen as the exact opposite of oxygen. Indeed a heated metal does not lose phlogiston but gains oxygen as it oxidizes.

Animals and plants inhale oxygen instead of releasing phlogiston. In 1774, the British Joseph Priestley, performed experiments on mice and deduced that dephlogisticated air (in fact pure oxygen) was like common air but with better properties in breathing and burning. By being the exact anti-oxygen, phlogiston was able to explain many chemical properties and its theory put a serious brake on the discovery of the oxygen element.

In the 1770's, Antoine Lavoisier abandoned the phlogiston theory that he replaced by the concept of "pure air". In fact it made no sense for him, that metals were losing phlogiston since they were gaining weight after combustion. Pursuing his experiments on acids, he called pure air : "oxygen" (acid producer) as he believed that all acids required oxygen. Lavoisier had to go through many polemics and fights against other scientists to make oxygen being accepted instead of phlogiston.

By the time oxygen was claimed as an elementary substance, hydrogen had already been found. Henry Cavendish, in 1766, was performing experiments on acid with metals. He regarded the gas that was released from the reaction as "pure phlogiston" or inflammable air (in fact hydrogen gas). Lavoisier, finally realized that the reunion of oxygen gas with inflammable air was giving water in a ratio of two volumes to one. He coined inflammable air : "hydrogen" (water producer) as an other element. He defended the recombination of elements, already proclaimed by Anaxagore of Klazomenae (fourth century BC), and was able to dissociate hydrogen from water by plunging a metal into the liquid. The metal would rust by being oxidized and hydrogen would be released. He stated the law of mass conservation as the maxim : "Rien ne se perd, rien ne se crée, tout se transforme[2]." For the first time, water was not seen as an elementary substance any more, but as a molecule formed by one oxygen and two hydrogens.

[2]Nothing gets destroyed, nothing gets created, everything gets recombined.

$$\frac{1}{2}O_2 + H_2 \longrightarrow H_2O \tag{1.1}$$

1.3 Physical and chemical properties of water

1.3.1 States of Water

The three water states can be observed almost everyday. At atmospheric pressure, water freezes at $32°F$ and vaporizes at 212°F. Further away from these usual conditions, water can be much more exotic.

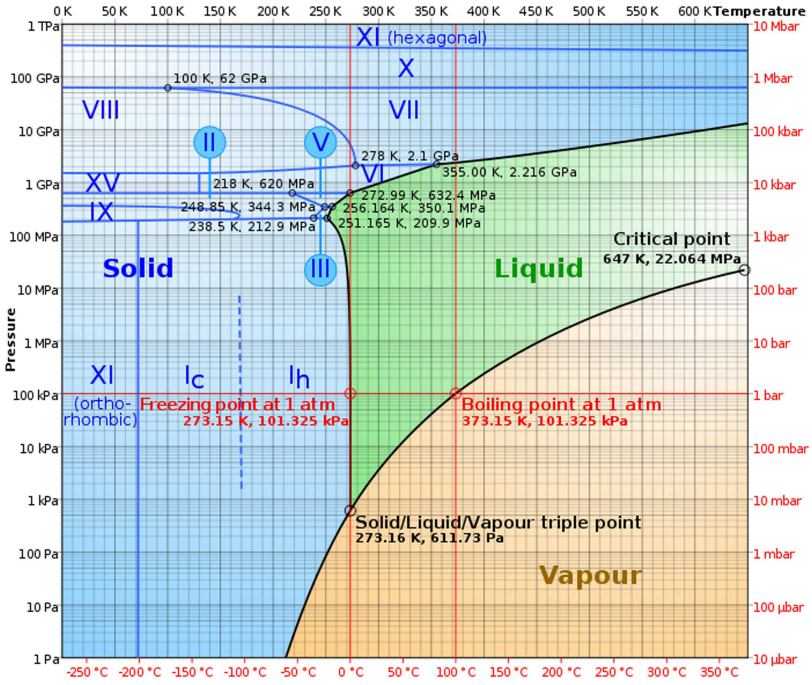

Picture from http://en.wikipedia.org/wiki/Phase_diagram
Author : Cmglee

Figure 1.2: Temperature/Pressure phase diagram of water. Blue region represents solid phase of water, green region liquid phase and orange region is the gaseous phase of water.

Phase diagram of water is shown in Figure: 1.2. The three water phases: solid, liquid, and gaseous, are respectively represented by the colors blue,

green and orange.

First, let's have a look at the red line located at atmospheric pressure (1 atm). There is a phase transition from solid to liquid at 273.15 K (32 °F) and another one from liquid to gas at 373.15 K (212 °F). Below 273.15 K, the solid phase we can observe is the so called I_h crystal ice. This structure, sometimes called ordinary ice, is practically the only structure present in the entire biosphere. It is characterized by a hexagonal symmetry and tetrahedral hydrogen-bonding. We see however, on the red line of Fig 1.2, that at atmospheric pressure and below 173 K, another crystal replaces hexagonal ice. Indeed, at very low temperatures (-148 °F), I_c crystal is present with its cubic symmetry. Cubic ice is a metastable structure that can be observed in small droplets of few μ-meters [80]. It has been reported [81] that, despite the generally accepted picture in which ice cloud in the atsmosphere was hexagonal I_h ice (formed from the homogeneous nucleation of ice in water droplets), cubic ice may form in the Earth's atmosphere. It could even be dominant when droplets freeze at a temperature below 190 K (temperature of clouds in tropopause region).

If we keep on decreasing the temperature at the same atmospheric pressure, we will reach another crystalline state of water, the orthorhombic ice XI (below 73 K or -328 °F). There are actually 13 different crystalline phases of water known today [20], and two glassy forms, sometimes called amorphous ice [74], this phenomenon is called polymorphism. Glassy states of water can be reached by freezing liquid water with a high cooling rate ($\sim 10^6$K/s). While almost non existent on Earth, glassy water may be the most common form of water in the universe [47]. The various crystalline forms originate from the high directionality of the intermolecular water-water bonds, called the hydrogen bonds (H-bonds).

Another interesting feature of the phase diagram on Figure 1.2 is the so

Figure 1.3: Ice sculpture, Lapland Finland. Photo: N. Poissier

called triple point at (273.16K,611.73Pa). At this particular point, water coexists in its three states: Solid, Liquid and Gas. Below this point, there is no liquid phase any more: solid water would go to its gas phase without passing through a liquid state upon heating (sublimation).

1.3.2 Supercooled water

The change of state, from liquid to crystal ice, needs the formation of a nucleus; a small crystal seed to which ice water can grow to. This process is called nucleation. Without nucleation, water remains liquid below its melting point temperature. It is said to be supercooled [20, 74]. Supercooled water is a metastable state, that stays observable until very low temperatures (235K or -36°F). Nucleation can be generated from a small perturbation [61], that triggers the transformation of the metastable liquid into ice.

In 1976, R.J. Speedy and C.A Angell [105] performed a series of experiments on isothermal compressibility of supercooled water. They wanted to continue mapping the water's response function dependency upon temperature. They could measure water's response function to temperatures down to 247K (-15°) and saw that as liquid water was cooled down, the compressibility increased dramatically. By extrapolating their data, they predicted a thermodynamic singularity at 228K (-49°). At this point, the compressibility would be infinite and water would collapse on itself. Since, experimentalists are trying hard to make liquid water survive such a temperature, but homogeneous nucleation (formation of ice without any seed or perturbation) always occurs. This hypothetical supercooled region is called the *No man's land* [77].

1.4 Anomalies and Exotic water properties

As a gas, water is very light, with a molecular weight of 18.016 only (Air is 29). Liquid water becomes unusually dense and solid water is then much lighter than expected. Water has got many unusual properties known as "anomalies", that make it to be an abnormal liquid as compared to most others [17, 24, 54].

1.4.1 Polarity, the hydrogen-bonding condition

A water molecule is formed by two strong OH covalent bonds ($\sim$ 5 eV). Each of these bonds share electrons. However, the oxygen atom is much more electronegative that hydrogens. This creates an asymmetry in the electronic charge distribution as the oxygen tends to retain more negative charge, that is redistributed towards its lone pairs (see Figure 1.4). For this reason, the molecule is said to be polar. Because of the water geometry, in particular with its $\sim$104.5° $\widehat{HOH}$ angle, water has a dipole moment (about

1.8D for gas monomer).

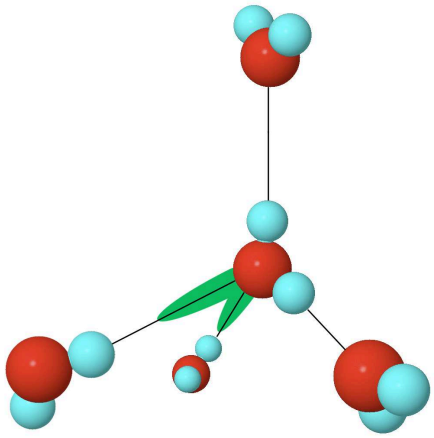

Figure 1.4: Water molecule H-bonded (straight black lines) in tetrahedral configuration with four water molecules. The center molecule accepts two H-bonds through its lone pairs (represented in green) and donates two H-bonds through its hydrogens.

Charge differences in atoms make water molecules attracted to each other. This attraction contributes to the intermolecular hydrogen-bond (H-bond) that occurs from the hydrogen of one molecule to the oxygen of another molecule. In average, bulk water has four H-bonds, formed in tetrahedral geometry (see Figure 1.4). While relatively weak ($E_{H-bond} \sim 0.25eV$) compared to the intramolecular covalent OH bond, the H-bond is responsible for the majority of water properties.

Water small size and polarity make it a very good solvent in particular to ionic or salt compounds. Indeed, compounds are surrounded and isolated by small water molecules that can present either a positive (H) or negative (O) charge to them.

1.4.2 High melting/boiling critical temperatures

Critical points of both melting and boiling temperatures are thankfully unusually high in water as compared to other compounds. This is the essential condition for having water in a liquid state on Earth.
Crystal water is arranged in tetrahedral configurations hold by strong H-bonds. The high organization in the crystalline structure makes the configurational entropy of ice being very low. At melting point, for a spontaneous phase transition, the variation in free energy ΔG has to be zero:

$$\Delta G = \Delta H - T\Delta S = 0 \tag{1.2}$$

With $\Delta H = \Delta U - P\Delta V$ the variation in Enthalpy, T is the temperature and ΔS is the change in Entropy. In order to melt, many H-bonds have to be broken. This is managed by the increase of Temperature. The very low configurational entropy together with the strength of H-bonds make the melting point relatively high, with $T_{melting}$=273K (32°F).

The boiling point is also high, with $T_{melting}$=373K (212°F). Again, the low configurational entropy , involved by the strong H-bond network in the liquid is at the origin of this unusual thermodynamical property.

1.4.3 Water density, the 4°C essential point.

Ice cubes float in a glass of water. At first sight, nothing peculiar here. However, for almost every element, a decreasing of temperature, increases the density. Indeed by decreasing the temperature, the kinetic energy caused by molecular thermal agitation also decreases and therefore atoms or molecules get closer to each other. Now it is peculiar.
Galileo believed, according to Archimedes' law of buoyancy that ice should have a lower density than liquid water. An experiment was performed [10, 73] by a group of Italian scientists in 1657, in which they filled and

Figure 1.5: Le trou du Souffleur (Blowing hole), Reunion Island. Photo: N. Poissier

closed tightly a jar with water and let it freeze. The jar exploded upon water expansion during the solidification, demonstrating Galileo's intuition. In a similar experiment, with water in a bulb with a long thin neck, they realized that during cooling, water was sinking towards the bulb. This was the first observation of the water maximum density.

Following this idea, in 1795, Lefevre-Gineau measured the weight of a copper cylinder plunged in water, as a function of water temperature [57]. He used thermal expansion corrections for the metal and measured

Figure 1.6: Outside pool next to sauna, Lapland Finland. Photo: N. Poissier

a maximum water density at around 4.0°C (39.2°F) [3]. The first accurate value of maximum water density was obtained. This property of water is considered to be an essential condition for life. Indeed, in natural water environments such as oceans, rivers or lakes, when water gets too cold and could potentially freeze, colder water goes to the surface and eventually freezes, making a natural protection for wildlife underneath, and prevents further freezing.

1.4.4 Viscosity and Pressure

Liquid water viscosity is quite high. Again, the well-ordered H-bond network maintains molecules together, making their mobility difficult. Under pressure however, where viscosity of most liquids lowers, because of a larger confinement, water's viscosity increases. Pressure is indeed deforming the network, which makes H-bonding weaker. This weakening in H-bonds is

[3] Actual maximum water density, at P=1bar is $\rho_{Max} = 3.978$°C [113].

increasing the molecules' mobility.

1.4.5 Specific Heat

The specific heat is the amount of heat required by a substance to change its temperature. Specific heat of liquid water is quite high as compared to its ice or vapor phases specific heats.

	$C_p(J/(g.K))$
Solid	2.1
Liquid	4.2
Gas	2.1

Table 1.1: Specific heat of the three water states.

High liquid specific heat can be explained by the fact that most of the energy used to heat up the liquid is used to distort intermolecular H-bonds [62]. The high value of the liquid water's specific heat is also the reason of the apparent coldness of water as compared to air ($C_p = 1.0(J/(g.K))$ at the same temperature.

1.4.6 Surface Tension and Capillarity

Cohesive intermolecular forces in water are responsible for another fascinating property. Surface tension of water is a force that tend to maintain the liquid together. It is the reason for the spherical shapes of water drops, in which the interface water/air is minimized. From a molecular point of view, surface tension can be understood by the fact that molecules at the interface (for instance air/water), are only partly bound to other water molecules, while bulk molecules are isotropically bound to other bulk molecules. This tends to favor interfacial water molecules cohesion with liquid rather than with the other media.

Figure 1.7: Victoria Falls, Photo: N. Poissier

Capillary effect (capillarity) is a combination of surface tension and adhesion between water and its container. It can make water to overcome gravitational force. For instance, a tall oak tree can release as much as 400 L of water per day from its leaves (called transpiration). The water goes from the roots to its leaves through the capillary effect.

Conclusion

All those properties together and many others make water a very special life molecule. H-bonding in water appears to be crucial for many effects. Its strength allows water to be essentially on its liquid state on Earth, but also to climb several feet against the gravitational force, or to protect wildlife during harsh winters. Water was, since the very early ages, one of the most studied molecule, however its secrets are not easily given away. Many classical models [6, 7, 48, 49, 67] have been built to reproduce and predict water properties. Quantum mechanics [32, 40, 86] is also broadly used to perform detailed electronic and structure calculations. Unfortunately so

far, none of them is able to fully characterize the complex molecule, and hard work is devoted every day, to achieve this exhilarating quest.

Chapter 2

Theoretical Background

Introduction

Over the past century, with the development of Quantum Mechanics, scientists have been able to dive more and more into a fine description of systems composed by many electrons and nuclei such as solids, liquids, or amorphous clusters of atoms. The mathematical heaviness of Quantum Mechanics considerably slowed down theoretical advancements. Solid state physics needed a major impulse to unlock the situation. This has been consecutively by the development of many-body theories (such as Hartree-Fock or theories based on the density functional) and by the boom of computers. Nowadays, calculations with thousands of atoms can be performed, and sharp descriptions of structural and electronic properties of systems can either confirm or predict experiments. Computational physics starts being a field of Physics on its own and can be considered as a "theoretical experiment", making a bridge between experiment and theory. This chapter is devoted to the approach and concepts of many-body solid state physics and especially to Density Functional Theory (DFT).

2.1 Many-body systems

Any many-particle problem starts with the many-body Hamiltonian :

$$\hat{\mathcal{H}} = -\sum_I \frac{\hbar^2}{2M_I}\nabla_I^2 - \frac{\hbar^2}{2m_e}\sum_i \nabla_i^2 + \frac{1}{2}\sum_{I\neq J}\frac{Z_I Z_J e^2}{\mathbf{R}_I - \mathbf{R}_J} + \frac{1}{2}\sum_{i\neq j}\frac{e^2}{|\mathbf{r}_i - \mathbf{r}_j|} - \sum_{i,I}\frac{Z_I e^2}{|\mathbf{r}_i - \mathbf{R}_I|} \tag{2.1}$$

Where i is used for electrons and I stands for nuclei. The first two terms are the kinetic energy of nuclei and electrons respectively. The third and fourth terms represent the nuclei-nuclei and electron-electron Coulomb interaction. Finally the fifth term is the electron-nuclei Coulomb interaction.

2.1.1 The Born-Oppenheimer approximation

The general, time-independent, Schrödinger equation can be written as :

$$\hat{\mathcal{H}}(\mathbf{r},\mathbf{R})|\Psi(\mathbf{r},\mathbf{R})\rangle = E(\mathbf{r},\mathbf{R})|\Psi(\mathbf{r},\mathbf{R})\rangle \tag{2.2}$$

In this equation the two variables $\mathbf{r}$ (for electronic coordinates) and $\mathbf{R}$ (for nuclei coordinates/ are coupled. Any variation on any electronic coordinate $\mathbf{r}$ will have an impact on every nuclei and electrons of the system. Born-Oppenheimer approximation [68] is based on the fact that the mass of nuclei is about two thousands times heavier than the mass of electrons. The latter has then the hypothetical ability to cover the entire phase space before any nucleus displacement. The wavefunction $|\Psi(\mathbf{r},\mathbf{R})\rangle$ can be decoupled as $|\Psi(\mathbf{r};\mathbf{R})\rangle = |\chi(\mathbf{R})\rangle|\Phi(\mathbf{r})\rangle$, where $\mathbf{R}$ is now a parameter of the wavefunction. Hence, the general Hamiltonian can be written as :

$$\begin{aligned}\hat{\mathcal{H}} &= \hat{T_{\mathbf{R}}} + \hat{T}_{\mathbf{r}} + \hat{U}(\mathbf{r};\mathbf{R}) \\ &= \hat{T_{\mathbf{R}}} + \hat{\mathcal{H}}_{\text{elec}}(\mathbf{r};\mathbf{R})\end{aligned} \tag{2.3}$$

With $\hat{T_{\mathbf{R}}}$, the nuclei kinetic energy and $\hat{\mathcal{H}}_{\text{elec}}(\mathbf{r};\mathbf{R})$ the electronic Hamiltonian.

Due to the decoupling between nuclei and electrons in the wavefunction $|\chi(\mathbf{R})\rangle|\Phi(\mathbf{r})\rangle$, the electronic Hamiltonian can be solved separately as :

$$\hat{\mathcal{H}}_{\text{elec}}(\mathbf{r};\mathbf{R})|\Phi(\mathbf{r})\rangle = E(\mathbf{R})|\Phi(\mathbf{r})\rangle \tag{2.4}$$

The Born-Oppenheimer approximation is often confusedly seen as the classical treatment of nuclei, in a quantum electronic description. This is misleading. Indeed, the electronic energy $E(\mathbf{R})$ can then be reinserted into equation 2.2 and quantum nuclei effects can be solved :

$$(\hat{T_{\mathbf{R}}} + E(\mathbf{R}))|\chi(\mathbf{R})\rangle = E|\chi(\mathbf{R})\rangle \tag{2.5}$$

The following sections of this chapter will be focusing on solutions of the electronic Schrödinger equation 2.4.

The general form of the Hamiltonian in the equation 2.4 within the Born-Oppenheimer approximation can always be expressed as :

$$\hat{\mathcal{H}}_{\text{elec}} = \hat{T}_r + \hat{V}_{\text{ext}} + \hat{V}_{\text{int}} + E_{\text{II}} \tag{2.6}$$

With,

$$\hat{V}_{\text{ext}} = -\sum_{i,I} \frac{Z_I e^2}{|\mathbf{r}_i - \mathbf{R}_I|} \tag{2.7}$$

$$\hat{V}_{\text{int}} = \frac{1}{2}\sum_{i \neq j} \frac{e^2}{|\mathbf{r}_i - \mathbf{r}_j|} \tag{2.8}$$

and,

$$E_{\mathrm{II}} = \frac{1}{2}\sum_{I\neq J}\frac{Z_I Z_J e^2}{\mathbf{R}_I - \mathbf{R}_J} \tag{2.9}$$

Within the Born-Oppenheimer approximation, the last term : E_{II} can be seen as an extra contribution in the total energy, but it does not contribute to the description of electrons.

2.2 Non interacting particles

The starting point of most methods of calculations that aim to solve the electronic time-independent Schrödinger equation, is based on the independent-electron approximation [40,68]. In this approximation, each electron can be seen being under an effective potential $V_{\mathrm{eff}}(\mathbf{r})$, and the Schrödinger equation of N electrons is replaced by N one-electron Schrödinger equations :

$$\hat{\mathcal{H}}_{\mathrm{eff}}\Psi_i(\mathbf{r}) = [-\frac{\hbar^2}{2m_e}\nabla^2 + V_{\mathrm{eff}}(\mathbf{r})]\Psi_i(\mathbf{r}) = \epsilon_i\Psi_i(\mathbf{r}) \tag{2.10}$$

This approximation assumes that electrons are uncorrelated, except for the Pauli exclusion principle, which is satisfied automatically with the orthogonalization of the wavefunction [68]. The electronic density can be defined as :

$$n(\mathbf{r}) = \sum_i |\Psi_i(\mathbf{r})|^2 \tag{2.11}$$

and the total energy as :

$$E = \langle\hat{\mathcal{H}}_{\mathrm{eff}}\rangle = \sum_i \epsilon_i \tag{2.12}$$

Different methods can be used to solve the general system governed by equation 2.10. While electronic correlation has been explicitly left behind, it will be shown later in this chapter that the density functional theory formalism can get round this problem by reintroducing a corrective term.

2.3 Hartree-Fock approximation

In 1930, Vladimir Fock developed a method to calculate the ground state energy of a many-particle system composed by N electrons. He first builds an antisymmetrized determinant wavefunction from the one-electron wavefunctions :

$$\Psi = |\phi_1(\mathbf{r_1}), \phi_{\mathbf{1}}(\mathbf{r_2}), ..., \phi_{\mathbf{2}}(\mathbf{r_1}), \phi_{\mathbf{2}}(\mathbf{r_2}), ..., \phi_{\mathbf{N}}(\mathbf{r_N})\rangle \tag{2.13}$$

The expectation value of the Hamiltonian 2.6 is :

$$\begin{aligned}\langle\Psi|\mathcal{H}_{\text{elec}}|\Psi\rangle = &\sum_i \int d\mathbf{r}\phi_i^*(\mathbf{r})[-\frac{1}{2}\nabla^2 + \hat{V}_{\text{ext}}(\mathbf{r})]\phi_i(\mathbf{r}) + E_{\text{II}} \\ &+ \frac{1}{2}\sum_{i,j}\int d\mathbf{r}d\mathbf{r'}\phi_i^*(\mathbf{r})\phi_j^*(\mathbf{r'})\hat{V}_{\text{int}}\phi_i(\mathbf{r})\phi_j(\mathbf{r'}) \\ &- \frac{1}{2}\sum_{i,j}\int d\mathbf{r}d\mathbf{r'}\phi_i^*(\mathbf{r})\phi_j^*(\mathbf{r'})\hat{V}_{\text{int}}\phi_j(\mathbf{r})\phi_i(\mathbf{r'})\end{aligned} \tag{2.14}$$

The first term represents the single electron expectation value, the second and third terms represent the direct and exchange interactions among electrons, those are responsible for the Pauli exclusion.

Hartree-Fock approach is to minimize the total energy with respect to all degrees of freedom with the constraint of orthonormality $\langle\Psi|\Psi\rangle = 1$. The total energy is defined as :

$$E = \frac{\langle\Psi|\mathcal{H}_{\text{elec}}|\Psi\rangle}{\langle\Psi|\Psi\rangle} \tag{2.15}$$

The stationary eigenstates of the Hamiltonian can be found by varying the ratio of equation 2.15. The method of Lagrange multipliers with the constraint $\langle\Psi|\Psi\rangle = 1$ can be used,

$$\delta[\langle\Psi|\mathcal{H}_{\text{elec}}|\Psi\rangle - E(\langle\Psi|\Psi\rangle - 1)] = 0 \tag{2.16}$$

Variations of $\phi_i^*(\mathbf{r})$ leads to the Hartree-Fock equations :

$$[-\frac{1}{2}\nabla^2+\hat{V}_{\text{ext}}(\mathbf{r})+\sum_j \int d\mathbf{r'}\phi_j^*(\mathbf{r'})\hat{V}_{\text{int}}]\phi_i(\mathbf{r})-\sum_j \int d\mathbf{r'}\phi_j^*\phi_i(\mathbf{r'})\hat{V}_{\text{int}}\phi_j(\mathbf{r}) = \epsilon_i\phi_i(\mathbf{r}) \tag{2.17}$$

The exchange term is summed over all orbitals and constitute the only many-body interaction. Nevertheless, all other correlation terms that constitute the many-particle effects have been forgotten here.

2.4 Exchange and correlation

Since the interactions always involve pairs of particles, discussions about the two body correlation are sufficient here. Without correlations, the joint probability $n(r, \sigma, r', \sigma')$ to find an electron in r with spin σ and an electron in r' with spin σ' can be defined as the product of single probabilities,

$$n(r, \sigma, r', \sigma') = n(r, \sigma).n(r', \sigma') \tag{2.18}$$

The correlation between electrons can thus be seen as :

$$\Delta n(r, \sigma, r', \sigma') = n(r, \sigma, r', \sigma') - n(r, \sigma).n(r', \sigma') \tag{2.19}$$

2.4.1 The exchange hole

Hartree-Fock approximation consists of neglecting all correlations except the Pauli exclusion principle. The exchange term in Hartree-Fock represents two effects :

a. The Pauli exclusion.

b. The self-term that must be subtracted to cancel the spurious self-term in the direct Coulomb energy.

The aim of exchange term is always to lower the energy of the system. That may be interpreted as the interaction of each electron with a positive

"exchange hole" surrounding it [68]. The exchange hole of an electron only involves electrons of same spin. The probability to find two electrons of same spin at the same point $r = r'$ must vanish. The exchange can be calculated analytically in Hartree-Fock and constitutes the best approximation of the many-body effects that can be achieved with wavefunction built with a single determinant. The improvement made in the wavefunction in order to include electronic correlation introduces new degrees of freedom. This has for effect to lower the energy for any state [63]. This energy lowering is called "correlation energy". The correlation energy is often defined as the energy difference between the exact many-body energy and the energy calculated with the Hartree-Fock method.

2.4.2 The correlation hole

We can define the correlation $n_c(r, \sigma, r', \sigma')$ as following :

$$\Delta n(r, \sigma, r', \sigma') = n_{xc}(r, \sigma, r', \sigma') = n_x(r, \sigma, r', \sigma') + n_c(r, \sigma, r', \sigma') \quad (2.20)$$

In general correlation is most important for electrons of opposite spin since electrons of same spin are automatically kept apart by the exclusion principle. One of the effects of correlation is the "screening", where particles collectively correlate to reduce the net interaction among any two particles. For repulsive interactions, the hole around each particle will produce a net weaker interaction strength. Screening is particularly important in metals, where the quasi-free electrons have the freedom to rearrange with a low energy cost.

2.5 Density Functional Theory

In 1927, Thomas and Fermi proposed a theory for quantum systems based on density functional [27, 107]. This approach, while not accurate enough to calculate precise electronic structures, represents the foundation of how density functional theory works. In their model, the total energy of a system depends on the electronic density only. They approximate the kinetic energy with an explicit functional of a non interacting homogeneous gas of electrons density.

$$\begin{aligned} E_{TF}[n] =& C_1 \int d^3r n(\mathbf{r})^{5/3} + \int d^3r V_{ext}(\mathbf{r}) n(\mathbf{r}) \\ &+ C_2 \int d^3r n(\mathbf{r})^{4/3} + \frac{1}{2} \int d^3r d^3r' \frac{n(\mathbf{r}) n(\mathbf{r'})}{|\mathbf{r} - \mathbf{r'}|} \end{aligned} \tag{2.21}$$

The equation 2.21 represents the Thomas-Fermi energy functional for electrons in an external potential $V_{\text{ext}}(\mathbf{r})$. The first term stands for the kinetic energy of electrons, the third one is the local exchange for the case of spins equally up and down, the last one is the classical electrostatic Hartree energy. This rough approximation is neglecting correlation between electrons, but is introducing a new concept : instead of dealing with rapidly varying wavefunctions with their many degrees of freedom, one may use the smoother, well defined (only 3 degrees of freedom), electronic density. Following this idea, Pierre Hohenberg and Walter Kohn formulate in 1964, in the famous "Inhomogeneous Electron Gas" article published in the Physical Review journal [43]. In this paper, they enunciate two theorems aiming to formulate density functional theory as an exact theory of many-body systems.

2.5.1 The Hohenberg-Kohn theorems

The most general many-body hamiltonian can be written as :

$$\hat{\mathcal{H}} = \hat{T} + \hat{V}_{\text{ext}} + \hat{U} \tag{2.22}$$

Where $\hat{T}$ stands for the electronic kinetic energy, $\hat{V}_{\text{ext}}$ is the total electron-nuclei interaction and $\hat{U}$ is the electron-electron interaction. This last term includes all electron-electron correlation effects.

The first theorem stipulates that *for any system of interacting particles in an external potential $V_{ext}(\boldsymbol{r})$, the potential $V_{ext}(\boldsymbol{r})$ is determined uniquely, except for a constant, by the ground state particle density $n_0(\boldsymbol{r})$* [68]. Since the hamiltonian is thus fully determined, then the many-body wavefunctions of all states are also determined. Therefore all properties of the system are completely determined given only the ground state density $n_0(\mathbf{r})$.

The second theorem proves that *a universal functional for the energy $E[n]$ in terms of the density $n(\boldsymbol{r})$ can be defined, valid for any external potential $V_{ext}(\boldsymbol{r})$. For any particular $V_{ext}(\boldsymbol{r})$, the exact ground state energy of the system is the global minimum value of this functional, and the density $n[\boldsymbol{r}]$ that minimizes the functional is the exact ground state density* [58,68].

$$E[n] = \int d^3\mathbf{r} V_{\text{ext}}(\mathbf{r}) n(\mathbf{r}) + F[n] \tag{2.23}$$

The corollary of the second theorem says that *the functional $E[n]$ (and hence $F[n]$) alone is sufficient to determine the exact ground state energy and density.*

The two Hohenberg-Kohn theorems made a giant step towards the characterization of realistic electronic structure calculations. The numerous degrees of freedom of many-particle wavefunctions were replaced by an actual smoother physical quantity with three degrees of freedom only, the electron density. Hohenberg and Kohn, however, gave no clue on how to define such

a functional, neither on how to solve the many-body problem in the presence of $V_{\text{ext}}(\mathbf{r})$.

In late 1965, Walter Kohn and Lu Jeu Sham were finishing the work by reformulating the original complex many-body problem by an independent-particle problem [52].

2.5.2 The Kohn-Sham approach

The ansatz

The Kohn-Sham approach replaces the complex many-body hamiltonian by an auxiliary independent-particle hamiltonian. This remains to solve a number of simpler independent equations that give the exact many-body solution up to the exactitude of the auxiliary hamiltonian.

Because there is no unique way of defining such an auxiliary independent-particle hamiltonian, Kohn and Sham defined an ansatz that claims that :
a. The exact ground state density can be represented by the ground state density of an auxiliary system of non interacting particles.
b. The auxiliary hamiltonian is chosen to have the usual kinetic operator and an effective local potential $V_{\text{eff}}(\mathbf{r})$.

They will include all many-body interactions inside a single term : the *"exchange and correlation potential"*.

The derivation of Kohn-Sham variational equations

Let us consider an auxiliary independent-particle system defined by the hamiltonian :

$$\hat{\mathcal{H}}_{\text{aux}} = -\frac{1}{2}\nabla^2 + \hat{V}(\mathbf{r}) \tag{2.24}$$

The system is composed by N independent electrons. The ground state

has one electron in each of the N orbitals $\Psi_i(\mathbf{r})$ with the lowest eigenvalues ϵ_i. (the spin is not considered here, as it does not modify the derivation). The density is given by :

$$n(\mathbf{r}) = \sum_i |\Psi_i(\mathbf{r})|^2 \tag{2.25}$$

The independent-particle kinetic energy T_s is given by :

$$T_s = -\frac{1}{2}\sum_i \langle \Psi_i | \nabla^2 | \Psi_i \rangle = \frac{1}{2}\sum_i \int d^3\mathbf{r} |\nabla \Psi_i(\mathbf{r})|^2 \tag{2.26}$$

And the classical Coulomb interaction between electrons (named as Hartree) can be calculated as the electron density interacting with itself :

$$E_{\text{Hartree}}[n] = \frac{1}{2}\int d^3\mathbf{r} d^3\mathbf{r'} \frac{n(\mathbf{r})n(\mathbf{r'})}{|\mathbf{r} - \mathbf{r'}|} \tag{2.27}$$

We can write the expression of the ground state energy by decomposing the independent terms and one extra term that contains all the many-particle effects $E_{XC}[n]$:

$$E_{\text{KS}}[n] = T_s[n] + \int d^3\mathbf{r} V_{\text{ext}}(\mathbf{r}) n(\mathbf{r}) + E_{\text{Hartree}}[n] + E_{\text{II}} + E_{\text{XC}}[n] \tag{2.28}$$

This expression has to be equal to the Hohenberg-Kohn 2.23 equation. Therefore a formal expression of $E_{\text{XC}}[n]$ can be deduced as :

$$E_{\text{XC}}[n] = \langle \hat{T} \rangle - T_s[n] + \langle \hat{V}_{\text{int}} \rangle - E_{\text{Hartree}}[n] \tag{2.29}$$

The ground state energy and density are finally calculated by minimizing the equation 2.28 with respect to the density. Since T_s is explicitly written as a functional of the independent wavefunctions Ψ_i and all other quantities are expressed as functionals of the density, one may minimize the equation 2.28 with respect to Ψ_i^* using the chain rule :

$$\frac{\delta E_{\mathrm{KS}}}{\delta \Psi_i^*} = \frac{\delta T_s}{\delta \Psi_i^*} + [\frac{\delta E_{\mathrm{ext}}}{\delta n(\mathbf{r})} + \frac{\delta E_{\mathrm{Hartree}}}{\delta n(\mathbf{r})} + \frac{E_{\mathrm{XC}}}{\delta n(\mathbf{r})}]\frac{\delta n(\mathbf{r})}{\delta \Psi_i^*} = 0 \tag{2.30}$$

We obtain the Schrodinger-like following expression :

$$(H_{KS} - \epsilon_i)\Psi_i(\mathbf{r}) = 0 \tag{2.31}$$

Where ϵ_i are the eigenvalues of the effective hamiltonian H_{KS}.

$$H_{\mathrm{KS}} = -\frac{1}{2}\nabla^2 + V_{\mathrm{KS}}(\mathbf{r}) \tag{2.32}$$

With,

$$V_{\mathrm{KS}}(\mathbf{r}) = V_{\mathrm{ext}}(\mathbf{r}) + \frac{\delta E_{\mathrm{Hartree}}}{\delta n(\mathbf{r})} + \frac{\delta E_{\mathrm{XC}}}{\delta n(\mathbf{r})} \tag{2.33}$$

By separating the independent-particle kinetic energy and the long range Hartree term form the exchange and correlation energy, one can approximate the latter by a local functional of the density :

$$E_{\mathrm{XC}}[n] = \int d^3\mathbf{r} n(\mathbf{r}) \epsilon_{\mathrm{XC}}([n], \mathbf{r}) \tag{2.34}$$

With $\epsilon_{\mathrm{XC}}([n], \mathbf{r})$ the exchange and correlation energy per electron at point $\mathbf{r}$.

2.5.3 The Exchange and correlation functionals

Thanks to the Kohn-Sham approach, the many-body problem has been replaced by manageable independent-particle equations. The complex behavior of many-particle systems has been isolated in a unique exchange and correlation term. The ability of density functional theory to describe physical systems depends almost entirely on a proper evaluation of the energy of exchange and correlation $E_{\mathrm{XC}}[n]$.

Local Density Approximation - LDA

The very first approximation Kohn and Sham proposed [52] was to consider that the exchange and correlation energy was locally the same as the one in a homogeneous electron gas $\epsilon_{\mathrm{XC}}(n(\mathbf{r}))$ with the same density.

$$E_{\mathrm{XC}}[n] = \int d^3\mathbf{r} n(\mathbf{r}) \epsilon_{\mathrm{XC}}(n(\mathbf{r})) \tag{2.35}$$

One needs to calculate, once and for all, the exchange and correlation energy of a homogeneous electron gas. The exchange energy of the homogeneous electron gas can be analytically calculated with the Hartree-Fock method. The correlation energy can be calculated with great accuracy with Monte Carlo methods [15, 68].

Generalized Gradient Approximations - GGA

As long as the electron density of the system is relatively homogeneous, or varies smoothly, which is the case on most of transition metals, the LDA approximation gives fairly accurate results and many physical properties such as the lattice parameter, the stress constant or the bulk modulus reproduce with great accuracy experimental data. However, most of systems require a better description of the exchange and correlation potential as the electron density varies much more rapidly. It becomes necessary to incorporate the first spatial derivative of the density as a variable in order to recover the hilly density landscape [25, 52]. This is the aim of the generalized gradient approximations (GGA), that can be defined as follow :

$$E_{\mathrm{XC}}[n] = \int d^3\mathbf{r} n(\mathbf{r}) \epsilon_{\mathrm{XC}}(n, |\nabla n|) \tag{2.36}$$

With $\epsilon_{\mathrm{XC}}(n, |\nabla n|)$ the energy of exchange and correlation per electron for a density n and a gradient of the density $|\nabla n|$. Equation 2.36 can be

rewritten as :

$$E_{\mathrm{XC}}[n] = \int d^3\mathbf{r} n(\mathbf{r}) \epsilon_X(n) F_{XC}(n, |\nabla n|) \tag{2.37}$$

With $\epsilon_X(n)$ the exchange energy of the homogeneous gas and $F_{\mathrm{XC}}(n, |\nabla n|)$ a dimensionless term called *exchange and enhancement factor*. Several forms of exchange and enhancement factors have been proposed [4, 38, 89, 90, 119, 120], they have been developed to reproduce accurately complex systems such as semiconductors, oxides [119], liquid water [38, 120] or ice [89,90]. each of them tends to reproduce the asymptotic behavior of the electron density, none of them is universal and the choice to treat a system with one another is very problem-related.

2.5.4 Solving the Kohn-Sham equations

In practice, solving Kohn-Sham equations has to be done recursively. Because the effective Kohn-Sham potential is a functional of the electronic density, the Schrodinger-like equation has to be solved respecting the consistency between input and output electronic density. This is done numerically by performing a self-consistent check over the density ρ :

$$|\rho_{\mathrm{output}} - \rho_{\mathrm{input}}| \leq a_0 \tag{2.38}$$

The absolute difference between the output density ρ_{output} obtained from the minimization and the input density ρ_{input} used to calculate the effective potential $V_{\mathrm{eff}}(\mathbf{r})$ has to be smaller that a small given criteria a_0. The procedure is summarized in Fig 2.1 [1]

The overall numerical procedure goes as follow :

1. First an electronic density is guessed and will be used to calculate the effective potential $V_{\mathrm{eff}}(\mathbf{r})$. This density can be constructed from the atomic

[1] Original schema from R. Martin, Electronic Structure, *Cambridge*, p. 173 [68].

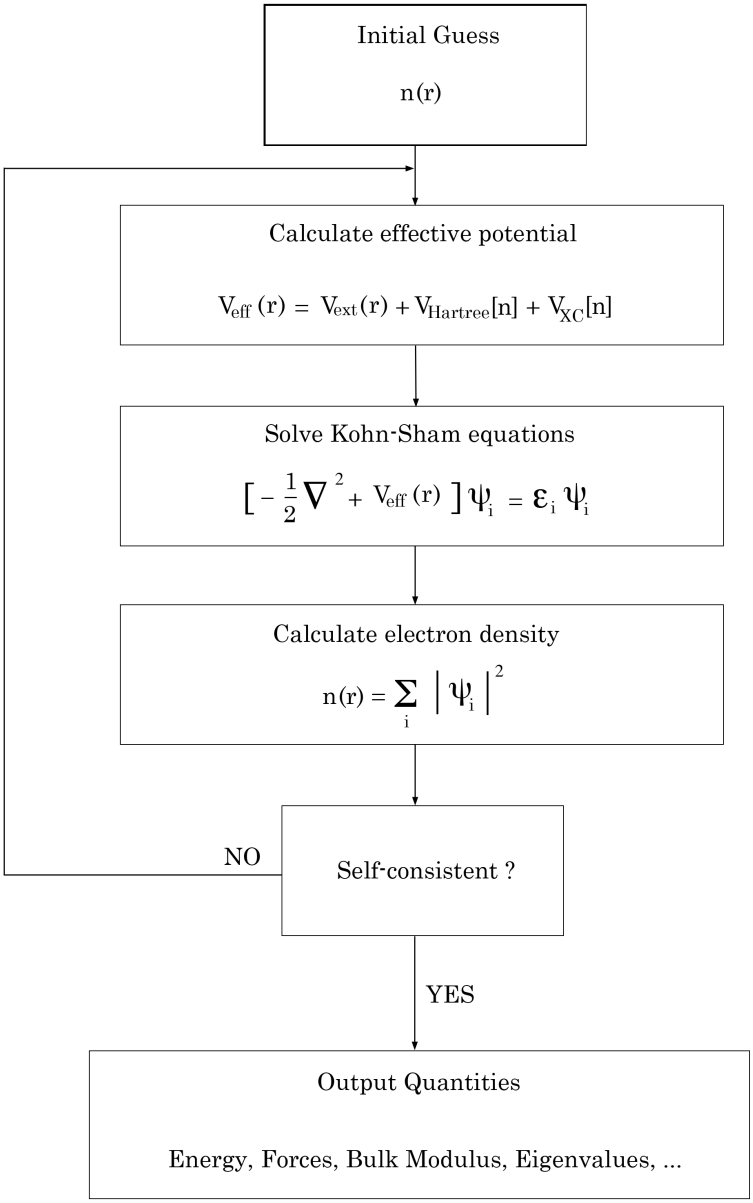

Figure 2.1: schema from R. Martin, Electronic Structure, *Cambridge*, p. 173 [68].

density of the system so it will not be too far away from a realistic guess.
2. The effective potential $V_{\text{eff}}(\mathbf{r})$ is calculated.
3. The Schrodinger-like equations can be solved by applying the variational principle of equation 2.30.
4. The electronic density is deduced from the Kohn-Sham wavefunctions that have been calculated in previous step.
5. The self-consistent check 2.38 is performed. It can either be satisfied and all physical quantities are calculated, or unsatisfied and the output density has to be reinjected on step 2 where the process can start over.

The way the output density is reinjected to become the input density of the next iteration usually follows an algorithm that makes sure that the variation is not too steep by transforming the new density with a linear mixing. A method often used is the Pulay algorithm [92] :

$$\rho_{\text{input}}^{n+1} = \alpha\rho_{\text{output}}^{n} + (1-\alpha)\rho_{\text{input}}^{n} \tag{2.39}$$

Where the guess for the $n+1$ iteration is constructed from the input and output densities of iteration n. α represents the mixing weight and its value is between 0 and 1.

2.5.5 Reciprocal space periodicity - The Bloch theorem

The apparent complexity of solid state systems comes from the intend of analyzing infinite or semi-infinite systems. Because of the infinite number of electrons in a solid and the gigantic number of electrons participating in most physical and chemical properties, the task appears unrealizable. The Bloch theorem [1, 51, 68] may certainly be the keystone that makes it possible.

The crystal structure of an infinite solid is periodic in the three spatial directions. It follows that the properties of crystal are invariant under a translational movement $\vec{R}$.

$$\vec{R} = n_1\vec{a_1} + n_2\vec{a_2} + n_3\vec{a_3} \tag{2.40}$$

Where n_1, n_2, n_3 are integers and $\vec{a_1}, \vec{a_2}, \vec{a_3}$, are a set of vectors forming a periodic basis. The equation 2.40 can be Fourier transformed in the so called reciprocal space.

$$\mathbf{G} = l_1\mathbf{b_1} + \mathbf{l_2}\mathbf{b_2} + \mathbf{l_3}\mathbf{b_3} \tag{2.41}$$

With $\mathbf{b_i}$, the reciprocal primitive cell vectors, defined by circular permutation :

$$\mathbf{b_i} = \mathbf{2}\pi\frac{\mathbf{a_j} \times \mathbf{a_k}}{|\mathbf{a_i}.(\mathbf{a_j} \times \mathbf{a_k})|} \tag{2.42}$$

Since the crystal is periodic, its potential at any point $\vec{r}$, $U(\vec{r})$, has to follow the same periodicity :

$$U(\vec{r} + \vec{R}) = U(\vec{r}) \tag{2.43}$$

The general time-independent Schrodinger's equation of electrons in a potential $U(\vec{r})$ can be written as :

$$\hat{\mathcal{H}}\Psi = (-\frac{\hbar^2}{2m}\nabla^2 + U(\vec{r}))\Psi = \epsilon\Psi \tag{2.44}$$

The periodicity of the potential $U(\vec{r})$ generates the Bloch theorem where the eigenstates Ψ of the hamiltonian can be chosen to have the form of a plane wave times a function with the periodicity of Bravais Lattice $\vec{R}$.

$$\Psi_{n,\vec{k}}(\vec{r}) = e^{i\vec{k}\vec{r}}u_{n,\vec{k}}(\vec{r}) \tag{2.45}$$

With,

$$u_{n,\vec{k}}(\vec{r}+\vec{R}) = u_{n,\vec{k}}(\vec{r}) \tag{2.46}$$

Where n is the band number and $\vec{k}$ represents the wave vector in reciprocal space. The Bloch theorem is often formulated with the alternative equivalent expression :

$$\Psi(\vec{r}+\vec{R}) = e^{i\vec{k}\vec{R}}\Psi(\vec{r}) \tag{2.47}$$

Equation 2.47 tells that any wave function in a solid can be fold back to a wave function of the unit cell times a phase factor. Therefore, all the information is contained within the unit cell. The reciprocal cell of this unit cell is called the Brillouin zone and contains all the physics.

2.5.6 Plane Waves vs Localized Orbitals

Two approaches can be used to numerically reproduce the infinite Hilbert space involved in solid state physics calculations. The space, evidently, has to be truncated to a finite basis set, which involves a loss of information. The first approach is to use orthogonal single electron plane waves $\Psi_i(\mathbf{r})$:

$$\Psi_i(\mathbf{r}) = \sum_{|\mathbf{G}|<G_{cutoff}} C_i(\mathbf{G})e^{i\mathbf{G}.\mathbf{r}} \tag{2.48}$$

With $\mathbf{G} = n_1\mathbf{b}_1 + n_2\mathbf{b}_2 + n_3\mathbf{b}_3$ Where the number of plane waves used to build the wave function of electron i is calculated by the relation $|\mathbf{G}| < G_{\text{cutoff}}$. G_{cutoff} being the wave vector cutoff above which one the space is not any more described. It corresponds to an energy E_{cutoff} with the relation :

$$\frac{1}{2}G^2_{\text{cutoff}} = E_{\text{cutoff}} \tag{2.49}$$

Another approach can be used to determine a physical basis set. One can use a set of atomic orbitals :

$$\Psi_i(\mathbf{r}) = \sum_j \alpha_j \Phi_j(\mathbf{r}) \tag{2.50}$$

Where j is a number that defines how many orbitals are used per electron. The cruder approximation is the so called single$-\zeta$ basis, where only one orbital is used per electron.
For example in the case of oxygen, with 6 valence electrons, the single$-\zeta$ basis set per atom would be composed by 2 s orbitals and 4 p orbitals. In general the basis has to be finer and basis such double$-\zeta$ polarized or triple$-\zeta$ basis are used (where 2 or 3 orbitals with different radii are attached per electron).

The two approaches have their own advantages and restrictions. Plane wave calculations use an orthogonal basis set, which is not localized in space, however it requires a large and computationally more expensive number of basis. Localized orbitals calculations readily uses chemical insights since it is based on atomic orbitals, the number of basis is much less than plane waves one and therefore the computational cost can be dramatically reduced even for a bigger number of atoms and a larger unit cell. However, an important drawback is that two different calculations with different atoms are harder to be compared since they do not involve the same basis set. This is called the Basis Set Superposition Error BSSE [118]. The BSSE can be reduced by using extra orbitals (sometimes called *Ghost Atoms*) at specific space positions .

2.6 Atomic relaxation and Molecular dynamics

Born-Oppenheimer approximation allowed the decoupling between electrons and nuclei. The nuclei have been left apart in the last sections. Indeed, it remained to solve the electronic Hamiltonian for a frozen snapshot. It is time to reintroduce them in the pot to complete the circle.

2.6.1 Conjugate Gradient Atomic Relaxation, Hellmann-Feynman Therorem

After solving the electronic hamiltonian one has the choice to treat nuclei quantum mechanically (Eq 2.5) or classically. This section and the following will be only based on a classical treatment of the nuclei as the quantum nuclei effects are several orders of magnitude below the electronic ones for the physics that is treated here.

The Hellmann-Feynman Theorem

At the correct ground state electronic density, the total electronic energy is at a minimum with respect to the electronic density. Therefore changes in the electronic density due to the moving of a nucleus do not contribute to first-order derivatives [31, 41, 68]:

$$\frac{\delta E[n]}{\delta n} = 0 \tag{2.51}$$

Therefore, since the only terms that depend explicitly on the position of nuclei are the interaction E_{II} and the external potential, one has that the force on nucleus I is :

$$F_I = -\frac{\delta E}{\delta \mathbf{R_I}} = -\int d\mathbf{r} n(\mathbf{r}) \frac{\delta V_{\text{ext}}(\mathbf{r})}{\delta \mathbf{R_I}} - \frac{\delta E_{\text{II}}}{\delta \mathbf{R_I}} \tag{2.52}$$

Forces on atoms are minimized using this variational principle, and the optimal atomic structure can be found. The total structure is said to be *relaxed* once the total force is less that a small criteria. Evidently, changing the nuclei coordinates will have for effect to modify the electronic density. Therefore after relaxing the atomic structure, one has to recalculate the ground state electronic density for the new geometry. The system is totally converged when both the atomic forces and the electronic energy are minimized.

2.6.2 Molecular Dynamics

Molecular dynamics can also perfectly be performed within the Born-Oppenheimer approximation. The entire density functional theory process for finding electronic ground state energy remains unchanged and again nuclei forces can be deduced from the Hellmann-Feynman theorem. A dynamics can be performed in which the electrons are treated with quantum mechanics and where the nuclei are treated classically within Newton's equation of motions.

Verlet Algorithm, a NVE ensemble

In any classical conservative system, one can apply Newton's equation of motions :

$$M_i \ddot{\mathbf{x}}_\mathbf{i}(t) = F(\mathbf{x_i(t)}) \tag{2.53}$$

With M the mass of particles, $\ddot{\mathbf{x}}(t)$ the acceleration of particle i at time t and $F(\mathbf{x_i(t)})$ the force that acts on the particle. This ensures the total energy conservation of the system. Verlet integration [112] is a numerical

algorithm that computes the second derivative of position by using central difference approximation :

$$\frac{\Delta^2 \mathbf{x_n}}{\Delta t^2} = \frac{\frac{\mathbf{x_{n+1}} - \mathbf{x_n}}{\Delta t} - \frac{\mathbf{x_n} - \mathbf{x_{n-1}}}{\Delta t}}{\Delta t} = \frac{\mathbf{x_{n+1}} - \mathbf{2x_n} + \mathbf{x_{n-1}}}{\Delta t^2} \tag{2.54}$$

This equation is used to determine the next dynamic iteration :

$$\mathbf{x}_{n+1} = 2\mathbf{x}_n - \mathbf{x}_{n-1} + \mathbf{a}_n \Delta t^2 \tag{2.55}$$

First time step integration

For the first time step integration :

$$\mathbf{x}_2 = 2\mathbf{x}_1 - \mathbf{x}_0 + \mathbf{a}_1 \Delta t^2 \tag{2.56}$$

One needs $\mathbf{x}_1$ which at first sight is unknown. However, considering that initial conditions are known, one has :

$$\mathbf{x}_1 = \mathbf{x}_0 + \mathbf{v}_0 \Delta t + \frac{1}{2}\mathbf{a}_0 \Delta t^2 \tag{2.57}$$

Which is also a known quantity. Therefore $\mathbf{x}_2$ can be computed.

Nose-Hoover Thermostat

Verlet integration is used to compute a molecular dynamics in the micro-canonical ensemble, where the number of particles, the total volume and the total energy of the system are conserved (NVE). Newton's second law does not conserve temperature and one has to go to another statistical model to be able to conserve it. Canonical ensemble, also called NVT ensemble uses a heat-bath that can either add or remove temperature to (from) the system in order to keep it constant through time. In molecular dynamics and especially for simulating liquid water, it is common to use a heat-bath, often with a Nose-Hoover [44, 82] thermostat in order to set up the liquid

to a certain temperature. This process is called the equilibration of the simulation. It is often performed at the beginning of a molecular dynamics before starting a Verlet NVE dynamics with good liquid initial conditions.

Chapter 3

The Water Dimer

Introduction

One of the most debated question among water scientists is the characterization of hydrogen bond (H-bond) [110]. While predominant, electrostatics cannot alone describe H-bonding properties [13, 91]. Covalent bonding behavior also has to be appreciated [46,87]. Therefore, the quantum character of electronic density has to be treated, and more recently, a quantum treatment of atomic nuclear motion [78] starts also being analyzed to apprehend the complexity of H-bond.

H-bonding network creates an even foggier picture, and notions such as water cooperativity [12] have to be developed. Cooperativity is the effect of enhancing the formation of H-bond by the presence of other already formed bonds. Indeed, a molecule that donates a H-bond, sees its OH bond being elongated. As a result, the electron density gets larger around its lone pairs and hence is favoring the acceptance of other H-bond. Similarly, the accepting molecule, by receiving a H-bond through its oxygen, will depopulate electrons of its hydrogens, enhancing their donations to other H-bonds. On the other hand, it is less favorable for a water molecule to accept a second H-bond through its free lone pair, if its first lone pair

is already receiving a H-bond. This is called the "anticooperativity". In a standard bulk *DDAA* model, a water molecule donates two H-bonds and receives another two, and an asymmetry in the strength of the accepting or donating H-bonds can be observed.
H-bonding is at the origin of most anomalies found in water and it gives to the latter most of its structural and electronic properties.
The dimer, with its two water molecules, appears to be the perfect system to start characterizing the nature of H-bonding. Indeed, this simple cluster counts only one single H-bond. The energy of the H-bond can be properly defined as :

$$E_{\mathrm{H-bond}} = E_{\mathrm{Dimer}} - E_{\mathrm{H_2O,1}} - E_{\mathrm{H_2O,2}} \tag{3.1}$$

Where E_{Dimer} is the total energy of the system composed by the cluster and $E_{\mathrm{H_2O,1}}$, $E_{\mathrm{H_2O,2}}$ are the total energies of isolated water molecules 1 and 2 respectively.
In this chapter, the H-bond of the dimer is analyzed as a function of the flap angle and the distances of intramolecular and intermolecular bonds. In a second part, electronic structure is discussed and projected density of states over the molecular orbitals is used to analyze the chemical nature of the H-bond.

3.1 The structure of the molecular water dimer

The strength of intermolecular H-bond is mostly dependent on two variables [30]. Evidently, the distance D between the donating hydrogen atom of molecule 1 and the accepting oxygen of molecule 2 is one of them. The second one is the so called *flap angle*.

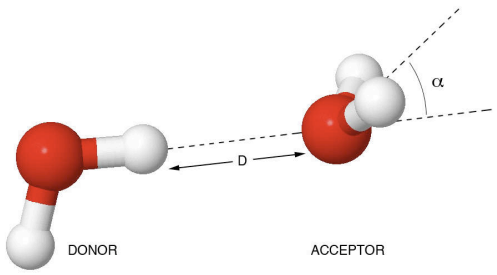

Figure 3.1: Asymmetric Water dimer making a H-bond. In the optimal configuration, the distance between the donating H and the accepting O is around $D \sim 1.95$ Å, and the flap angle is about $\alpha \sim 53°$.

3.1.1 The Flap Angle

Flap angle can be defined as the angle between the vector $\overrightarrow{OH}$ of the donating molecule and the plane that contains the accepting molecule. This angle is labeled α in the Figure: 3.1.

The H-bond energy as defined in Eq 3.1 has been calculated as a function of the flap angle. Calculations have been performed within the DFT formalism, using the localized-orbital first-principle code SIESTA [84,103]. Exchange and correlation has been computed with the PBE [89] GGA functional. Norm-conserving pseudopotentials of the Troullier-Martins [109] type have been used and an extra large double$-\zeta-$polarized basis has been set up to reproduce the long-range water interaction [91]. Results are reported on the Figure: 3.2. For this set of calculations, intermolecular O–H distance D has been rigidly kept to 1.95 Å. The energy minimum, at about $\alpha = 53°$, corresponds to the optimized structure. The H-bond survives ($E_{H-bond} < 0$) until a tilting of around 130°. The maximum repulsion between the two water molecules is reached at 180°. It corresponds to a geometry very electrostatically unfavorable with two positively charged hydrogens facing each other.

Interestingly, the energy that corresponds to a flap angle of $-53°$ (equiv-

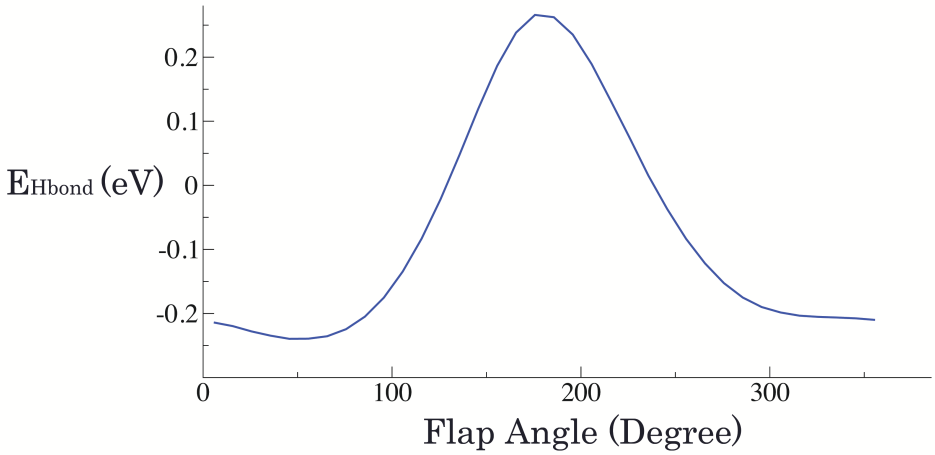

Figure 3.2: H-bond energy calculated from Eq 3.1, as a function of the flap angle α. Global minimum is found for $\alpha = 53°$.

alent on Figure: 3.2 to 307°) is not as low as the energy at 53°. Indeed, this water dimer is said to be asymmetric. This is due to the fact that the two orientations α and $-\alpha$ are not geometrically equivalent since the hydrogen-hydrogen distances are not conserved.

3.1.2 Intra/Intermolecular bonds

Intramolecular covalent OH bond of the donating molecule is varied together with the intermolecular H-Bond for a fixed flap angle of about 53°. Two-dimensional map of the total energy of the dimer can be obtained. Figures: 3.3 and 3.4 respectively show the 3 dimensional and isolines view of the total energy of the molecular dimer as a function of these two distances. Evidently, the energy is more sensitive to a small variation of the intramolecular OH distance. This bond is the more energetic ($\sim$ 5 eV) and a variation along its equilibrium center (about 0.98 Å) is accompanied with strong energy variation.

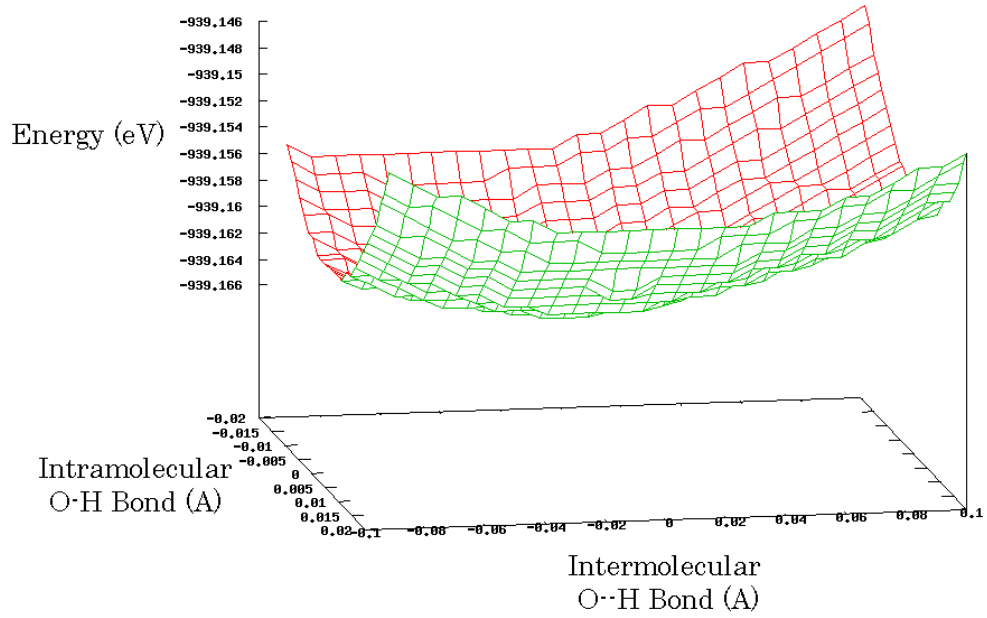

Figure 3.3: Two-dimensional plot of total dimer energy as a function of intermolecular and intramolecular bonds.

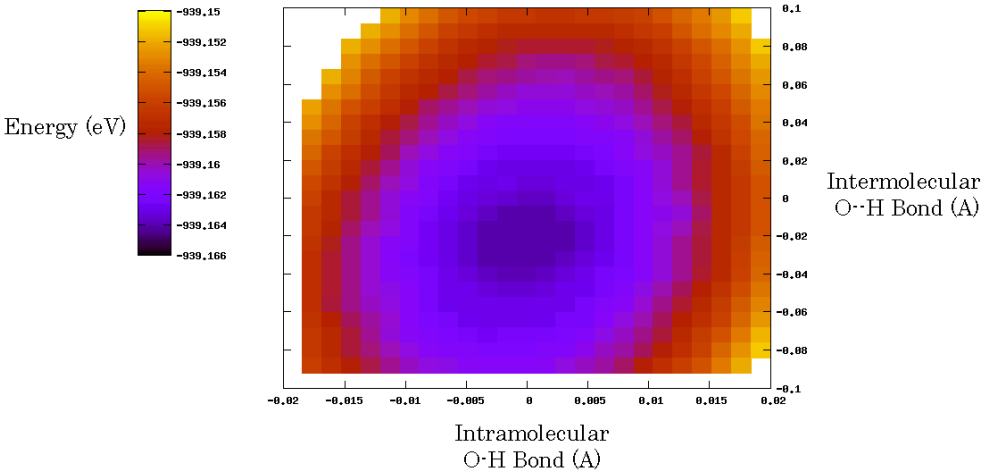

Figure 3.4: Isolines representation of the total dimer energy as a function of intermolecular and intramolecular bonds.

3.2 Projected Density of States over the Water Molecular Orbitals

The projected density of states (PDOS) is a powerful tool to study electronic structure of a system. It gives information about a particular region and is directional enough to target the role of a specific state on the overall system. Water, with its limited number of Molecular Orbitals (MO) gives a perfect set of states to be projected on. It is straightforward to identify the contribution of a particular MO on the total hybridized system. PDOS $\rho_\nu(E)$ can be written as :

$$\rho_\nu(E) = \sum_n |\langle\nu|\Psi_n\rangle|^2 \delta(E - E_n) \tag{3.2}$$

With $|\nu\rangle$ being the water MO and $|\Psi_n\rangle$ the states of the system at the energy E_n.

The five first water MO are shown in the Figure: 3.5. There names refer to the groups of symmetry they belong to. Hence the MO $2a1$, $3a1$ and $4a1$ are symmetric to the plane formed by the three atoms of the water molecule and symmetric with the plane perpendicular to the molecule that contains the HOH bisector. The $1b2$ and $1b1$ MO are respectively antisymmetric and symmetric to the plane of the molecule and respectively symmetric, antisymmetric to the plane perpendicular to the molecule.

The Figure: 3.5 represents the PDOS projected on water MO of both the isolated water molecule (dashed red line) and the acceptor molecule of the dimer system (solid blue line). The energy levels appear to be deeper for the dimer system. It shows that the formation of the H-bond is lowering the MO energy levels of the accepting molecule. This is the result of the hybridization of the lone pair that participates in the H-bond.

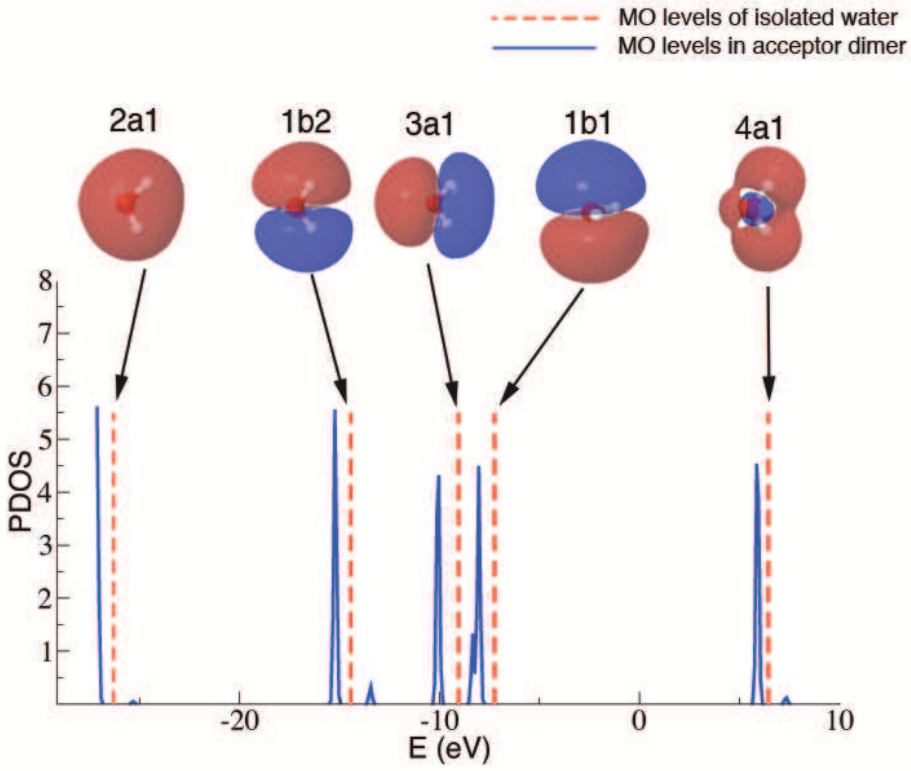

Figure 3.5: Five first molecular orbital (MO) levels of isolated water (dashed red line) and dimer acceptor (solid blue line). The four first MO are filled with electrons. The $4a_1$ MO is empty.

The lone pair can be decomposed as a linear combination of the $3a1$ and $1b1$ molecular orbitals. Figure: 3.6 shows the PDOS projected on the $3a1$ and $1b1$ MO for both of the donor (dashed red line) and the acceptor (solid blue) molecules in the dimer at the optimal orientation. The graph also shows the energy levels of the $3a1$ and $1b1$ MO of the isolated water (dashed black straight lines).

As it has been already pointed out in the Figure: 3.5, the MO of the acceptor molecule are lowered in energy with respect to the isolated water

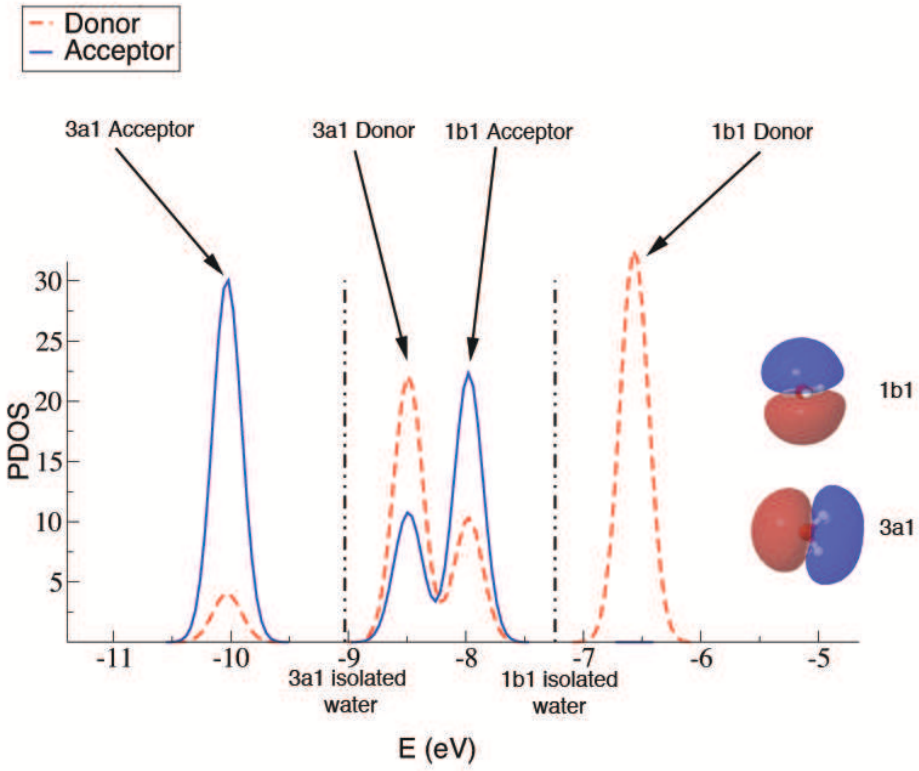

Figure 3.6: $3a1$ and $1b1$ MO of donor (dashed red line) and acceptor (solid blue) molecule in the molecular dimer at the optimal orientation.

by about 1 eV. On the contrary both the $3a1$ and $1b1$ MO of the donor molecule appear to be raised as compared to an isolated molecule by about 0.7 eV. A strong hybridization of the $3a1$ donor molecule and the $1b1$ acceptor level is also clearly visible and the two MO of the two water molecules produce a mixed state which is the main contribution of the formation of the H-bond. The acceptor $3a1$ seems to play a role also by hybridizing with a small fraction of the donor $3a1$ MO. However, the donor $1b1$ does not seem to contribute significantly to the formation of the H-bond.

3.3 The Nature of the hydrogen bond

The optimized geometry is the result of several physical contributions to the H-bond interaction [30, 50, 91]. The acceptor water molecule, due to a locally attractive electrostatic potential associated to the donor H atom, is polarized. This polarization occurs through an elongation of the lone pair involved in the bond [99]. As a consequence of this intermolecular polarization, a small acceptor-donor charge transfer occurs. The charge transfer occurs though the highest occupied molecular orbital (HOMO) of the accepting water molecule, $1b1$ orbital. This MO is the oxygen atom p_z orbital, which is perpendicular to the plane of the molecule. Hence, the maximum polarization for this orbital will occur when the main axis of the $1b1$ acceptor MO is oriented parallel to the donor OH bond axis, i.e. for a 90° flap angle. If the energy of the pair could be divided into donor and acceptor components, for the acceptor water molecule this orientation would give the strongest H-bond energy. However, a second, counterbalancing effect, needs to be taken into account. Pauli repulsion occurs due to the orthogonalization of the acceptor lone pair [102] with the MO associated to the OH covalent bond of the donating H. This is a repulsive exchange interaction and as a result, the donor OH bond will be weakened after formation of the H-bond. The net H-bond interaction is a balance between attractive intermolecular polarization, intramolecular polarization and repulsive Pauli exchange. This repulsive exchange will have the effect of increasing the internal energy of the pair, mostly associated to the destabilization of the donor OH intramolecular bond donating the H to the H-bond. In order to minimize this energetically unfavorable effect, the two molecules find an optimal orientation through a tilting of the flap angle. Therefore, the optimal flap angle of the acceptor molecule in the dimer, is a function of the inter-oxygen separation. The closer the molecules, the

less the flap angle of the acceptor molecule will be, given that the repulsive Pauli exchange will be large, and for long O-O distances a larger flap angle will be allowed.

Conclusion

In this chapter, the investigation of the optimized structure of the water dimer, with its great dependency upon the flap angle has revealed the incompleteness of a classical electrostatics description alone. Molecular orbitals, especially the $3a_1$ and $1b_1$ HOMO, play an important role in the formation and strength of the H-bond. A small charge transfer occurs between the lone pair of the accepting orbital and the hydrogen of the donating molecule. The role of donating and accepting water molecule is therefore quite different. Donating molecule imposes a particular geometry (in the flap angle) to minimize the Pauli exclusion, while the accepting molecule would prefer to allow more charge transfer (by a 90° flap angle). As a result, a compromise is found, with a flap angle of about 53°, to hybridize lone pairs of accepting molecule, without increasing too much the electronic instability of the donating one.

Chapter 4

Interaction of a water monomer and a metallic surface

Introduction

Much effort is being devoted to the understanding of water-substrate interactions at metallic [16, 22, 26, 33, 71, 72, 75, 83, 93, 94] surfaces with catalytic properties. The nature of these interactions involves an entangled balance between water-water and water-substrate interplay. In order to characterize specifically the water-substrate interaction, we reduce, in this chapter, the system to its simplest form. Thus, only one water molecule (monomer) is considered on top of a Pd $\langle 111 \rangle$ surface[1].

Michaelides *et al.* performed a detailed DFT study of the adsorption of water monomers [72] on $\langle 111 \rangle$ surface of a series of transition metal systems. They found that the energy of adsorption of these structures, varies depending on the metal. This variation is due to the different chemical interaction between the water's molecular orbitals (MO) and the surface states of the metal.

[1] $\langle 111 \rangle$ surface corresponds to the plane perpendicular to the (111) axis of the crystalline structure.

However, to date, all these theoretical studies are performed with the same exchange and correlation (XC) density functional [89] (DF), which was chosen as the optimum compromise for obtaining an accurate description of both H_2O molecules and the metallic slab. The limitations of DFT for describing liquid water are well known [29, 37, 97]. Compared with experiments, *ab initio* molecular dynamics simulations (AIMD) of liquid water show an over-structured liquid with low diffusivity and incorrect equilibrium density at room temperature [29, 96, 115].

One source of error has been related to the classical treatment of the nuclear coordinates in the AIMD calculations [78]. But reconciliation between theory and experiment cannot be achieved simply with this argument. It is well known that the structure of DFT water depends strongly on the XC functional used [111, 115], mainly due to the variation in strength of the hydrogen bond (H-bond) interaction observed for different XC functionals, together with the consideration of non local van der Waals correlations in the intermolecular interaction.

In this chapter, I perform a detailed study of the adsorption of a water monomer on top of Pd$\langle 111 \rangle$ surfaces and explore a number of DFs, specifically, those developed within the generalized gradients approximation (GGA) framework to improve the performance of PBE [89] in bulk systems [119] and in surface-related problems [120]. I also study the effect of non-local correlations using the van der Waals density functional (vdW-DF) of Dion *et al.* [21].

I will show that the interaction between the molecules and the metal is very similar to the H-bond interaction between water molecules. For this reason, I name this interaction *pseudo hydrogen bond*; its origin and properties are presented in detail.

4.1 Description of the system

To study the interaction of a water monomer with a Pd $\langle 111 \rangle$ surface, first-principle calculations within the DFT approach have been performed with the SIESTA code [84, 103]. Exchange and correlation potential has been treated with different GGA functionals such as, PBE [89], WC [119], a revised version of PBE, named revPBE [120], and the van der Waals XC functional DRSLL [21]. An extra large double$-\zeta-$polarized has been used to compute water related atomic orbitals and a double$-\zeta-$polarized has been set up for the metallic atoms. A Pd slab of 5 layers cut perpendicularly to the (111) axis has been built (in addition, a 6th layer of ghost atoms has been set up as an extra set of orbitals [34]). A picture of the simulation is shown on Figure: 4.1.

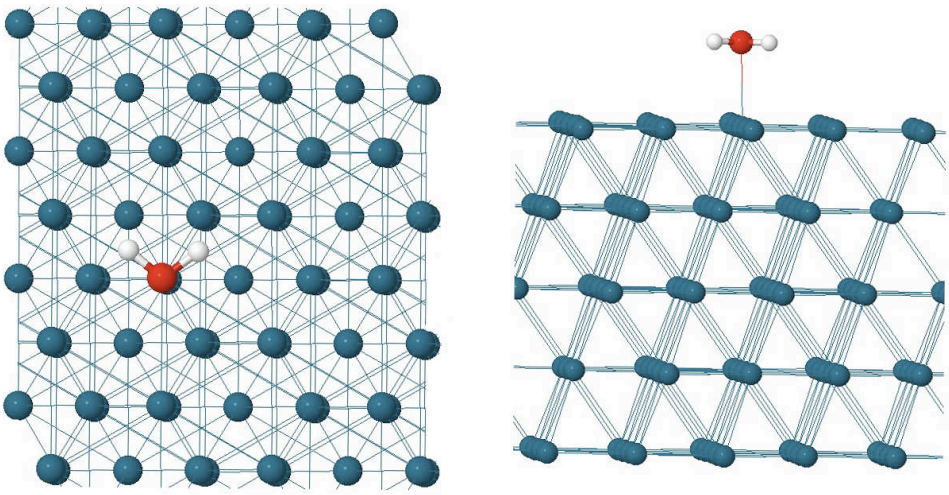

Figure 4.1: Top view (Left) and Side View (Right) of a water monomer on top of a Pd $\langle 111 \rangle$ surface. A 5-layer slab is shown on the Side view.

As it has been explained in the theoretical background chapter, density functional theory uses the periodicity of a unit cell. It has been set up to reproduce a semi-infinite metallic surface in X and Y. However, a 70 Å

vacuum has been established in the Z direction, to break the periodicity of the calculation along this axis. The cell also needs to be large enough in X and Y to ensure the non interaction between the water monomer with the monomer from the cell ± 1 (see Figure:4.2).

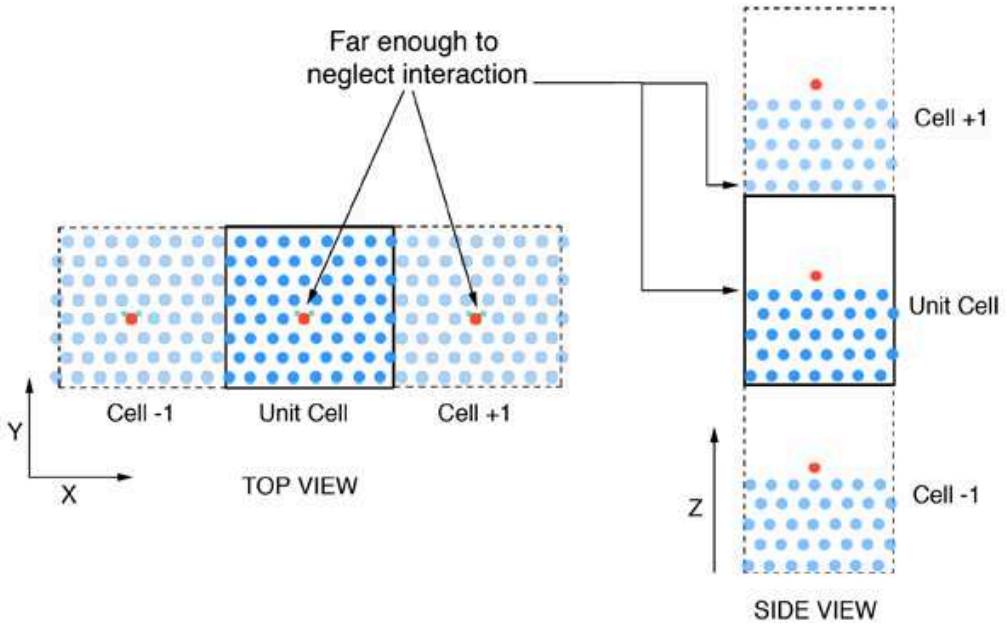

Figure 4.2: Top (left) and Side (right) sketch of periodicity of the system. Surface is periodic in X and Y but the unit cell has to be large enough to neglect interaction between 2 monomers (in red). In Z, large vacuum is introduced to break the periodicity imposed by DFT.

The two first slab layers are relaxed with a conjugate gradient method that satisfies the Hellman-Feynman theorem. Other layers are frozen to bulk geometry. The system geometry is optimized with a maximum tolerance for the forces of 0.01 eV/Å. Water-substrate interaction is expected to be weak (few meV). This makes the potential energy surface flat, with many local minima. In order to obtain the optimal chemisorption site and

geometry, many different surface sites and water orientations are tested.
In the following section, the convergence of different approximations including the size of the system and k-point sampling is analyzed in detail. The largest system is a $3\sqrt{3} \times 3\sqrt{3}.R(30)^\circ$ unit cell (27 Pd surface atoms, 135 Pd atoms in total). Brillouin-zone k-point sampling is performed with the Monkhorst pack [76] approach, with a maximum of $4 \times 4 \times 1$ k-points for the largest unit cell.

4.2 Size effects

As previous DFT studies have shown [13, 72], an isolated water molecule is nearly parallel when chemisorbed on $\langle 111 \rangle$ transition metal surfaces, deviations from the perfectly horizontal orientation depending on the metal considered. In this section, the problem is revisited, focusing only on the Pd $\langle 111 \rangle$ surface.
DFT takes advantage of the Bloch theorem to reduce the system size, to its unit cell thanks to the real space periodicity of the system. This also reduces the reciprocal cell to its first Brillouin zone. Numerically, Brillouin zone is being sparsely integrated with the use of k-points of high symmetry (called the k-point sampling). Considering the monomer alone, if the size of the unit cell is too small (lattice parameter of 4.5 Å or less), the electrostatic interaction between water molecules in neighboring cells makes the horizontal configuration (an infinite arrangement of dipoles parallel to a plane) more than 100 meV favorable with respect the vertical configuration (an infinite arrangement of dipoles perpendicular to a plane). In monomer calculations and especially for polar molecules that are highly sensitive to long-range Coulomb interactions, large unit cells have to be used [11, 91]. *Ab-initio* codes based on localized orbitals, allow going farther beyond the usual unit cell size than those based on plane-wave formalism, without

increasing much the computational cost.

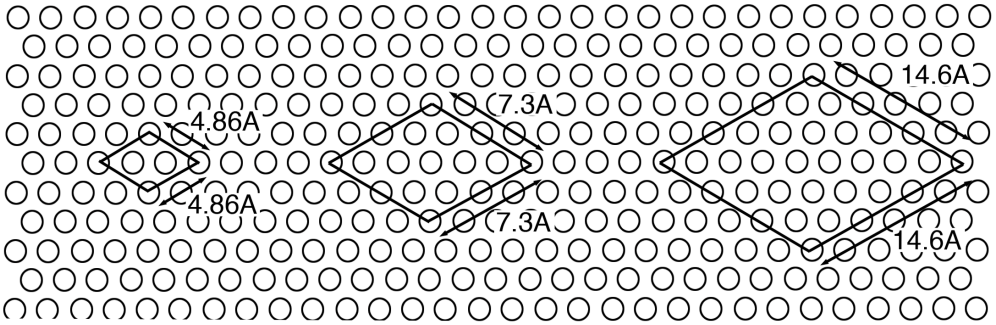

Figure 4.3: a. $\sqrt{3} \times \sqrt{3} \times R(30°)$, 3 atoms per unit cell. b. $2\sqrt{3} \times 2\sqrt{3} \times R(30°)$, 12 atoms per unit cell. c. $3\sqrt{3} \times 3\sqrt{3} \times R(30°)$, 27 atoms per unit cell.

Here the size of the unit cell is carefully analyzed by comparing the geometry and adsorption energy of three different unit cells (from small to large) shown in Figure: 4.3. k-sampling dependency of the first Brillouin zone is also analyzed and the number of k-points is varied from a gamma calculation, with no k-points, to calculations with a total of 432 k-points.

We define the adsorption energy of the water monomer as:

$$E_{Ads}^{Monomer} = E_{H_2O/Metal} - E_{H_2O} - E_{Metal} \tag{4.1}$$

Table 4.1 shows the dramatic impact of the unit cell size on the adsorption energy strength. For an equivalent number of $k-$points, the 1×1 and 2×2 unit cells show an adsorption energy importantly lower than the 3×3 cell (0.40eV). The orientation of the monomer on top of the surface is also quite different depending on the unit cell and the increasing of the size has the tendency of decreasing the distance water-substrate. The monomer also appears to be nearly flat with respect to the surface with an flap angle of 1.6°.

Results show that both the geometry and adsorption energy are strongly influenced by the number of k-points. Even for a relatively large unit cell

Table 4.1: Adsorption energy and geometry of a water monomer on top of Pd ⟨111⟩ calculated using GGA PBE [89]potential as a function of the size of the unit cell and the reciprocal k-points sampling.

Energy - $E_{Ads}^{Monomer}$										
cell	a(Å)	$\sqrt{3}\times\sqrt{3}$				$2\sqrt{3}\times2\sqrt{3}$		$3\sqrt{3}\times3\sqrt{3}$		
k-point grid		6×6 (108)		12×12 (432)		6×6 (432)		Γ (27)		4×4 (432)
	3.97	0.24 eV		0.21eV		0.28eV		0.51 eV		0.40 eV

Geometry										
cell	$\sqrt{3}\times\sqrt{3}$				$2\sqrt{3}\times2\sqrt{3}$		$3\sqrt{3}\times3\sqrt{3}$			
k-point grid	6×6 (108)		12×12 (432)		6×6 (432)		Γ (27)		4×4 (432)	
	flap	D_{O-Pd}	flap	D_{O-Pd}	flap	D_{O-Pd}	flap	D_{O-Pd}	flap	D_{O-Pd}
	-7.2°	2.53 Å	−5.6°	2.52Å	3.0°	2.4Å	6.5°	2.36 Å	1.6°	2.39 Å

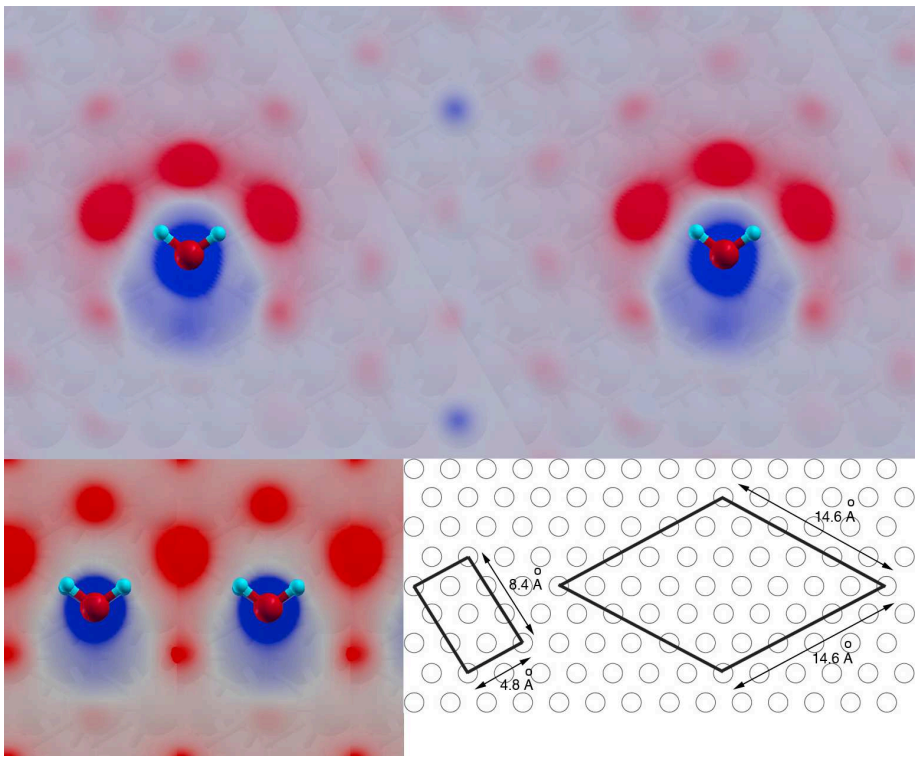

Figure 4.4: Screening charge formed at the ⟨111⟩ surface of a Pd slab to screen an adsorbed water molecule. The screening charge density is calculated as $\rho_{scr} = \rho_{Pd+H_2O} - \rho_{Pd} - \rho_{H_2O}$ for two different surface periodicities. Top, $3\sqrt{3} \times 3\sqrt{3}R(30)^\circ$ unit cell. Bottom left, rectangular cell with 4.8Å × 8.4Å sides. Bottom right, sketch of the two cell periodicities. The image plane is located at≈ 1 Å above the Pd surface layer. Blue colors represent electron depletion regions (positive charge), while red regions represent electron accumulation regions (negative charge). Notice how the screening charge shape and spread is very sensitive to the unit cell size.

(∼15 Å × 15 Å), a Γ calculation does not provide converged calculation, either in geometry or energy. The effect of the unit cell size on the energy and geometry of adsorption is associated with the extension of the image charge distribution. As shown in Figure: 4.4, the charge distribution suffers important changes when going from a small $p2 \times 2$ rectangular cell to a

$3\sqrt{3} \times 3\sqrt{3}$ cell. Only a fully converged image charge distribution will provide an accurate electrostatic interaction between the molecule and its image.

4.3 A critical system for the XC density functionals

Given that the description of liquid water is well known to be strongly dependent on the XC choice, a similar behavior for water-metal interactions can be anticipated.

To explore this, a set of commonly used XC DFs is chosen. All of them contain different modifications to the functional form of the exchange enhancement factor [68], and share a common description of the correlation part of the potential.

The XC functionals are PBE [89], revPBE [120] (a minor modification of PBE proposed to improve its performance for surface-related systems), and the lately popular Wu-Cohen (WC) [119] potential, designed to improve the treatment of metals and oxide systems.

To assess the role of vdW interactions on the binding of water to metal surfaces, the recent Dion *et al.* vdW-DF [21] is also tested here, and will be denoted DRSLL after its authors. The results for this functional will be analyzed separately.

4.3.1 Adsorption energy and geometry

Table 4.3.1 shows the adsorption energy and geometries of the different XC functionals. All the calculations have been performed with the large $3\sqrt{3} \times 3\sqrt{3} \times R(30°)$ unit cell and with a k-points sampling of 4×4×1 (equivalent 432).

The four different XC functionals provide quite different adsorption energies and geometries. Both PBE and WC provide much larger adsorption energies (more than 0.3 eV larger) than revPBE and DRSLL. These results correlate well with DFT studies of liquid water that show how PBE overestimates the intermolecular H-bond interaction in the liquid [37, 115] whereas revPBE presents a less structured liquid, with larger H-bonded O-O distances than PBE.

	a	$E_{Ads}^{Monomer}$	Geometry	
			flap	D_{O-Pd}
PBE	3.97 Å	0.40 eV	1.6°	2.39 Å
WC	3.91 Å	0.43 eV	2.3°	2.28 Å
revPBE	3.99 Å	0.10 eV	6.8°	2.47 Å
DRSLL	4.01Å	0.35 eV	14.4°	2.48 Å

Table 4.2: Adsorption energy and geometry of a water monomer on top of Pd $\langle 111 \rangle$ calculated using GGAs PBE [89], revPBE [120], WC [119] and DRSLL [21] XC potentials.

It is known [30] that the formation of H-bonds between molecules in liquid water and ice increases the molecular polarization and therefore the dipole moment of condensed phases of water, as compared to the gas phase. This increase makes the formation of subsequent H-bonds favorable, a phenomenon called H-bond cooperativity [28]. This bond-induced polarization has its major effect on the lone pairs of the oxygen atoms, which are also the electrons involved in the formation of H-bonds (as shown in the water dimer chapter). As a consequence of this polarization, when a H-bond is formed,

there is a small (few milli-electrons) [50] negative charge transfer from the lone pair of the acceptor molecule to the donor molecule. This transfer weakens the covalent intramolecular OH bond of the acceptor molecule. This effect is the reason for the red shift of the OH stretching frequency in ice versus liquid water [8], given that ice has much stronger H-bond network than liquid water. This shift also correlates with a blue shift of the H-bond vibrational band (water librations) in ice versus water. The origin of this weakening is the Pauli repulsion between the H-bonding lone pair of the acceptor molecule and the MO associated to the OH covalent bond of the donor molecule [102]. The consequence for the donor molecule is a net polarization, where electrons are shifted toward the Oxygen atom, therefore increasing its molecular dipole.

4.3.2 van der Waals Density Functional

Dispersion interactions are neglected by current local density approximation [14] (LDA) and generalized gradients approximation [3,56,88,89] (GGA) XC functionals. In these formalisms, interactions are treated as local or semi-local effects and approaches that are very well-suited for the characterization of homogeneous systems such as simple metals or semiconductors (with LDA functionals) or inhomogeneous ones such as transition metals, ionic crystals, surfaces, organic compounds, etc. GGA functionals, semi-local, are the choice in this case. van der Waals (vdW) or dispersion interactions are, by definition, non-local and long-ranged interactions. We have also evaluated the effect of non local vdW type correlations on the adsorption of water onto Pd. To do so, we have used the vdW density functional (vdW-DF) first introduced by Dion *et al.* [21], DRSLL. DRSLL is a functional with approximate inclusion of non local dispersion interactions. It is capable of describing semi-quantitatively weak dispersion interactions, without compromising the accuracy of the best GGA functionals

for stronger ionic, covalent and metallic bonds. The main reason why, to date, this functional has not been used widely is because its evaluation for large systems is very expensive. The Roman-Perez and Soler [95] implementation of this functional has been used, within the program SIESTA, which reduces the computational cost of the calculation.

In the construction of the DRSLL functional, the local exchange interaction is taken from the revPBE formulation. The choice of revPBE as the basis for the exchange in DRSLL is motivated by the well known over-binding effect produced by PBE in situations where no exchange-induced binding should exist (like the noble gases binding) [21].

When we compare the geometry and energetic results of DRSLL to those of revPBE we observe large differences. vdW interactions clearly increase the binding energy. While revPBE provides the lesser binding (0.1 eV), DRSLL binds nearly 3 times as much (0.28 eV). This increase in energy occurs without changing the chemisorption distance D_{O-Pd} (2.48 Å for revPBE against 2.47 Å for DRSLL).

Interestingly the flap angle in DRSLL is larger than in any other functional (twice as much as revPBE and nearly 10 times as much as PBE), indicating that when vdW interactions are taken into account, the weight of the charge transfer decreases and the electrostatic energy component (which favors a perpendicular orientation) increases. Also, vdW interactions favor the facing of polarizable charge clouds [115], which also explains the vertical tilting of the molecule when DRSLL is used instead of any of the GGAs.

As the exchange part of the interaction is treated by revPBE, in its current form, DRSLL is not a good choice of XC functional to study water-related problems [115]. At the same time, results obtained here indicate that vdW interactions are very important and they might change the structure of water at metallic interfaces computed with XC functionals that do not ac-

count for vdW correlations. However, the exchange part of the interaction needs to be well described and for the moment PBE is a better choice of functional. In a different study [115] it has been shown that DRSLL underperforms other functional in the description of the structure of liquid water. In the same study, it was shown that replacing the local revPBE exchange by PBE in DRSLL improves largely the overall description of liquid water.

4.3.3 Vibrational properties

In order to understand the origin of the differences of the binding energy, the three vibrational frequencies of water, both isolated and adsorbed to Pd are also computed. Table 4.3 shows the results. The OH stretching vibrational energies for the monomer on top of the surface vary by an amount of about $4-5\%$ depending on the different XC functionals while they only vary by $0.5-0.6\%$ for the isolated monomer, one order of magnitude less.

As mentioned before, the OH stretching vibration energy of water measures the strength of the intramolecular OH bond. Similarly, the strength of the H-bond interaction in water is inversely related to the frequency of the intramolecular OH stretching vibration. We conclude from table 4.3 that the binding of the water to the metal, exactly as it occurs in liquid water, strongly modifies the intramolecular OH bond.

revPBE water barely binds to the metal (see table 4.3.1) as it describes a more covalent water molecule, with a stronger OH bond and with less tendency to be polarized by the metal substrate. This is the reason why the stretching frequencies calculated with revPBE undergo a small (2%) change after adsorption onto the substrate. WC water strongly binds to the metal; it describes a more ionic molecule, with weaker OH bonds. This is the reason why the stretching frequencies experience a 6% change after binding. PBE water is in between these two extremes, with a frequency

	H_2O on Pd			H_2O in vacuum		
	B	S	AS	B	S	AS
PBE	1611	3640	3737	1649	3797	3896
WC	1573	3593	3698	1636	3812	3914
revPBE	1627	3707	3814	1653	3798	3896
DRSLL	1636	3660	3760	1667	3774	3870

Table 4.3: Bending (B), symmetric stretching (S) and anti-symmetric stretching (AS) vibrational modes (in cm^{-1}) of a water monomer on top of Pd $\langle 111 \rangle$ (left panel), and isolated (right panel) calculated using three different GGAs (PBE [89], WC [119], revPBE [120]) and the vdW-DF DRSLL. [21]

change of ≈4%.

4.4 Interaction Water/Metal, the pseudo-H-bond

Only after bonding to the metal, the intramolecular OH covalent bond reveals its sensitivity to the polarizability of the molecules. In the optimum adsorption geometry, so called "horizontal" adsorption, the oxygen atom forms a bond with the metal that resembles an accepting H-bond through the $1b1$ Molecular Orbital. The screening charge formed at the surface of the Pd slab is calculated. This image charge can also be seen as the "real" image charge density, and is calculated as $\rho_{scr} = \rho_{Pd+H_2O} - \rho_{Pd} - \rho_{H_2O}$. The screening charge of the water molecule inside the metal, is shown in Figure: 4.4. It resembles an "anti-water molecule" (positively charged oxygen-like and negatively charge hydrogen-like charge distribution). Therefore the metal effectively acts as a pseudo water molecule, forming a *H-bond-type* interaction with the adsorbed molecules. Strong similarities between this interaction, that I name *pseudo hydrogen bond* and the real H-bond in water can be noticed.

It can also be seen in Figure: 4.4 that the shape and spread of the screening charge is strongly sensitive to the in-plane periodicity of the unit cell, which might be part of the reason for the large energy differences presented in table 4.1. The large $3\sqrt{3} \times 3\sqrt{3}R(30)^\circ$ cell provides an image charge closer to the fully converged one.

4.4.1 Electronic structure of the H- and *pseudo-H*-bonds

In water-metal interaction, the metal, with the creation of an image charge, plays the role of a second water molecule, This will always be the case, no

matter the orientation of the water molecule with respect to the metallic substrate, as shown in Figure: 4.4. If O faces the substrate, the lone pairs will face a locally attractive potential that will enhance their polarization toward the metal. Charge transfer between the two systems will happen and will depend on the relative position of the monomer-metal or donor-acceptor (in the dimer) chemical potentials. For PBE, about 10% of an electron (mulliken charge) is transfered to the metal.

The chemical potential of a molecular system can be very roughly approximated as the average between the highest occupied molecular orbital energy E_{HOMO} and the lowest unoccupied molecular orbital energy E_{LUMO} [19]:

$$\mu_{\mathrm{H_2O}}^{\mathrm{DFT}} \approx \frac{E_{\mathrm{HOMO}} + E_{\mathrm{LUMO}}}{2} \tag{4.2}$$

For the metal the chemical potential is given by the energy of the HOMO level, $\mu_{Pd}^{\mathrm{DFT}} = E_{\mathrm{HOMO}}(Pd\langle 111\rangle)$ [19]. These will depend on the orientation of the monomer with respect to the surface, or in the relative orientation of the two molecules in the dimer.

To study this, the projection of the Kohn-Sham states, ϕ_n has been computed , from the calculation of the complex (water-metal and water dimer) onto the acceptor water molecule Kohn-Sham orbitals, ψ_ν, (MOs) as computed in a separate calculation of the isolated acceptor monomer in the same geometry as in the complex.

$$MOPDOS(E,\nu) = \sum_n \langle\psi_\nu|\phi_n\rangle\delta(E - E_n) \tag{4.3}$$

This molecular orbital projected density of states (MOPDOS) is computed for three different relative orientations (perpendicular, intermediate and parallel) and the projection onto the acceptor HOMO ($1b1$) and HOMO-1 ($3a1$) orbitals are shown in Figure: 4.5. Water molecule lone pairs are a linear combination of these two orbitals and therefore they are the acceptor's MOs with major participation in the bond formation [50].

The comparison of the MOPDOS for the dimer Figure: 4.5 (top) and water-metal complex (bottom) shows that the HOMO-1, $3a1$, orbital has a very similar energy dependence in the two systems. Its energy is minimized at the perpendicular configuration (flap=0°, solid line) and maximized at the horizontal one (flap=90°, dashed line). The maximum polarization of this orbital occurs along the dipole moment direction [85], reinforcing the gain in electrostatic energy of this orbital when the molecule is perpendicular to the substrate. The energy behavior of the HOMO, $1b1$, orbital as a function of the angle is different for the two systems. For the water dimer, the two peaks appearing in the MOPDOS of the $1b1$ orbital of the acceptor molecule show that this orbital is a linear combination of two water MOs of the global system. One (with large weight) being the $1b1$ MO of the acceptor molecule in the complex and the second (small weight, lower in energy) showing the hybridization of this orbital with orbitals of the donor molecule upon formation of the H-bond. For this orbital, the intermediate geometry (flap=45°,dotted line) is the most favorable energetically. This can be seen by taking the weighted average of the energy of the two peaks that contribute to the $1b1$ band. In the perpendicular configuration (solid line) the nodal plane of the $1b1$ MO faces the donor H atom, preventing the intermolecular polarization of this orbital (which is needed to the formation of the H-bond). The parallel configuration (dashed line in Fig. 4.5) is not favorable, even if in this case the charge transfer and intermolecular polarization of the $1b1$ acceptor MO is a maximum. However because of this also the repulsive Pauli exchange is a maximum and dominates the energy of this configuration.

In the metal-water complex, the Pauli repulsion energy is much smaller since the metal states are delocalized and not directional, which allows a much larger orbital flexibility. It is not unfavorable for the metal to receive charge from the $1b1$ water MO, i.e. the metal is a very good electron

acceptor. The optimal orientation of the monomer is therefore horizontal, maximizing the electronic delocalization of the monomer $1b1$ MO. This is the reason why in Fig. 4.5 (bottom) the spread of the peak increases with the angle of adsorption, indicating a larger hybridization between monomer and metal states.

It is worth noticing that the relatively large value of the cohesive energy (0.40 eV for PBE) is also explained by the formation of two other *pseudo-H-bonds* through the hydrogens (with negatively charge hydrogen images induced by screening). Indeed, when the monomer is physisorbed vertically, with the two H atoms facing the metal, this geometry is found to be stable, even if the binding energy is only 0.13 eV, with PBE. In this geometry the charge transfer is reversed. The water molecule now acts as the H-bond donor (two of them one through each H) and the image charge HOMO state mixes in with the donor states. As explained before the donor molecule is destabilized due to Pauli repulsion. At the same time, when only the electrostatic interaction is accounted for, the perpendicular geometry is energetically favored. The perpendicular geometry, with the two hydrogens facing the metal surface should be energetically stabilized in the liquid-metal interface. The reason being that once this interfacial donor molecule is able to form accepting H-bonds with the bulk water, the overall Pauli repulsion associated to this geometry, due to making two donating H-bonds to the metal will be reduced. The molecule will lower its energy by accepting two H-bonds from the bulk water. Therefore the binding energy will increase and this geometry will compete with horizontally adsorbed molecules.

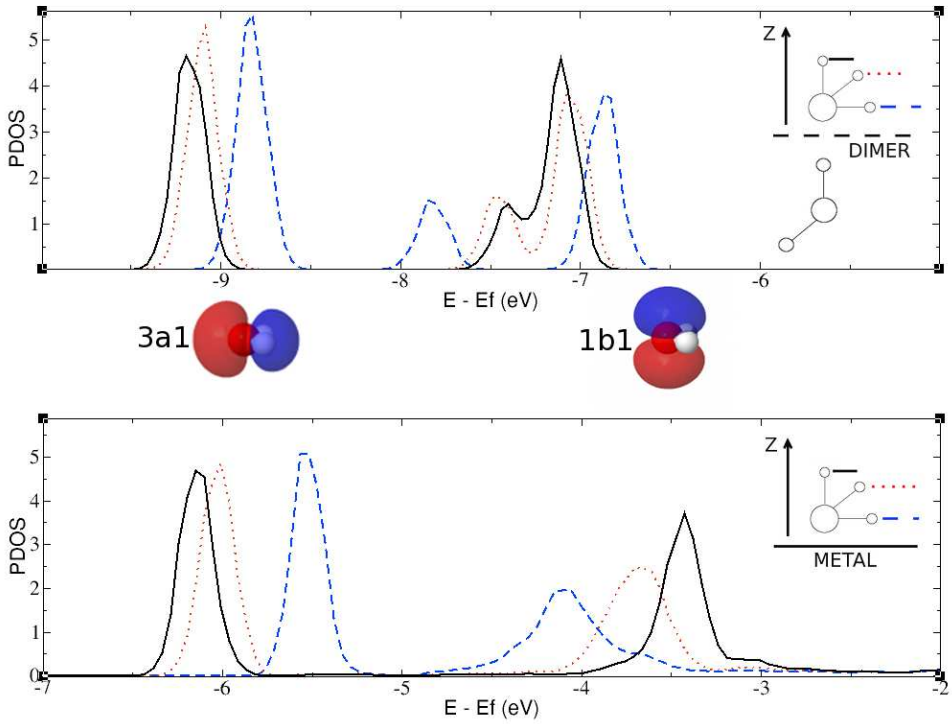

Figure 4.5: Density of states projected onto the water $3a1$ and $1b1$ molecular orbitals (shown in the middle inset) calculated for the water dimer (top) and the water monomer on top of a Pd $\langle 111 \rangle$ surface (bottom). The Fermi energy has been shifted to 0 eV in both cases. The arrows indicate the energy regions of the $3a1$ and $1b1$ projections for each plot. Projections are performed for three different orientations of the acceptor molecule, as shown in the insets. The three orientations for the dimer depend on the angle α formed between the plane of the acceptor molecule and the donor O-H bond. For the water-Pd complex the orientations depend on the angle α formed between the plane of the water molecule and the normal direction to the surface. Full (black) lines, $\alpha = 0^o$. Dotted (red) lines, $\alpha = 45^o$. Dashed (blue) lines, $\alpha = 90^o$.

Conclusion

In this chapter, it has been shown that the size of unit cells is critical to properly describe systems with large polarity such as water. Long-range

Coulomb interactions must be controlled to avoid spurious neighboring interactions and extra large cells must be used.

Exchange and Correlations (XC) potentials are also a determinant parameter to have under control. While revPBE underestimates the interaction water/metal, WC tends to enhance the interaction by making a highly polar water. This polarity emphasized the electrostatic weight of the interaction.

XC functionals, however, can be used as a tool, to understand the physics of the interaction. It is known that revPBE understructures liquid water by "making" a water molecule too covalent. On the contrary, WC is overstructuring liquid water by building much more ionic water molecules. These XC characteristics can then be used as computational tools to emphasize one effect or the other in order to deduce the nature of the interaction.

van der Waals functional, with its revPBE exchange term, does not appear to reproduce physical water/metal interaction. This XC functional is strongly enhancing the electrostatically unfavorable facing of polarizable charge clouds.

Finally it has been shown that the water/metal interaction is comparable to a H-bond interaction. Indeed, the metal by screening a locally charged water, is creating an opposite charge to the water molecule. This charge cloud is playing the role of either an accepting or donating water-like molecule, and a *pseudo H-bond* is formed.

Chapter 5

Water monolayer covering a metallic surface

Introduction

The previous chapter was aimed for the understanding of the basic interaction between a water molecule and a metallic surface. Experiments [16] however, focus on the wetting of metallic surfaces with a water monolayer. Covering can be controlled from nano-structures (hexagons, heptagons) to a complete covering of the surface by a water monolayer. From a fundamental point of view, understanding the nucleation of ordered arrangements of water molecules at metallic interfaces is a prolific area of scientific effort [16, 22, 26, 33, 42, 71, 72, 75, 83, 93, 94]. Experimental observation of hexagonal [16] clusters of water grown at low temperatures and low coverages on top of hexagonal closed packed metallic (HCP) surfaces and pentagonal [71] clusters at non HCP surfaces, motivates the theoretical study of the origin of this nucleation. Density functional theory [43, 52] (DFT) studies of water adsorption at Pd [72], Ru [26], Cu [94], Ni [33] show that water molecules can adsorb in three different configurations at these surfaces; these configurations can combine to build a two dimensional ice

structure when repeated periodically following the lattice symmetry of the metallic surface. In some cases, the strong interaction between H_2O and the substrate can lead to dissociation of the molecules [26, 116], or to the formation of 2D ice monolayers [16], often confusedly called bilayers due to its water buckling.

Here, the adsorption of an ordered water monolayer is studied on the Pd⟨111⟩ surface. Previous studies, based on the use of the PBE [89] GGA functional [9, 16, 70], showed that one of the two possible ordering of the monolayers (with half of the water molecules oriented with a hydrogen atom oriented toward the Pd surface) was energetically more favorable than the opposite ordering (with half of the water molecules oriented with a hydrogen atom oriented away from the Pd surface). In this work, different DF are tested. Again, they are used as a tool to understand the physics behind the heterogeneous interaction. The stability of these over-layers are compared by studying the strength of the different hydrogen bond interactions, and it can be shown that the two over-layers are very different in nature.

5.1 Description of the system

⟨111⟩ transition metal surfaces offer a lattice parameter comparable to the intermolecular O-O distance (a =2.81 Å for Pd). It has been shown [16,22, 83] that a monolayer of ice binds to ⟨111⟩ transition metal surfaces in an hexagonal arrangement, following a 2 dimensional structure, called *2D ice rule*. This arrangement imposes the water oxygen atoms to form hexagonal structures on top of Pd atoms, following the ⟨111⟩ surface symmetry, while one and only one hydrogen lies in between two oxygens, as shown in the Figure: 5.1, top view. The formation of a perfect, infinite, monolayer brings another restriction; half of the molecules must lie parallel to the surface, and the other half have one OH bond parallel to the surface while the

other OH bond is pointing either away (up) or towards (down) the surface. Figure: 5.1, side view, represents an arrangement of flat, down molecules.

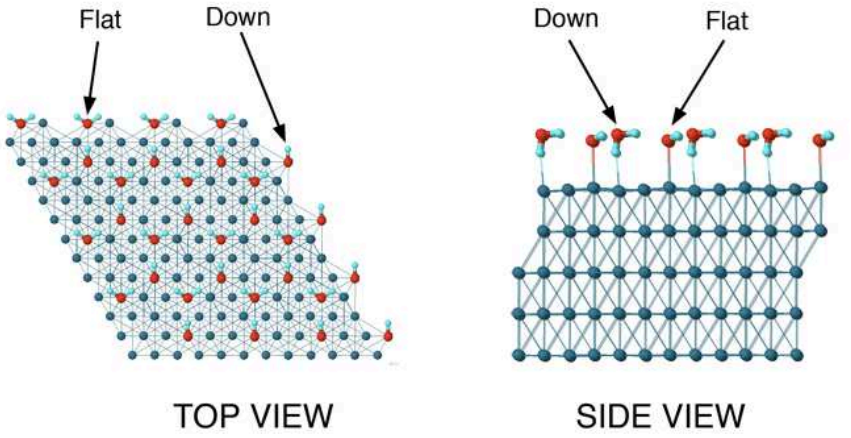

Figure 5.1: Top (Left) and Side (Right) view of a water monolayer on top of a Pd $\langle 111 \rangle$ surface. This perfect monolayer is made with a hexagonal arrangement of Flat and Down water molecules that respect the *2D ice rule*: the oxygens lie on top of Pd atoms forming hexagons, while one hydrogen lies in between two oxygens, ensuring H-bonding.

5.1.1 Configurational entropy

The configurational entropy can be defined as the number of different water configurations that can be performed to respect the *2D ice rule*, in a perfect monolayer surface coverage. For instance, the smallest possible $\sqrt{3} \times \sqrt{3}R(30°)$ unit cell (see Figure: 5.2) is composed by two water molecules. One of the molecules has to be flat, while the other one can be either up (one H is pointing away from the surface) or down (as in Figure: 5.1), with one H pointing down towards the surface.

The configurational entropy for the smallest cell has a set of two elements that are $\{(\text{Flat,Down}); (\text{Flat,Up})\}$.

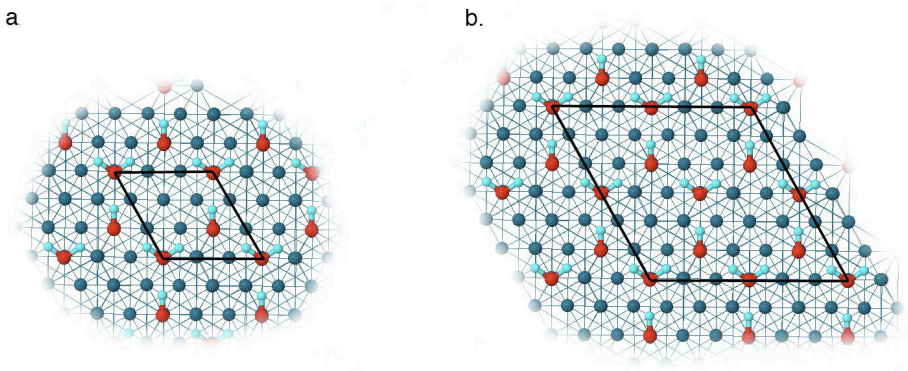

Figure 5.2: a. $\sqrt{3} \times \sqrt{3}R(30°)$ and b. $2\sqrt{3} \times 2\sqrt{3}R(30°)$

The configurational entropy increases dramatically with the size of the unit cell. We analyze in this chapter the substrate induced effects on this hexagonal two dimensional H-bond network. We compare the two systems formed by the smallest unit cell allowing a complete coverage of the metal by water after imposing the *2D ice rule* constraint. The first one, labeled H-down, is composed by a Flat and a Down pair of molecules. The second system, referenced as H-up, is formed by a Flat and a Up pair. Both of the calculations are performed using a $\sqrt{3} \times \sqrt{3}R(30°)$ unit cell.

5.2 Energy and Geometry

The cohesive energy of the adsorbed 2D ice layer is defined as:

$$E_{\text{Cohesive}} = E_{2\text{H}_2\text{O/Metal}} - 2E_{\text{H}_2\text{O}} - E_{\text{Metal}} \tag{5.1}$$

While in appearance this energy is identical to the monomer adsorption energy (Eq:4.1), its meaning is not quite the same. The cohesive energy represents the total energy of forming a 2D ice layer on top of a Pd $\langle 111 \rangle$ surface from gas water. In this definition, water-metal interactions are obviously taken into account but water-water interactions are also included

in the overall counting.

In order to compare the cohesive energy with the adsorption energy per monomer, the cohesive energy per molecule is introduced. In the $\sqrt{3} \times \sqrt{3}R(30^\circ)$ unit cell, (2 water molecules) it is defined as :

$$E_{\mathrm{Cohesive/H_2O}} = \frac{1}{2}(E_{\mathrm{2H_2O/Metal}} - 2E_{\mathrm{H_2O}} - E_{\mathrm{Metal}}) \tag{5.2}$$

The cohesive energy per H_2O is expected to be greater than the monomer adsorption energy due to water-water H-bonds. Table 5.1 shows the cohesive energy per H_2O for the two systems, H-down and H-up, for all the XC functionals used in this study.

As it was already pointed out [16, 70], the two systems appear to be stable and the cohesive energy per molecule is close to the monomer adsorption energy. The H-down monolayer is confirmed to be the most stable for all the GGA functionals, although the cohesive energy is strongly dependent on the XC potential (revPBE is much weaker than WC). This is in agreement with the calculations discussed in the previous chapter on the monomer adsorption (see Table: 4.3.1). The energy difference between the two systems: H-down and H-up, is also dependent on the XC choice. We observe differences of ≈15% for PBE, ≈14% for WC and ≈ 16% for revPBE.

The results obtained using the vdW-DF DRSLL are notoriously different. As compared to revPBE, the cohesive energy is increased by 70% and the same energy is obtained for both configurations. Two physical reasons must be pointed out to explain these results. The first one is that, as shown by Wang *et al.* [115] vdW interactions increase the H-bond strength, therefore the H-bond component of the cohesive energy dominates the overall energy. The second one is that the so called vdW bond [115] favors the facing of polarizable charge clouds. In water, the vdW bond is an O-O bond unmediated by Hydrogen atoms. In the 2D ice-Pd complex this vdW

	Energy (eV)		Geometries (Å)					
	H-down	H-up	H-down			H-up		
	E_{Ads/H_2O}	E_{Ads/H_2O}	$D_{O_1O_2}$	$D_{O_1Pd_1}$	$D_{O_2Pd_2}$	$D_{O_1O_2}$	$D_{O_1Pd_1}$	$D_{O_2Pd_2}$
PBE	0.47	0.40	2.8	2.6	3.1	2.8	2.7	3.3
WC	0.69	0.59	2.8	2.6	3.1	2.9	2.5	3.0
revPBE	0.25	0.21	2.9	2.6	3.1	2.9	2.9	3.5
DRSLL	0.42	0.42	2.9	2.7	3.2	2.9	2.9	3.5

Table 5.1: Adsorption energy per water molecule (E_{Ads/H_2O}) and geometries of a 2-dimensional (2D) layer of ice adsorbed onto a Pd$\langle 111 \rangle$ as shown in Figure: 5.1, calculated using three different GGAs (PBE [89], WC [119], revPBE [120]) and the vdW-DF DRSLL [21]. Two 2D structures can be studied, which differ on the orientation of one hydrogen atom in the molecule perpendicularly adsorbed to the surface, H-down and H-up (see Figure: 5.1). The adsorption energy is the sum of water-metal water-water (each water participates ion three pure H-bonds) interactions. D_{OO} is the average oxygen-oxygen distance. D_{O-Pd} is the O-Pd distance for the flat, up or down water molecules.

bond makes the H-up configuration (with the lone pairs of the H-up water molecule facing the metal) more favorable than with GGA functionals. It is interesting to note that the vdW-DF DRSLL does not change much the geometry of the water layers when compared to its GGA counterpart, revPBE. This is not unexpected [115], given that the H-bond geometry for these two functionals is very similar. However the compressibility of the water over-layers is expected to be very different, given that, as shown in the next section, the average H-bond strength is not the same for the two overlayers.

The O-O distances are all identical in the H-down structure, making the water pattern perfectly hexagonal, with O-O distance $D_{O-O} = 2.8$ Å, that respects the hexagonal Pd lattice parameter. However, the H-up configuration represents distorted water hexagons, with a short oxygen-oxygen distance, $D_{O-O} = 2.7$ Å and a long one ; $D_{O-O} = 2.9$ Å (not seen on table 5.1 since the average value is taken). Interestingly, this effect; called anticooperativity, is well known in pure water complexes. One H-bond is favored while the other one is weakened. In our case, this would mean that the H-up system behaves much more like pure water, with therefore a much weaker water-metal interaction.

Finally, the distance oxygen-palladium D_{OPd}, is shorter for the H-down structure for all the XC functionals. The interaction Water-metal is therefore stronger for the H-down monolayer.

5.3 How to quantify the strength of the H-bond?

5.3.1 Cohesive energy fails to provide decomposed energy contributions

As it has been said in the previous section, one has a conceptual problem when trying to separate the different contributions to the cohesive energy from the subsystems forming the ice-Pd complex. Indeed, the cohesive energy can be rewritten as :

$$E_{\text{Cohesive}} = 3E_{\text{H-bond}} + E_{\text{adsorption}}^{\text{monolayer}} \tag{5.3}$$

where $E_{\text{H-bond}}$ is the energy to form a H-bond between two water molecules ($\approx$ 0.25 eV in the water dimer) and $E_{\text{adsorption}}^{\text{monolayer}}$ represents the energy gained by approaching a hexagonal water layer from infinity to the metal (with PBE, 0.16 eV for H-down and 0.07 eV for H-up). Therefore, for PBE Eq. 5.3 would predict a cohesive energy per molecule 0.045 eV larger for the H-down monolayer. This is very different from what is shown in Table: 5.1. The question that cannot be solved by the analysis of the cohesive energy, is what is the strength of the interaction water-metal? Indeed, how to make sure that most of the energy does not come from an unusually strong water-water H-bond? Can it be possible to estimate the energy contributions coming from H-bond formation and the one coming from the water-metal interaction? The only way to answer this question is to isolate the H-bond contribution.

Let's consider a few definitions of the H-bonds energy involved in the system. The $\sqrt{3}\times\sqrt{3}R(30^\circ)$ unit cell has with its two water molecules, a total of three H-bonds. This H-bond energy, E_{H-bond} can be defined as :

$$E_{\mathrm{H-bond}} = \frac{1}{3}(E_{\mathrm{Cohesive}} - 2E_{\mathrm{Ads}}^{\mathrm{Monomer}}) \tag{5.4}$$

Where $E_{\mathrm{Ads}}^{\mathrm{Monomer}}$ is the adsorption energy of a water monomer as defined in the Eq 4.1. It appears that this definition will have the tendency to strengthen the water-metal interaction, since it considers twice the energy of a relaxed monomer in its optimal orientation.

To correct this overestimation, one could calculate two separate systems of monomers frozen at the Flat and Down (or Up) monolayer geometry. Then, the H-bond energy will be defined as :

$$E_{\mathrm{H-bond}} = \frac{1}{3}(E_{\mathrm{Cohesive}} - E_{\mathrm{Ads}}^{\mathrm{Flat}} - E_{\mathrm{Ads}}^{\mathrm{Down}}) \tag{5.5}$$

With $E_{\mathrm{Ads}}^{\mathrm{Flat}}$ and $E_{\mathrm{Ads}}^{\mathrm{Down}}$ the adsorption energy of a frozen Flat and Down molecule respectively. However, here again, the definition is not totally correct since neither the Flat nor Down molecules bind on the surface separately and therefore they do not exist as stable monomers on metal. They would have the effect (for the Down orientation) do give a negative adsorption energy coming from a repulsive interaction.

Finally one can define the H-bond energy as the difference between the total cohesive energy and the adsorption of an isolated, already formed, 2D water monolayer :

$$E_{\mathrm{H-bond}} = \frac{1}{3}(E_{\mathrm{Cohesive}} - E_{\mathrm{Ads}}^{\mathrm{Monolayer}}) \tag{5.6}$$

Where $E_{\mathrm{Ads}}^{\mathrm{Monolayer}}$ is the adsorption energy of a water monolayer coming from infinite to the Pd $\langle 111 \rangle$ surface. This definition, however forgets to take into account the interaction water-metal, and only the H-bonds of an isolated 2D water monolayer is considered (see Figure: 5.4).

The table 5.2 relates the H-bond energy of the system according to the three different definitions.

Table 5.2: H-bond energy according to different equations. None of the definitions are totally correct as they omit or overestimate system interactions.

	$E_{\mathrm{H-bond}}$
Eq 5.4	0.15 eV
Eq 5.5	0.32 eV
Eq 5.6	0.24 eV

The H-bond energy calculated with the Eq. 5.4 appears to be the smallest, with only 0.15 eV. Indeed the overestimation of the water-metal interaction in the overall interaction tends to weaken the remaining H-bond interaction. Oppositely, the H-bond energy calculated from the Eq 5.5 is the greatest with 0.32 eV. By forcing a non-physical monomer adsorption geometry, a spurious repulsive water-metal interaction is counted in the total calculation, giving more weight to the other part (the H-bond energy). Finally, the Eq. 5.6, while correct in appearance, neglects entirely the contribution of the water-metal interaction in the overall cohesive energy, and then makes the H-bond energy identical to the one contained in pure water (≈ 0.25 eV).

There is no definition based on energy decoupling, capable of giving the actual strength of the H-bond interaction. The problem of Eq.5.3 is that the binding energy of the ice monolayer, i.e. the energy of the 3 H-bonds, changes dramatically when the monolayer is adsorbed onto the metal substrate. This energy is of the same order of magnitude as the monolayer adsorption energy, and therefore the two contributions cannot be separated as done in Eq. 5.3. This effect can be compared to the

cooperative enhancement of the H-bond interaction in water. Instead, a study of charge density partition such as the Mulliken population analysis, can give a better understanding of the actual ice-metal interaction.

5.3.2 The Mulliken Population

Mulliken population analysis can be used as a tool to understand the different contributions of the cohesive energy. The overlap population indicates that the strength of the binding is different in the two structures.

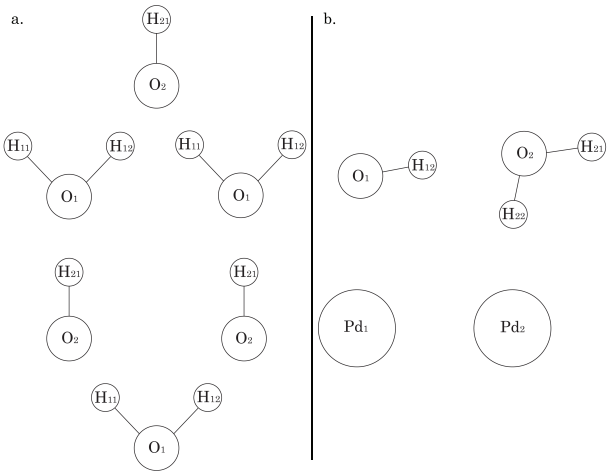

Figure 5.3: Sketch of 2D layer of ice on top Pd $\langle 111 \rangle$. The figure is for the H-down structure: top view (a) and side view (b). The H-up structure is similar to this one, but with atom H_{22} located above O_2.

In reference [30] it was shown that bond orders are a very natural choice to characterize the strength of the H-bond interaction. The bond order between two atoms, 1 and 2 is $Q_{1,2} = \sum_\mu \sum_\nu \rho^{\mu\nu} S_{\mu\nu}$, where $\mu(\nu)$ sums over the basis functions associated to atom 1 (2) and ρ and S are the density and overlap matrices, respectively. The absolute value of bond orders is basis set dependent, but relative changes of bond orders are meaningful quantities to characterize the electronic signature of H-bond [30].

	H_{12}/O_2	H_{11}/O_2	H_{21}/O_1	O_1/Pd_1	O_2/Pd_2	H_{22}/Pd_2
				PBE		
H-Down	0.028	0.028	0.026	0.028	-0.022	0.043
H-up	0.018	0.018	0.028	0.006	-0.007	-
2D ice vacuum	0.025	0.025	0.032	-	-	-
				DRSLL		
H-Down	0.020	0.020	0.020	0.013	-0.017	0.030
H-up	0.013	0.013	0.024	-0.006	-0.008	-
2D ice vacuum	0.015	0.014	0.028	-	-	-

Table 5.3: H-bonds Mulliken overlap populations (in units of electrons) between H–O atoms as labeled in Figure: 5.3. H-down: two-dimensional (2D) ice structure adsorbed on a $\langle 111 \rangle$ surface of a Pd slab with non H-bonding H atoms oriented toward the slab. H-up: same as H-down but with non H-bonding H atoms oriented away from the slab. 2D ice vacuum refers to an infinite 2 dimensional isolated layer of ice.

Table 5.3.2 shows the Mulliken bond orders, also known as bond overlap populations [79], calculated using PBE and the vdW-DF DRSLL. For each system, we consider the atoms participating in the water-water H-bond, as shown in Figure: 5.3. Atoms O_1, H_{11} and H_{12} belong to molecule 1 and atoms O_2, H_{21} and H_{22} to molecule 2. The three H-bonds are therefore : H_{11}–O_2, H_{12}–O_2 and H_{21}–O_1. H_{22} does not form any water H-bond, since it is either pointing away from the surface (up), or pointing towards the surface (down).

First we notice that the overlap populations H_{12}/O_2 and H_{11}/O_2 are identical in the two (up/down) structures.

The overlap oxygen-palladium is much more important for the H-down configuration than the H-up. Indeed, the charge overlap is about $\sim 70\%$ larger in the H-down system. This is already enough to conclude that the H-down system is much more bonded to the metal than H-up. This strength could not be seen from the cohesive energy analysis, where the difference in energy between the two systems was only about 15 %.

A very large overlap between the hydrogen from the down molecule and the palladium beneath it can be also noted.

The overlap between atoms participating in the H-bond is also significantly different. A homogeneous overlap (0.028e) is obtained for the two H-bonds in the H-down configuration, while for H-up, the overlap reveals two different H-bonds (0.018e and 0.028e). This weak/strong behavior is characteristic of liquid water (anticooperativity). This shows that the water-metal is weaker for the H-up overlayer. These results indicate that H-down overlayer has a large cohesive energy because of the binding to the metal, while the H-bonds in this structure are weaker than in the H-up structure.

As all water molecules make 4 H-bonds each (three to water and one to the metal), H-down forms a very stable and semi-hydrophobic layer that will not favor the growth of additional water on top. The 2D H-up ice

layer is very different. While the cohesive energy is not far from that of the H-down, it seems that the origin for this is due to the strengthening of the H-bonds of this layer with respect to H-bonds of the 2D layer in vacuum, due to substrate induced enhanced polarization, as proposed by Cabrera-Sanfelix *et al.* [12]. this is a highly hydrophilic structure that will favor the growth of additional water on top.

Conclusion

Infinite ice monolayers can be formed with an arrangement of either Flat/Down or Flat/Up waters on top of $\langle 111 \rangle$ transition metals. The similar values of metal lattice parameter and O-O distances, allow water to form hexagonal patterns by respecting the *2D ice rule*.

The configurational entropy of the unit cell $\sqrt{3} \times \sqrt{3}R(30^\circ)$ is composed by two configurations, each with two molecules $\{(\text{Flat,Down}); (\text{Flat,Up})\}$. The two configurations, called H-down and H-up appear to be energetically stable, and therefore any of them may be experimentally observed. Overall cohesive energy of H-down happens to be lower than H-up. However, their respective H-bond strengths may be different as the analysis of charge distribution with mulliken is showing.

A definition of the water-metal interaction strength, coming from energetics calculations only is not straightforward and further analysis must be performed. Bond order appears to be a powerful tool to characterize relative binding strengths. Others,such as projected density of states or molecular vibrations may also appear relevant to complete the overall picture of this complex interaction.

In this chapter, the ice monolayer H-down system sees all its H-bonds already formed. No further bonds can be made to any water, which makes the layer hydrophobic to the growth of additional water molecules. The

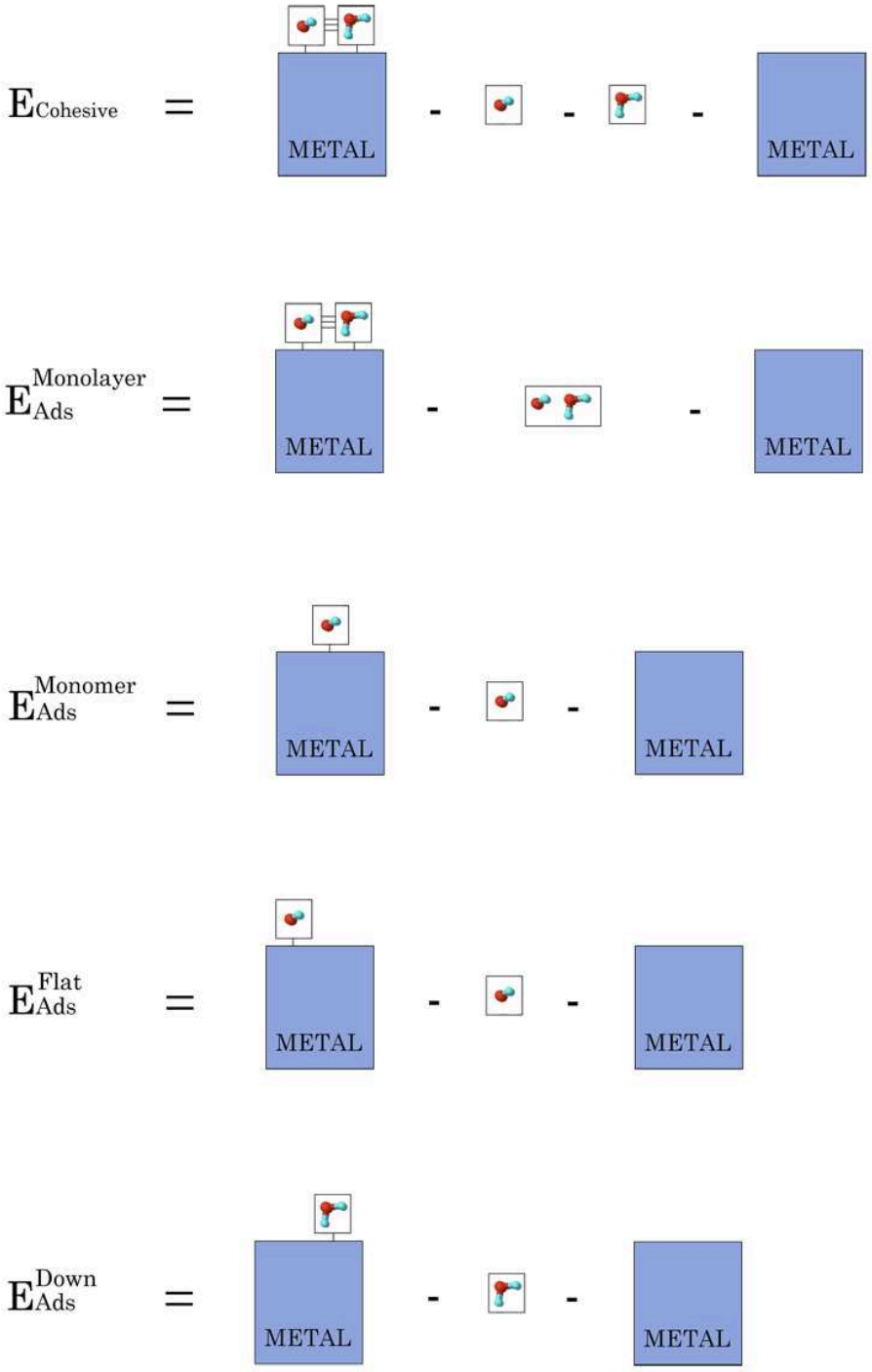

Figure 5.4: Schemas of the different Adsorption Energy calculations.

H-up system, however, is still capable of donating one H-bond to an additional water molecule through its H-up molecule. That would make this

layer hydophilic. In order, to confirm or undermine this idea, *ab-initio* molecular dynamics simulations of water confined between metallic plates are performed. Results are discussed in the next chapter.

Chapter 6

Liquid Water confined between metallic plates

Introduction

The last chapters have characterized the interaction of a single water monomer on top of a metallic surface, as well as a monolayer of ice on a metal. To go further and to converge to an even more realistic picture of the water-metal interaction, one need to include more water on top of the water monolayer. Confined liquid water represents a great interest for physicists and chemists interested in state-of-the-art technologies such as, fuel cells, where concentration of hydrogen atoms have to be controlled, nano-sensors, heterogeneous catalysis, or nano-fluids. A molecular dynamics of liquid water confined between hydrophobic walls [35] has shown dramatic dependence between water structure and density. Below a critical water density, the structure is a bilayer and above a density of 0.95 g/cm^3 a trilayer is formed between walls separated by a distance of 8 Å. It has also been shown in that study that interfacial water has a crystal-like character and does not diffuse while central water is liquid-like and is able to diffuse easily.

Relevant dependence of the classical model used for water has been

highlighted by different studies [36, 69]. The use of a rigid SPC [7] model in Ref [69] tends to make a confined water between 9×9 CNTs less mobile, while the flexible SPC model used in Ref [36] claims a higher mobility for similar systems.

The need of first principles calculations becomes crucial to draw more solid conclusions. With the more powerful computationally available resources, dynamical properties of confined water have been investigated by means of first principles calculations [18, 45, 98]. Properties of liquid water confined between plates [98] or inside carbon nanotubes (CNT) are of first importance for applications in nanofluidics and biosensors [18, 45]. It has been shown that the nature of confinement is strongly dependent on the type of surface, in particular, noticeable features in the far IR spectra are proving the water molecules sensitivity to the surface electronic charge fluctuations [98, 108].

In this chapter, a detailed first-principle investigation of liquid water, confined between periodical palladium slabs is given. Dynamical structure of water will be analyzed and competition between ice and liquid water will be discussed. Insights of electrochemistry will also be an important part of the discussion here, as water seems to polarize the metal slab by a mechanism of charge transfer.

6.1 Description of the system

Calculations of confined water between $\langle 111 \rangle$ palladium slabs are performed by means of first-principle molecular dynamics simulations. A $4-$layer slab is constructed with a surface of 9.71×16.83 Å^2. A box of liquid water is cut from an equilibrated classical molecular dynamics simulation and inserted on top of the slab.

Liquid water in *ab-initio* molecular dynamics simulations reproduce ex-

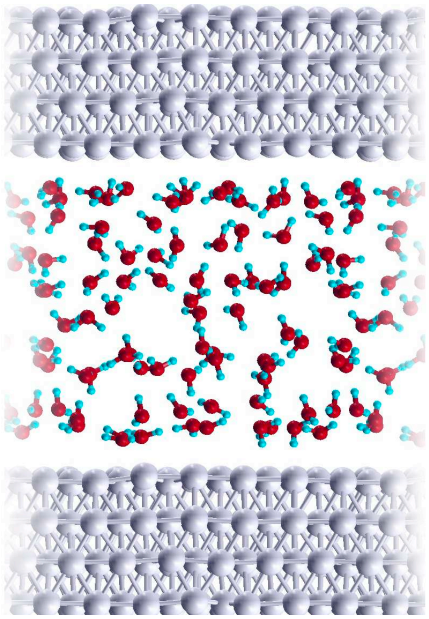

Figure 6.1: Snapshot of confined water between ⟨111⟩ 4-layer Pd slabs.

periment with a better agreement by simulating a slightly lower density lower than the actual one under normal pressure and temperature conditions. In the present simulations, periodic boundary conditions ensure that water is confined at a density of $0.97 g/cm^3$. A snapshot of simulations is presented on figure 6.1.

6.1.1 Initial conditions

The two water layers (top and bottom) in direct contact with metal are referred to *interfacial water*. They play a key role on the overall water chemistry. In order to avoid an eventual potential energy surface local minimum which would artificially constrain water to a particular structure, a set of two distinct simulations have been performed with different initial conditions. The first simulation, called RUN A, is built from the assembling of two monolayers of ice on each metallic surface, with another 48 liquid bulk water molecules. 16 water molecules cover each metallic surface in a

perfect hexagonal arrangement, and the inside liquid bulk water has been first equilibrated with a 20ps classical molecular dynamics [5,60]. A total of $16 + 16 + 48 = 80$ water molecules are then confined between the Pd slabs, with a water density of 0.97 g/cm^3. The second simulation, that is referred as RUNB, contains the same total number of molecules, but no particular arrangement at metallic surfaces has been performed. 80 molecules of liquid bulk water are inserted between two metallic slabs. from an equilibrated classical molecular dynamics at $0.97 g/cm^3$. The sketch of figure 6.2 shows the two different initial conditions used for RUN A and RUN B.

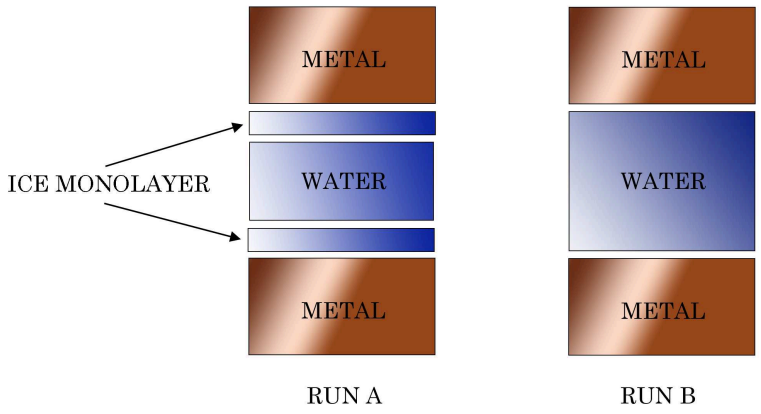

Figure 6.2: This cartoon represents the initial configurations that were used to start the molecular dynamics simulations. RUN A has been initialized with two monolayers of water (2×16 molecules) in interaction with metal slabs, the empty space has been filled with 48 water molecules (from an equilibrated classical molecular dynamics simulation [5, 60]). RUN B has been initialized with 80 water molecules from an equilibrated classical molecular dynamics simulation. No interaction with metal slabs has been favored.

6.1.2 *ab initio* molecular dynamics

Molecular dynamics simulations have been prepared with the following procedure : Water molecules have been first equilibrated during 20 ps by means of a classical molecular dynamics, with the code GROMACS [5, 60]. Then, an *ab initio* molecular dynamics equilibration has been performed with a Nose-Hoover thermostat [44, 82] to set a temperature at 300K for 10 ps. Finally, a Verlet algorithm [112] has been performed for the two simulations for more than 10 ps ; this final dynamics is the set of data that is going to be analyzed in this chapter.

No k-points were sampled ; this approximation is reasonable due to the large size of the cell in X and Y. A long range optimized basis has been utilized to described water and a double-ζ-polarized basis is describing the Palladium atoms. Exchange and correlations energies have been computed with the PBE [89] functional.

6.2 Structure Analysis

6.2.1 Radial Distribution Functions

Radial distribution functions (RDF), also called pair correlation functions give the probability of finding a particle at a particular distance r from another particle. They reveal the structure and arrangement in liquids. For water, pair correlation O-O, O-H and H-H are computed. Experimentally RDFs can be obtained from X-ray scattering [55, 104].

RDF of the oxygen-oxygen distribution is computed and compared on Figure 6.3. The top graph shows a comparison between confined water from RUN A and a simulation of pure liquid water at a density of 0.95 g/cm^3 with the same exchange and correlation potential obtained by J. Wang and al. [115]. From this graph two features can be emphasized :

1. The first peak of the two simulations is located at the same distance. It corresponds to the location of first oxygen neighbors and is very sensitive to the water density. The agreement between the two peaks is ensuring that the density of the confined simulations has been properly set up.
2. The second coordination shell is better structured for confined water, while slightly further away from the first shell than the pure liquid water at the same density. There is also a much more marked separation between the first and second coordination shells in the case of confined water.

Confinement appears to induce an over-structuration of the liquid under the same density and pressure with respect to pure liquid. This second point is particularly interesting in that it resembles structural properties of hexagonal ice [53, 117]. Indeed in ice, the separation between first and second coordination shells is bigger, because of the elongation of the H-bond network and the arrangement of shells is also evidently sharper and structured due to the crystalline behavior of ice. The similarity between confined water and ice could come from the interfacial waters which tend to stay structured as a 2D monolayer of ice, as shown in the previous chapter. The bottom graph of Fig 6.3 shows the oxygen-oxygen radial distribution functions for both of the simulations RUN A and B. The two RDFs almost perfectly match together. The different initial conditions do not appear to affect the water structures.

Fig 6.4 represents the radial distribution functions of the oxygen-hydrogen pair. The top graph compares pure liquid water from the Ref [115] with confined water of RUN A. The first peak corresponds to the intramolecular OH bond. This strong bond is clearly not affected by the confinement of water. Properties of confined water molecules should be the same as the ones in pure liquid water. Second peak corresponds to distance of H-bond ; the intermolecular bond. This average bond however, suffers a slight elongation in the case of confined water with respect to pure liquid water.

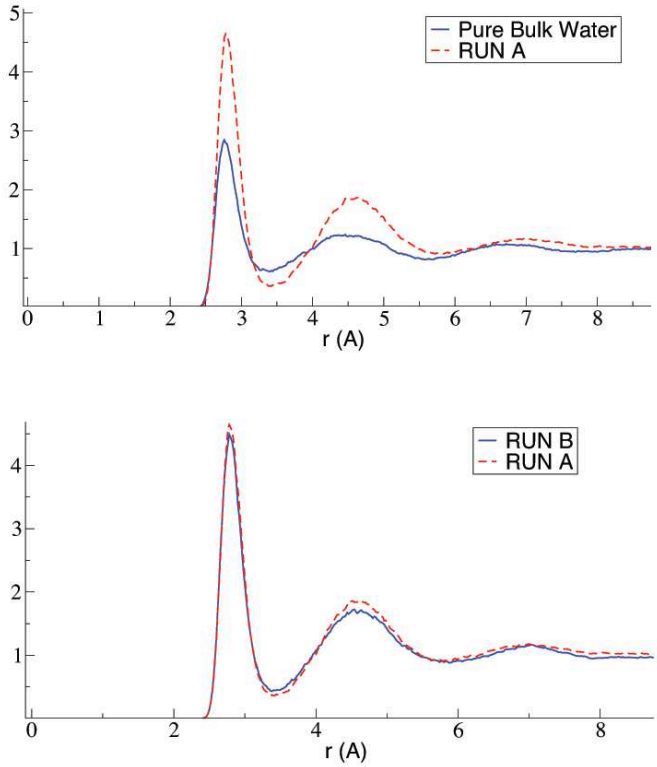

Figure 6.3: Comparison of OO radial distribution functions between pure liquid water from Ref [115] and confined water RUN A (Top graph). Comparison of OO radial distribution functions of confined water from RUN A and B (Bottom graph).

That confirms that confined water tends to an ice-like structure as it was already pointed out from Fig 6.3. Again, from the bottom graph, no significant differences can be observed and the two simulations seem to obey the same dynamics.

6.2.2 Z-density

We will refer as Z-density, the probability of finding an oxygen or hydrogen atom at a given z distance ; Z being the axis perpendicular to the metallic

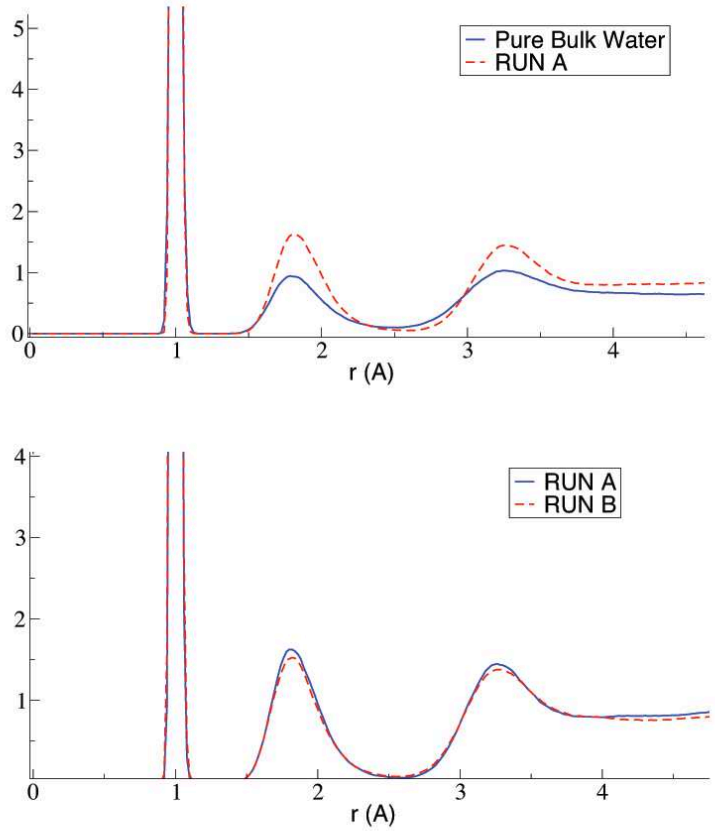

Figure 6.4: Comparison of OH radial distribution functions between pure liquid water from Ref [115] and confined water RUN A (Top graph). Comparison of OH radial distribution functions of confined water from RUN A and B (Bottom graph).

slabs. Figures 6.5 and 6.6 represent the Z-densities for RUN A and B respectively. Metallic surfaces are shown with straight black lines at 0 and 20 Å. Probabilities have been computed by averaging the distance of water atoms from metal for all water molecules over the whole simulation time. On each simulation, there are two water-metal interfaces. There will be referred as Left and Right interfaces, Left being the interface formed

between the metal and water at 0 Å. Right represents the water-metal interface at around 20 Å. On both figures, oxygen atoms are seen in solid blue curves while hydrogens are shown with dashed red curves.

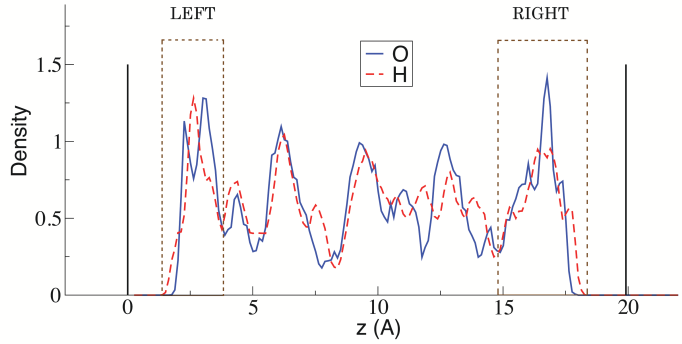

Figure 6.5: Atomic densities of oxygen (solid blue curve) and hydrogen (dashed red) computed along the distance (in Å) separating the metallic slabs for RUN A. Slabs surfaces are shown in solid black lines.

On Fig 6.5, Left interfacial oxygen atoms form a double peak at about 2.5 Å and 3.08 Å from the surface. This formation is similar to the 2D ice structure [16,91], where a monolayer of water covers a metallic surface with a hexagonal arrangement of flat and up(down) water molecules. In a standard monolayer of ice on top of a $\langle 111 \rangle$ metallic surface, flat water molecules tend to closer to the surface than the up(down) by around 0.5 Å. The double peak on the Left interface of Fig 6.5 could represent an arrangement of flat (first peak) and up(down) (second peak) water molecules. ice-like ordering of liquid water under confinement has already been revealed [35] where a trilayer fluid was acting, under confinement at 300 K, as ice. Here, however, the larger number of water layers (around five), restricts the possibility of a global crystal ordering at 300 K. Nevertheless, the structure of interfacial Left layer, clearly resembles that of 2D ice. The probability to find hydrogen atoms is shown with the dashed red curve. The maximum of

probability to find hydrogens at the Left interface is right between the two oxygen peaks. This peak corresponds to the H-bonding that occurs within the interfacial layer.

The Right interface however, presents a broad peak located at 16.8 Å (3.2 Å from the surface), surrounded by two smaller peaks at 16.0 Å and 17.4 Å (respectively 4 Å and 2.6 Å from the metallic surface). In average, water molecules from the Right interface are further away from the metal than molecules of Left interface. Down water molecules (*ie* molecules that have at least one H pointing towards the surface), at both interfaces, can be seen as the tail of H Z-density that is closer to the surface than O. The number of down molecules appears to be greater at the Right interface.

Inside these Left and Right interfacial water layers, a bulk water region can be delimited from 3.08 Å to 16.0 Å. Water in this region is still strongly layered with a total of 6 oxygens peaks. This is the signature of a nano-confined system [18, 98].

Fig 6.6 corresponds to the Z-density of RUN B. Here also, the Left interface shows a clear double-layer structure with maximum of probability to find oxygen atoms at 2.3 Å and 3.1 Å from the surface. The Right interface seems to favor water molecules further away from the metallic surface, with an important peak located at 3.2 Å from the metallic surface. Nevertheless, a smaller peak can be observed at 2.5 Å from the surface. Right interface appears to have many more down water molecules than Left interface as revealed by the height of the H Z-density tail.

Both of the simulations are asymmetric. The Left interface with its clear 2 peaks, reveals a well-ordered structure, reminiscent of 2D ice. The Right interface, however, looks more unstructured, with a broader peak.

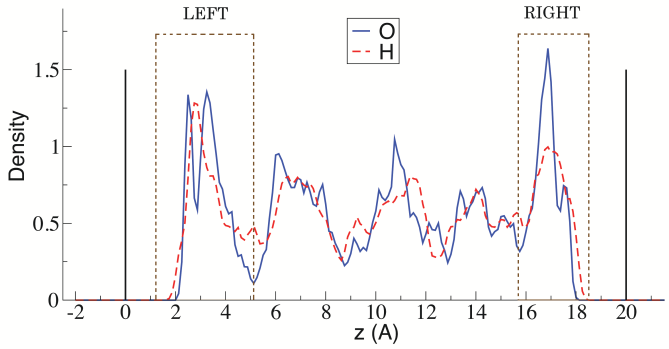

Figure 6.6: Atomic densities of oxygen (solid blue curve) and hydrogen (dashed red) computed along the distance (in Å) separating the metallic slabs for RUN B. Slabs surfaces are shown in solid black lines.

6.2.3 Water structure at the interface

Deeper analysis of the Left/Right structures can be performed by looking at the probability to find an atom at a particular position on the XY plane, near the surface, along the simulation. Probabilities have been calculated by counting the number of occurrences an atom appears at a specific (x, y) point on the surface plane for each water molecule inside the LEFT (RIGHT) window (see Figures 6.5, 6.6), for the whole simulation time. Those calculations are coined "XY surface probabilities".

Figure 6.7 represents the XY surface probabilities of RUN A. Left panel is showing a strong water ordering. Oxygen atoms (yellow) are organized in hexagons and heptagons, hydrogen atoms (blue) ensures the satisfaction of the 2D ice rule by being located in between oxygens, making a H-bond. The structure differs, however, from the perfect ice monolayer on top of a Pd $\langle 111 \rangle$ studied in the previous chapter. Indeed, oxygen atoms do not bind right on top of a Pd atom. Instead, some of them bind at hollow sites, located between two Pd atoms. This may come from two facts :

First, the presence of temperature increases the configurational entropy

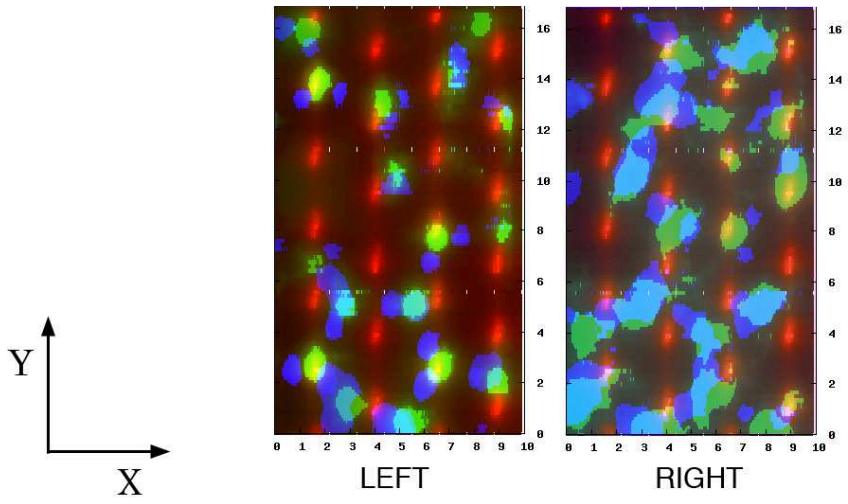

Figure 6.7: LEFT : Probability to find oxygen (yellow) or hydrogen (blue) in the region of Left interfacial water, for RUN A. Pd atoms are shown in red. RIGHT : Probability to find oxygen (green) or hydrogen (blue) in the region of Right interfacial water, for RUN A. Distances in X, Y are in Angstroms.

of the system. Second, the presence of liquid bulk water on top of the monolayer also interacts with interfacial water and a competition between optimized water-metal interaction and liquid water interaction, balances the ordering of interfacial water.

Waters at the Right interface, do not appear to be as strongly structured. Oxygen atoms (green) and hydrogens (blue) are forming more extended clouds. Those atoms are moving much more around an equilibrium position than at the Left interface. Nevertheless, a hexagonal ice-like structure, centered around the coordinate $(3, 3)$, is visible. Finally, the Left side counts 7 flat molecules (with 4 on top of Pd), while the Right side only has 3 flats molecules (only 1 on top of Pd). Flat water has been shown, in the two previous chapters, to be the one making the real strong interaction with metal, through the hybridization of the out-of-plane $1b_1$ molecular orbital.

Figure 6.8 shows the XY surface probability of RUN B. Again, the Left side is clearly ordered. Oxygen atoms (yellow) form hexagonal and pentagonal patterns. Hydrogens ensure the 2D ice rule construction. 5 flat molecules (with 4 right on top of Pd) can be identified. Probability clouds of finding atoms are well localized.Water molecules at this interface are very stable ; once they bind to the surface, they stay for the entire simulation. On the Right interface, however, oxygens (red) and hydrogens (blue) appear much more delocalized and faint (as for RUN A). Water molecules at this side are unstructured and no crystal-like pattern can be found from the figure.

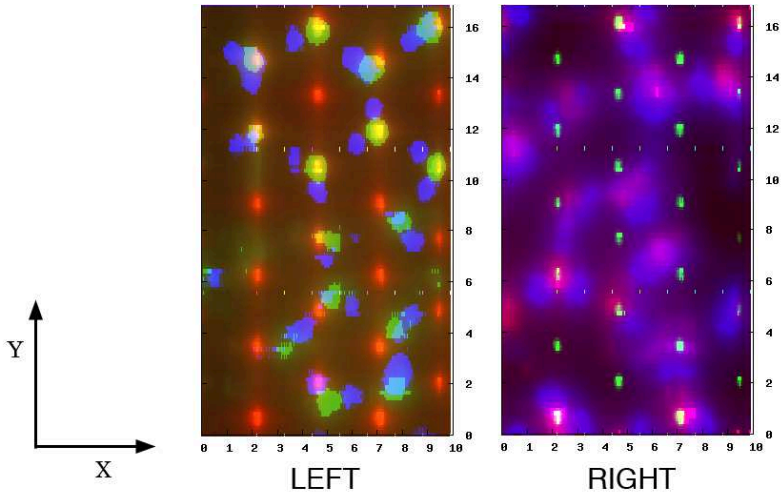

Figure 6.8: LEFT : Probability to find oxygen (yellow) or hydrogen (blue) in the region of Left interfacial water, for RUN B. Pd atoms are shown in red. RIGHT : Probability to find oxygen (red) or hydrogen (blue) in the region of Left interfacial water, for RUN B. Pd atoms are shown in bright green. Distances in X, Y are in Angstroms.

On the two simulations, a Left/Right asymmetry is seen. The Left side seems to favor an ice-like structure while the Right side appears to be more liquid. RUN A has been performed from an initial condition that was

forcing pure ice monolayers at each surface. The spontaneous symmetry breaking along this simulation, shows that the asymmetry is much more energetically favorable than having two ice-like structures at each metal interface.

It has been shown that the metal screening creates an anti-charge near the surface. Depending upon the orientation of the water molecule towards the surface, metal may screen a negative or a positive charge. Therefore, a majority of water molecules with different orientations on Left and Right surface side, would tend to favor a spontaneous polarization of the slab. A simplistic picture of this idea is sketched on Fig :6.9.

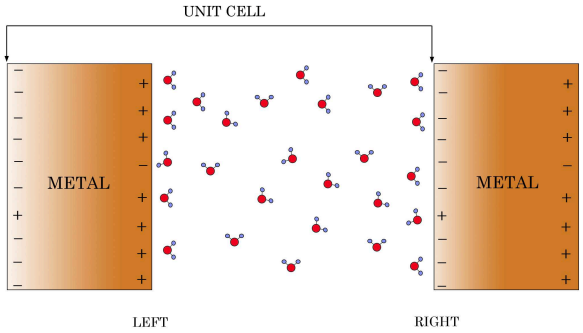

Figure 6.9: Cartoon representing the possible polarization of metal that occurs because of a asymmetric Left/Right surface screening of water molecules. When oxygen is oriented towards the surface, metal screens a negative by creating a positive charge. When hydrogen points towards the metal, opposite behavior happens and metal creates a negative charge at its surface. A Left/Right asymmetry could locally charge the metal surfaces.

Electronic analysis is performed for the two simulations by calculating all electronic properties of RUN A and B, for a sample of 200 snapshots,

equally spaced, along each simulation.

6.3 Electrochemical insights

Electronic projected density over water states have been computed to explore the metal-water interaction in three different regions.

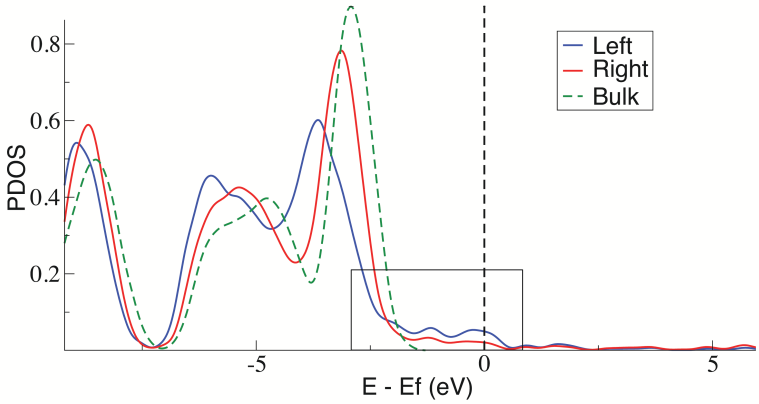

Figure 6.10: PDOS of three region of water confined between Pd ⟨111⟩ slab. Interaction with Left side of the slab is represented by a solid blue curve, Right side of the slab interaction is the solid red curve, and liquid bulk water region is the dashed green curve. Fermi energy has been shifted to 0 eV and is represented by a dashed black straight line. PDOS have been averaged from 200 snapshots among the RUN A, over the whole simulation.

Figure: 6.10 shows the water PDOS, averaged from 200 snapshots along RUN A, over the entire simulation. Three different regions have been delimited, denoted as Left (Right), which stands for the water molecules interacting with metal on the left (right) metal surface and Bulk, that refers to water molecules in the interior bulk liquid region. Fermi energy has been shifted to 0 eV and is represented with a straight dashed black

line. Close to the Fermi energy (inside the window on Figure 6.10), are the hybridizations of water with metal.

There is evidently no hybridization for bulk water, since it is not in contact with any metal surface. Left side water appears to have a greater hybridization than the Right one. This confirms the fact that Left water has a stronger interaction with metal than Right side water. Around -2.5 eV with respect to 0 eV Fermi energy, are the peaks corresponding to the highest occupied $1b_1$ molecular orbitals of water. This peak is much narrowed for the bulk water which keeps of molecular behavior, while Left and Right interacting water show a peak that is spreading out. One of the reason of the spreading is the hybridization around the Fermi energy. It is also noticeable that the $1b_1$ orbital-like for Left water, clearly seems to be the deepest in energy. As it has already been pointed out, it is really favorable for the $1b_1$ to delocalized its electrons. The metal is a very good electrons acceptor and does not pay the penalty (Pauli exclusion) that the water donor would pay. A strong hybridization with metal, tends to stabilize the energetics of interfacial water molecules by transferring charge to the metal. A small charge transfer is also occurring at the Right interface but few electrons are injected to the metal.

6.3.1 Mulliken Population Analysis

Palladium slab counts 4 layers. Each layer has 24 atoms. Mulliken population on Pd atoms have been computed for 200 snapshots and averaged as a function of the layer.

Table above presents the average Mulliken population difference between $Pd + water$ with Pd alone, as a function of the layer, along the simulation time. Calculation is expressed in equation 6.1 :

	$\overline{\Delta Q(z_{layer})}$ (e)	
	RUN A	RUN B
LEFT	0.000	0.000
INT 1	0.011	0.013
INT 2	0.020	0.021
RIGHT	0.023	0.024

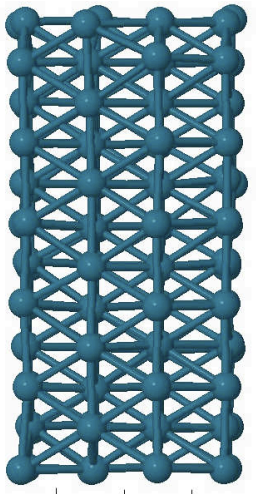

Figure 6.11: Average Mulliken population difference between $Pd + water$ with Pd alone, as a function of the layer, for the simulation time (Eq 6.1). Left and Right layers refer to the Left and Right surface interaction **with water** ; this is why they appear in reversed order on the figure. INT 1 and 2 layers refer to the two Pd interior layers.

$$\begin{aligned}\overline{\Delta Q(z_{layer})} &= \frac{1}{Ntime}\sum_{i}^{Ntime}\int dxdy\Delta q_i(x,y,z_{layer}) \\ &= \frac{1}{Ntime}\sum_{i}^{Ntime}\int dxdy[q_i^{Pd+water}(x,y,z_{layer}) - q_i^{Pd}(x,y,z_{layer})]\end{aligned} \tag{6.1}$$

This average can be seen as the metal polarization along the z direction. For both simulations, the LEFT layer slab does not contain any extra charge. Then, negative charge starts accumulating in the two interior layers and finally the RIGHT layer presents an important negative charge accumulation. Therefore, LEFT side, with the stronger water interaction does not appear charged. Negatively charged oxygen, bind to the LEFT surface, mostly through the $1b_1$ molecular orbital. Metal receives some

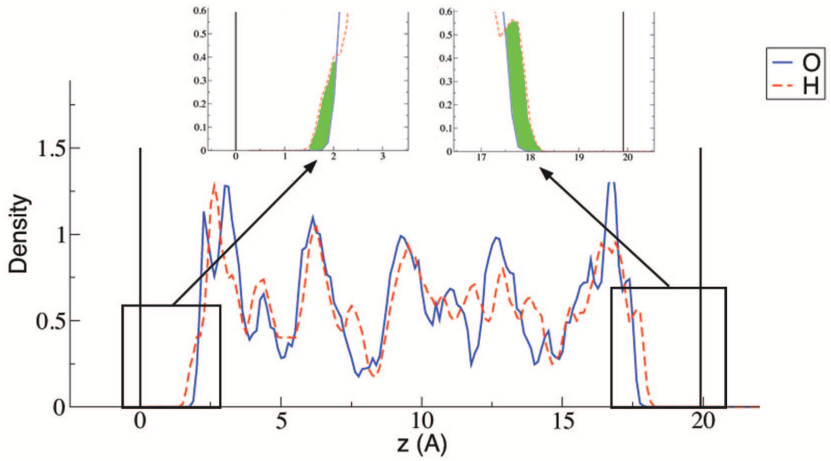

Figure 6.12: Atomic Z-density of RUN A. More hydrogens pointing down (green region) are found on the RIGHT side.

charge transfer from those water molecules but also has to screen the water molecule by creating a positive charge. Excess of charge that metal receives is driven away from the region of water-metal interaction. In the mean time, on the other side, water "sees" a negatively charged metal surface. It is not much favorable any more to bind and the surface becomes hydrophobic.

Figure 6.12 shows the Z-density of atoms for the RUN A. Hydrogens from water molecules pointing down towards the surface are found to be more prolific on the RIGHT side than on the LEFT one. This is explained by the fact that the RIGHT side is negatively charged, and therefore enhance a positive hydrogen attraction.

6.3.2 Molecular dipole moment

The dipole moment of water molecules has been computed with a method which takes into account the rearrangement of electronic density around molecules (see Appendix A). Therefore, charge transfer that occurs at the

metal interface and elongation of the density are taken into account.
Table 6.3.2 presents the dipole moment of a water molecule in a Flat or Down orientation towards the metallic surface. As compared to the 2.05 D of pure liquid water, the dipole moment of a flat molecule increases. Despite the charge transfer (evaluated to be 10% of an electron per molecule) that would reduce the dipole, the elongation of the electronic density near the oxygen is responsible for the increasing of the dipole. The Down orientation, however, sees its dipole moment decreasing by about 12%. In this case, hydrogen atoms get more electronically charged by making a bond to metal; this reduces the net dipole moment of the molecule.
Again, water-metal interaction is found to be similar to a pseudo hydrogen-bond interaction. In a pure water H-bond, the donor molecule reduces its electronic dipole moment (hydrogen atom gets negative charge from lone pair of the acceptor), while the accepting molecule sees its dipole increasing (elongation of its lone pair extends the distance between the electronic center of charge and nuclei center of charge).

	Dipole Moment
Flat	2.34 D
Down	1.81 D
Isolated gas	2.05 D

Table 6.1: The dipole moment has been calculated for water on top of $\langle 111 \rangle$ Pd surface with a Flat or Down orientation. Isolated gas water is also shown here.

In order to point the effect of the interaction metal-water, it is relevant to compare the change in dipole that is involved by the presence of the metal. To do so, two sets of 200 calculations have been performed. In the first one, the dipole moment of every water molecules is calculated from 200 snapshots of the RUN A. In a second, the metal is removed, and the same

water dipole moments are calculated. The difference in dipoles between the two systems is called $\Delta\mu$. It is calculated for each water molecule as:

$$\Delta\overrightarrow{\mu} = \overrightarrow{\mu}^{Pd/water} - \overrightarrow{\mu}^{water} \tag{6.2}$$

Figure: 6.13 shows the z component of $\Delta\mu$ for 200 events along the simulation. Metal surfaces are represented by red dashed lines. Dipoles (black dots) are located at the oxygen atom position for each snapshot.

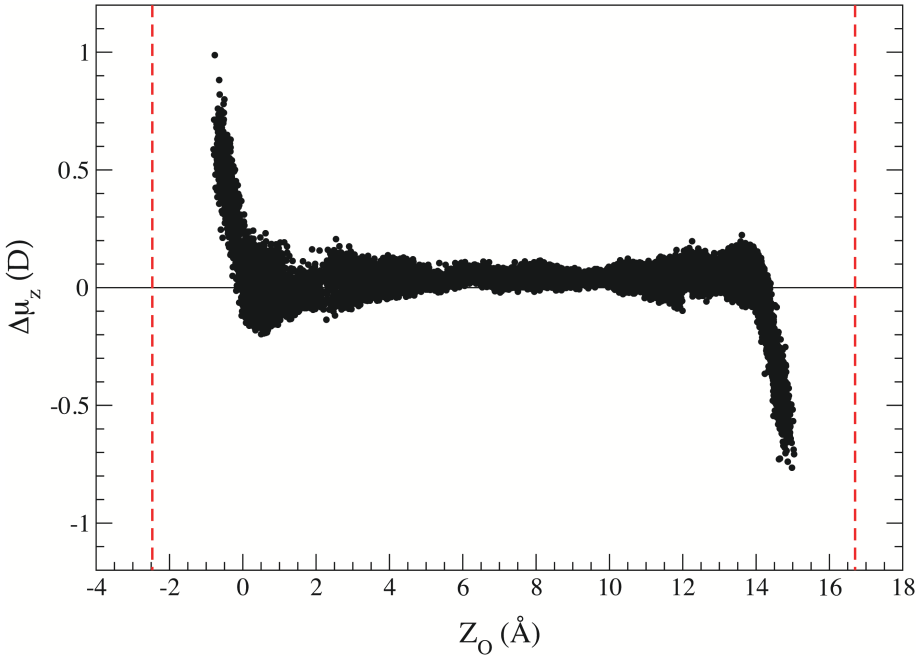

Figure 6.13: Change of dipole in z calculated form Eq. 6.2 for each water molecule for 200 snapshots along the whole 10 ps RUN A.

The change in z of dipoles in the bulk liquid region is very close to zero. This is not surprising since the interaction of bulk molecules with the metal slab is almost absent. However, a strong change can be seen close to the Left and Right interfaces. It is important to note that no change can be induced by geometry since they remain exactly the same for the calculations of the two systems. In that sense, any dipole variation is purely electronic, and the charge rearrangement involved by the metal

interaction is the main contribution to this variation. Again, it is noticeable that the Left side presents a greater variation (up to 1D) than the Right one (only 0.7D).

Figure: 6.14 represents the magnitude of dipole variation of equation 6.2. Again, no variation is clearly noticeable in the bulk liquid region, while important change is seen at the two metallic interfaces.

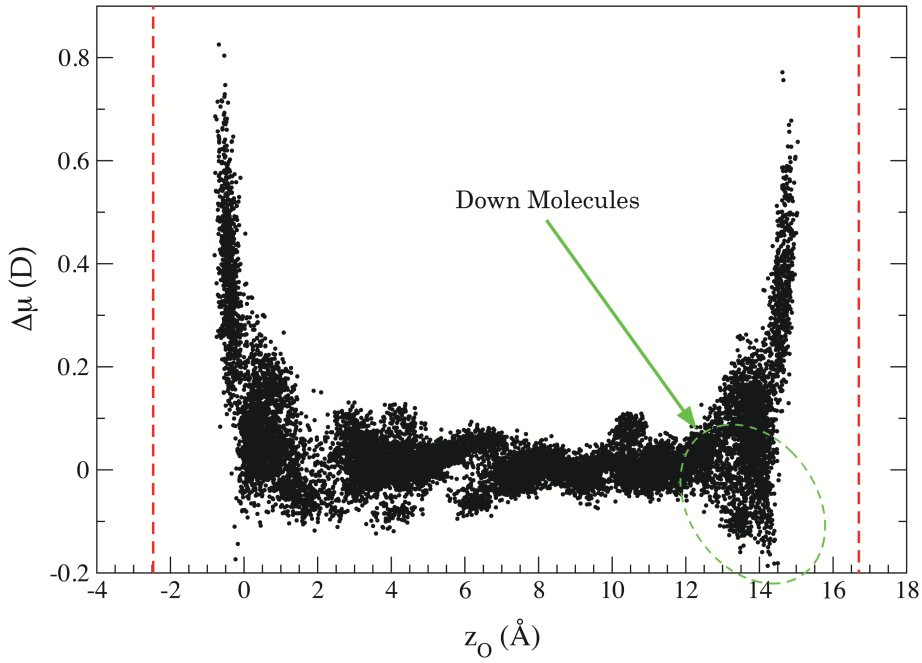

Figure 6.14: Change of dipole (magnitude) calculated form Eq. 6.2 for each water molecule for 200 snapshots along the whole 10 ps RUN A.

This Figure shows that the molecular dipole moments on the Left side are increasing. This is characteristic of the important presence of Flat molecules (as seen in Table: 6.3.2) . Right side, also shows the presence of Flat molecules, with an increasing of dipole moments. However, an important number of molecules, with a reduction of their dipole moment (pointed with the green ellipse), are representative from a binding of Down molecules. This binding has been favored by the negative charge present at this side of the slab (see Table: 6.3.1).

6.3.3 The nature of the asymmetry

The actual cause of the structural asymmetry is not yet clear. The relatively small size of the slab (4 layers of 24 atoms each) could restricts the metal to give optimal screening properties. This poor metal screening would give rise to local charge arrangements at the metal surfaces and therefore would affect the water binding energy and ordering at those surfaces.

On the other hand, the asymmetry could perfectly be an intrinsic property of the water-metal interaction. In this case, effects would remain unaffected by the size of the metal or the amount of water.

Opened boundaries calculations have been performed for several snapshots. By introducing a large vacuum either right after the metal or after water, the two systems "ordered water-metal" and "disordered water-metal" have been constructed. Total surface binding energies have then been calculated with BSSE corrections [118] and averaged binding energies values show that the ordered interface is more strongly bound to metal than disordered one, by 0.46 eV (about 16 water molecules appear to take part in the water-metal interface for each side).

This work has demanded a tremendous computational cost both in time and memory and calculations have reached todays limitations of *first-principle* molecular dynamics simulations. Nevertheless, the role of the metal slab in the asymmetry has to be established and further calculations need to be performed by varying the number of metallic layers.

Despite the fact that the cause of the asymmetry appears unclear, consequences do seem to be physical and effects may not be artifacts. This study has revealed that a specific bias could control the binding of water on metals. Hence, a positive bias would favor a strong water binding, and make the metallic surface hydrophilic. A negative bias, however, would restrict

water to bind to the metal, making the metallic surface hydrophobic.

Conclusion

While very different at the beginning, with two distinct initial conditions, the two *ab-initio* molecular dynamics simulations are showing a very similar behavior. A Left/Right asymmetry appears spontaneously in the two systems, and persists along the 10ps equilibrated simulations.

This structural asymmetry is clearly observable with a Left, well structured monolayer and a Right, more amorphous liquid-like structure. Left side layer presents a great majority of ordered patterns that reminds those of ice monolayer, with hexagons and pentagons structures. Molecules chemisorbed at the Left interface appear very stable and almost no in-plane diffusion is observed. On the Right side interacting layer, however, in-plane diffusion is more present (as seen in Figures: 6.7 and 6.8), and no explicit ice pattern are observable.

The physical cause of the asymmetry is still unclear; indeed it has not yet been concluded whether this comes from a poor description of the metal screening or whether this is an intrinsic property of the water-metal interaction. Nevertheless, consequences of this asymmetry are well established and properties do not constitute spurious physical effects. It has been shown that a change of bias would modify the nature of binding of water on metals. A positive bias would allow a strong water binding, making the metallic surface hydrophilic, while a negative bias would restrict water to deposit on the metal, making the surface hydrophobic.

Calculations with a number of layers more important and opened boundary conditions should dispel doubts about the role of the metal description in the structural asymmetry.

Chapter 7

Liquid water confined between GaN (10$\underline{1}$0) surfaces

A great challenge in new sustainable energies is the production of hydrogen. Fuel cells are a few steps away from being a first-rank source of energy. CO_2 free, sustainable, and efficient, they constitute an important hope for replacing the environmentally unfriendly fossil fuel energies such as coal, petroleum or gas.

Introduction

Energy produced by the reunion of hydrogen and oxygen gas has been experienced for a long time (Cavendish 18th century). The reaction produces water and is accompanied with a strong heat release. Fuel cells have also been proved to be a very promising method for providing electricity. The process is the formation of water molecules from its sub-elements oxygen and hydrogens. A fuel cell contains three main elements : the anode, cathode and a membrane, used to make the proton exchange.

A polymer exchange membrane fuel cell works as the following : Hydrogen gas (H_2) is stored in the anode side, while Oxygen gas (O_2) is stored

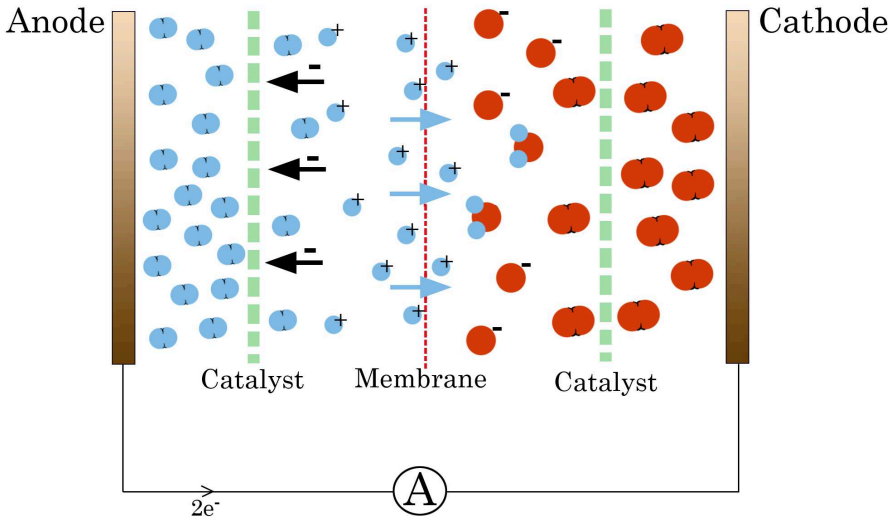

Figure 7.1: Cartoon of a proton exchange membrane fuel cell. H_2 gas is stored in the anode side, while O_2 is stored in the cathode. The reaction between H_2 and a catalyst, produces $2H^+$. From this reaction $2e^-$ are released and captured by the anode. On the cathode side, O_2 gas reacts with a catalyst and produces $2O$. A membrane in between only allows the transfer of protons H^+ towards the cathode side. Reaction between H^+ and O produces H_2O. In the mean time, electrons travel from the anode to the cathode producing an electrical current.

in the cathode of the cell. On the anode side, H_2 gas is forced through a catalyst (Pt) by pressure. Once in contact with the catalyst, H_2 starts the reaction :

$$2H_2 \longrightarrow 4H^+ + 4e^- \tag{7.1}$$

The $4e^-$ are released into the anode and start their way towards the cathode. H^+ are able to go to the cathode side through the proton exchange membrane that only accepts positively charged ion and blocks electrons. During that time, on the cathode side, O_2 gas is forced through

the catalyst by pressure and separates into 2 oxygen atoms. The strongly electronegative O atoms attracts the positive H^+ in the reaction :

$$O_2 + 4H^+ + 4e^- \longrightarrow 2H_2O \tag{7.2}$$

The $4e^-$ that came across an external circuit participate in the reaction 7.2. The overall reaction of the fuel cell is :

$$2H_2 + 2O_2 \longrightarrow 2H_2O \tag{7.3}$$

And only water has been created during the process. The migration of electrons from the anode to the cathode can be used to generate electricity. While the principle of fuel cells has been well established, the major problem remains the production of molecular hydrogen. Indeed the gas, very reactive, does not exist on the planet on its own. Therefore it needs to be produced and stored.

To this end, photocatalysis appears to be a very promising technique for the hydrogen production [64–66, 101, 106], in which water is split into its constituents with the help of a semiconducting catalyst and a photon reaction.

7.1 Photocatalytic water splitting reaction

In a photocatalytic reaction, a photon is absorbed by the semiconductor. It creates an electron/hole pair according to the reaction:

$$Semiconductor + 2h\nu \longrightarrow 2e^- + 2h^+ \tag{7.4}$$

The holes, located in the valence band edge (VBE), can then be used for the water oxidation reaction:

$$H_2O + 2h^+ \longrightarrow 2H^+ + \frac{1}{2}O_2 \tag{7.5}$$

Finally the proton reduction takes place as:

$$2H^+ + 2e^- \longrightarrow H_2 \tag{7.6}$$

The overall reaction is then:

$$H_2O + 2h\nu \longrightarrow 2H_2 + \frac{1}{2}O_2 \tag{7.7}$$

In 2006, Domen *et al.* [65] found a very promising alloy composed by a solid solution of GaN and ZnO semiconductors. The yellowish color of the solution was indicating the absorption of visible light (in the blue region). Several factors seemed to have been brought together to satisfy the photocatalytic water splitting reaction:
While GaN is known to absorb light in the UV range, the solid solution GaN:ZnO has been shown theoretically [59, 65, 66, 100] and experimentally [39] to absorb photons in the 420-440 nm wavelength visible region. This is of first importance for the use of photocatalyst with direct sunlight. Moreover, the quantum efficiency for the water oxidation appears to be around 50% [65]. Finally, the valence band edge (VBE) and the conduction band edge (CBE) of the alloy are located around the region of the water splitting reaction [64, 66].
The present work is based on the structural study made by Jue Wang [114] on water confined between pure GaN (10$\underline{1}$0) surfaces. Electrochemical insights are discussed in order to understand the very first steps of water dissociation in presence of a heterogeneous photocatalyst.

7.2 Description of the system

Ab-initio molecular dynamics simulation have been performed with the code SIESTA [84, 103]. The system is composed of 94 water molecules, confined between GaN slabs. A five-layer GaN slab is cut along the (10$\underline{1}$0)

surface. Periodicity in Z, perpendicular to the surface slabs is imposed as shown on the Figure 7.2.

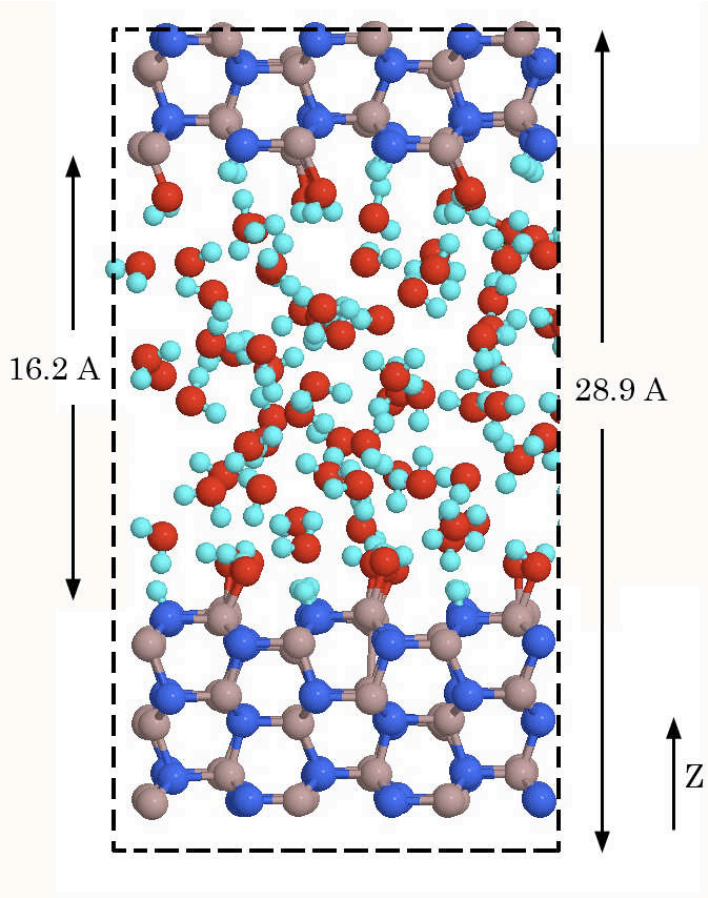

Figure 7.2: 94 water molecules confined between a GaN 1010 5-layer slab.

Exchange and correlation functionals are computed by PBE [89] within the GGA approximation. Extra large optimized double$-\zeta-$polarized basis are used to described the water orbitals. $3d$ atomic orbitals are included as valence electrons of Ga atoms [114]. Norm-conserving Troullier-Martins pseudopotentials [109] are used to describe core electrons.

7.3 Structural properties

7.3.1 Spontaneous water dissociation on the surface

Ab-initio molecular dynamics simulation has been performed to the system in the following way:

First, a water box of 94 water molecules has been cut from a 20ps classical molecular dynamics, at the dimensions of the system in order to conserve the proper liquid water density.

Then, a quantum equilibration has been performed to the confined system by applying a Nose-Hoover thermostat at 300K for 10 ps. During this equilibration, about 20% of water molecules got spontaneously dissociated by binding to the GaN surfaces. The very reactive Ga atoms, with their dangling bonds, attract water molecules and dissociate them into OH^- and H^+. OH^- are strongly chemisorbed to Ga, while H^+ are bound to the free surface N.

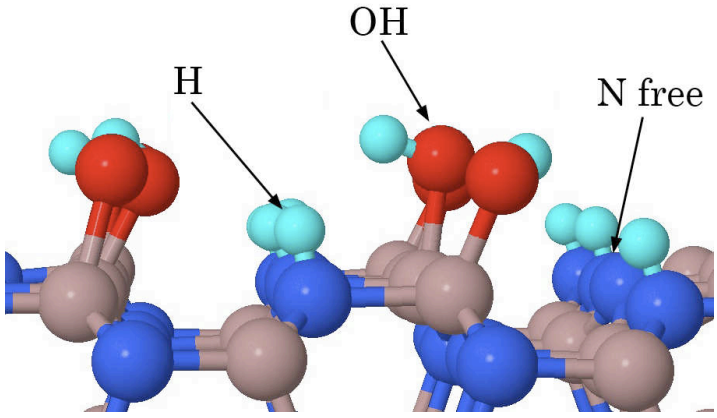

Figure 7.3: H^+ and OH^- bound to N and Ga atoms respectively. N free surface atoms are also shown here. Liquid bulk water has been removed from the picture for more clarity.

Only 83% of N are accepting H^+ (17% remain free). Similarly, 83% of

Ga are bound OH^-, however, the remaining 17% are making a bond to undissociated water.

Finally, a 20 ps *ab-initio* NVE molecular dynamics is performed with the Verlet algorithm. This simulation is being analyzed in detail here.

7.3.2 Z-density

Probability of finding oxygen (red) and hydrogen (blue) atoms at a particular Z distance from the surfaces is shown on Figure 7.4.

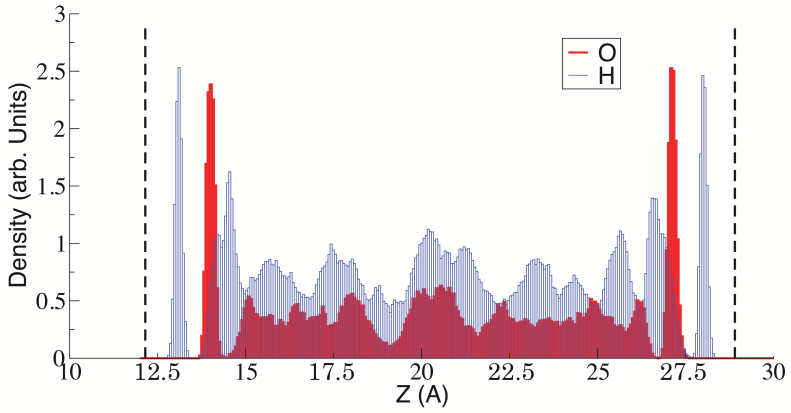

Figure 7.4: Probability (arbitrary units) to find Oxygen (red) and Hydogen (blue) at a distance Z from the GaN surfaces. GaN surfaces are shown in black dashed lines at about 12 Å and 29 Å.

Semiconducting surfaces are represented by the two black dashed lines. Two clear blue peaks (at 13 Å and 28 Å) represent the dissociated H^+ that are bound to surface N. The averaged distance is found to be D_{N-H}=1.02 Å. Inside these peaks, red peaks of about the same height (at 14 Å and 27 Å), are the O component of the OH^- bound to surface Ga, with an averaged distance of D_{Ga-O}=1.93 Å. The similar height between the blue and red peaks, tells us that the number of dissociated hydrogens bound to N is equivalent to the number of OH^- bound to Ga, therefore there are no

free protons in the liquid bulk region of the simulation. The H component of those surface OH^- are seen with blue peaks (at 14.5 Å and 26.5 Å). We notice an overlap between the blue and red curve responsible for the OH^- molecules. This means that some OH^- are flat with respect to the surface. Others, ensure the connection to liquid bulk water by H-bonding. Inside, liquid bulk water keeps a strong layering, characteristics of water confined systems. The overall picture is symmetric and the two semiconducting surfaces have dissociated the same number of molecules (20 on each side out of 24 available sites).

7.3.3 Surface OH^-

Conduction band edge of the system is characterized by surface Ga. They act as an electron acceptor, that can trigger the water dissociation into OH^- and H^+, by strongly favoring electronegative oxygen binding. This binding, while similar in nature, is stronger than the intramolecular OH bond. An unstable hydronium-like Ga-H_2O molecule is formed and eventually H^+ is ejected from the molecule. Surface Ga plays the same role as a hydrogen atom and a very stable Ga-OH^- water-like molecule is formed and remains for the entire simulation (see Figure 7.3).

Free H^+ are instantaneously attracted by surface N that form the valence band edge of the semiconductor. Interestingly, two different types of Ga-OH^- can be identified. There are denoted by *in-plane* and *out-of-plane* as they are flat on the surface or directed towards the liquid bulk water respectively as seen in the Figure 7.5.

Geometries of the two molecules are shown in table 7.1.

Electronic structure of those two species is also quite different. Figure: 7.6 shows the projected density of states averaged over all OH species for 50 snapshots of the whole 10ps simulation.

While the peak that corresponds to the HOMO level, is quite the same

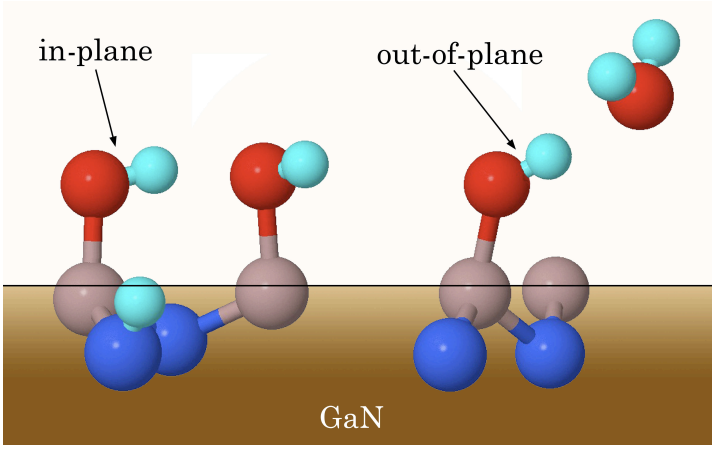

Figure 7.5: In-plane and out-of-plane OH^- molecules chemisorbed on surface Ga. In-plane molecule donates a H-bond to another surface OH^-. Out-of-plane donates a H-bond to a liquid bulk water.

	D_{O-Ga} (Å)	$\widehat{GaOH}(^\circ)$
in-plane	1.81	106.4
out-of-plane	1.87	118.5

Table 7.1: O-Ga distance D_{O-Ga} in Å and $\widehat{GaOH}$ angle in degrees of in-plane and out-of-plane OH^- molecules bound to surface Ga.

for the two, in-plane and out-of-plane, OH species, there is clear shift in energy for the states around -3 eV with respect to the 0 eV Fermi energy. Out-of-plane OH seems to lower its HOMO-1 level as compared to in-plane OH. This is, again, the response of non equivalent H-bonding environment. Indeed, in-plane OH is always donating a H-bond to another surface OH (this is the reason of its planar orientation), while out-of-plane OH will donates fitfully a H-bond to a bulk liquid water. It has already been pointed out that the donation of a H-bond is quite electronically unstable for the donor, and it requires the acceptance of H-bonds to lower this instability. As shown by Wang [114], in the Figure: 7.7, 100% of in-plane OH donates a H-bond, where only 75% of out-of-plane are donating a bond. However,

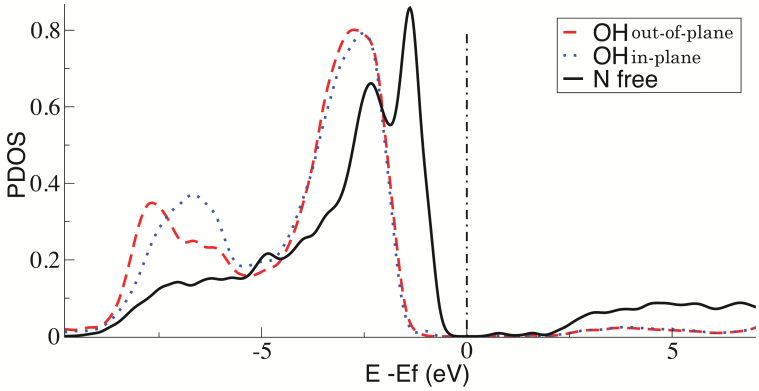

Figure 7.6: Averaged PDOS of in-plane OH (dotted blue) and out-of-plane OH (dashed red). Levels of free N are shown in black. Fermi energy has been shifted to 0.

the latter accept two H-bond with a probability of 55%, when in-plane OH is only fully solvated with a probability of about 42%. This H-bonding environment represents the main variation in the electronic structure of the two surface OH compounds.

7.4 Electrochemical insights

Averaged PDOS over water states has been performed for 50 snapshots of the entire simulation. Water contributions have been separated into different groups, such as, bulk water (in red), water bound to surface Ga (blue) and water on top of free N (green). Levels of free N, that represent the valence band edge of the system is shown in black on the Figure: 7.8.

Waters bound to Ga appear to be the most stable in energy. This comes from the fact that these waters are able to delocalized electrons through one of their lone pairs towards Ga. This is reminiscent of the stabilization of the accepting water molecule during the formation of the H-bond.

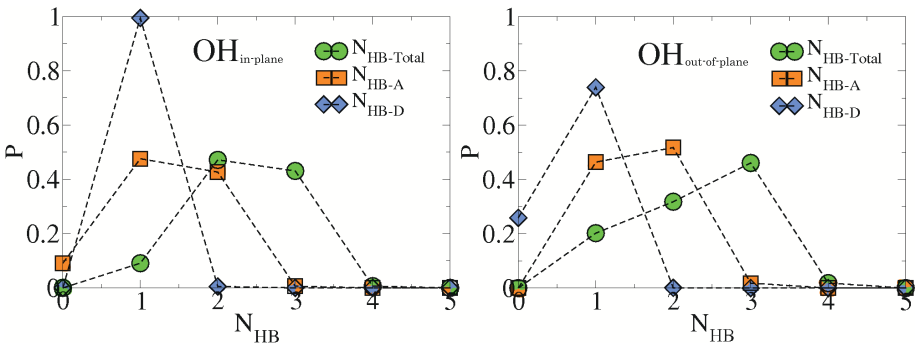

Figure 7.7: Statistical probability for both the in-plane (Left) and out-of-plane (Right) OH surface H-bonds. Orange squares refer to the probability of accepting a certain number of H-bond, Blue diamonds are the probability to donate a certain number of Hbond, and the green circles count the probability of forming (either accept or donate) a certain number of H-bond.

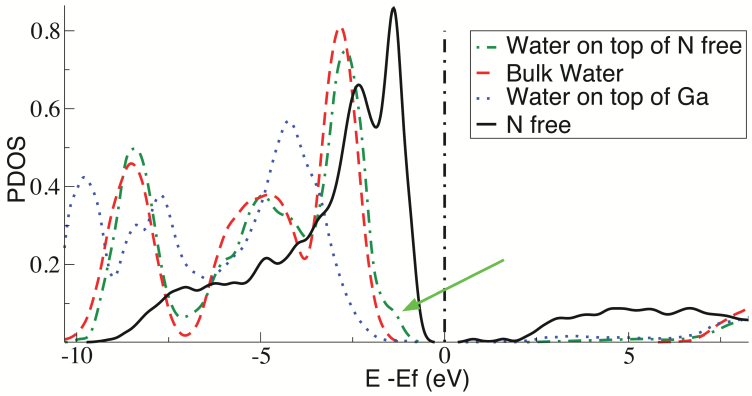

Figure 7.8: Averaged PDOS of water discriminated between bulk (dashed red), bound to Ga (dotted blue), or on top of free N (dashed green). Levels of free N are shown in black. Fermi energy has been shifted to 0.

Interestingly, a noticeable difference can be observed between bulk water molecules and waters on top of a free N. Indeed, while weak in appearance (bond constantly breaks and reforms), the bond formed between water and

a free N through one of its hydrogen, changes its energetic behavior. A small hybridization occurs close to the valence band edge (VBE) of the system (shown in Figure: 7.8 with green arrow). This effect needs to be taken with great consideration since it represents the perfect location for an eventual hole. Indeed, by being the closest to the VBE, waters "H-bonded" to free N, could be the first targets to the chemical reaction defined in equation 7.5, and therefore, semiconducting surfaces with many free N, should favor such a photocatalytic reaction.

Conclusion

Semiconducting GaN (10$\underline{1}$0) surface has shown to be very reactive, by spontaneously dissociating water. Surface Ga atoms, with their 4p dangling-bond states, can initiate the splitting in attracting H_2O in a first step, and by forming an unstable hydronium-like compound. Stronger, Ga-O bond is preferred and one OH bond is sacrificed. The free proton is instantaneously chemisorbed to a free surface N to form a very stable NH pair.

Two sorts of surface OH^- have been observed, and their geometrical and electronic structures are noticeably different, and governed by a specific H-bonding environment.

Waters that stay on top of a free N can hybridize with the valence band edge of the system. They are found to be great candidates to be the most photocatalytically active in the overall process.

Bibliography

[1] N.W. Ashcroft and N.D. Mermin. *Solid State Physics*. W.B. Saunders Company, W.B. Saunders Company, Philadelphia, 1976.

[2] P. Ball. *H_2O a biography of water*. Orion Books Ltd, Clays Ltd, St Yves plc, 1999.

[3] A. D. Becke. Density-functional exchange-energy approximation with correct asymptotic behavior. *Phys. Rev. A*, 38:3098, 1998.

[4] A.D. Becke. Density-functional exchange-energy approximation with correct asymptotic behavior. *Phys. Rev. A*, 38:3098–3100, 1988.

[5] Berendsen, H.J.C., van der Spoel, D., and R. van Drunen. GROMACS: A message-passing parallel molecular dynamics implementation. *Comp. Phys. Comm.*, 91:43, 1995.

[6] H. J. C. Berendsen, J. R. Grigera, and T. P. Straatsma. The Missing Term in Effective Pair Potentials. *J. Chem. Phys.*, 91:6269, 1987.

[7] H. J. C. Berendsen, J. P. M. Postma, W. F. van Gusteren, and J. Hermans. in Intermolecular Forces, edited by B. Pullman (Reidel, Dordrecht, 1981) p. 331.

[8] J.E. Bertie, H.J. Labbe, and E. Whalley. Absorptivity of Ice I in the Range 4000-30cm-1. *J. Chem. Phys.*, 50:4501, 1969.

[9] M.L. Bocquet and N. Lorente. Probing the proton location in a water bilayer on Pd(111) by inelastic spectroscopy simulations. *J. Chem. Phys.*, 130:124702, 2009.

[10] I. Brovchenko and A. Oleinikova. Multiple phases of liquid water. *Chem. Phys. Chem*, 9:2660–2675, 2008.

[11] P. Cabrera-Sanfelix, A. Arnau, A. Mugarza, T.K. Shimizu, M. Salmeron, and D. Sánchez-Portal. Decisive role of the energetics of dissociation products in the adsorption of water on O/Ru(0001). *Phys. Rev. B*, 78:155438, 2008.

[12] P. Cabrera-Sanfelix, M.V. Fernandez-Serra, A. Arnau, and D. Sanchez-Portal. Substrate-induced coopetative effects in water adsorption form density functional theory calculations. *Phys. Rev. B*, 82:125432, 2010.

[13] J. Carrasco, A. Michaelides, and M. Scheffler. Insight from first principles into the nature of the bonding between water molecules and 4*d* metal surfaces. *J. Chem. Phys.*, 130:184707, 2009.

[14] D. M. Ceperley and B. J. Alder. Ground state of the electron gas by a stochastic method. *Phys. Rev. Lett.*, 45:566, 1980.

[15] D.M. Ceperley and B.J. Alder. Ground state of the electron gas by a stochastic method. *Phys. Rev. Lett.*, 45:566–569, 1980.

[16] J. Cerdá, A. Michaelides, M.L. Bocquet, P.J. Feibelman, T‘. Mitsui, M. Rose, E. Fomin, , and M. Salmeron. Novel Water Overlayer Growth on Pd(111) Characterized with Scanning Tunneling Microscopy and Density Functional Theory. *Phys. Rev. Lett.*, 93:116101, 2004.

[17] Martin Chaplin. Water Structure And Science. `http://www.lsbu.ac.uk/water/index2.html`, November 2011.

[18] G. Cicero, J.C. Grossman, E. Schwegler, F. Gygi, and G. Galli. Water confined in nanotubes and between graphene sheets: A first principle study. *Journal of the American Chemical Society*, 130(6):1871–1878, 2008.

[19] Xavier Crispin, Victor Geskin, Annica Crispin, Jerome Cornil, Roberto Lazzaroni, William R. Salaneck, and Jean-Luc Bredas. Characterization of the interface dipole at organic/ metal interfaces. *J. Am. Chem. Soc*, 124:8131, 2002.

[20] P.G. Debenedetti and H.E. Stanley. Supercooled and glassy water. *Phys. Today*, 56:40–46, 2003.

[21] M. Dion, H. Rydberg, E. Schröder, D. C. Langreth, and B. I. Lundqvist. Van der waals density functional for general geometries. *Phys. Rev. Lett.*, 92(24):246401, 2004.

[22] D.L. Doering and T.E. Madey. The Adsorption of H2O on Clean and Oxygen-Dosed Ru(001). *Surf. Science*, 123:305, 1982.

[23] D. Eisenberg and W. Kauzmann. *The structure and Properties of Water*. Oxford University Press, Oxford Unversity Press Inc. New York, 2005.

[24] J.R. Errington and P.G. Debenedetti. Relationship between structural order and the anomalies of liquid water. *Nature*, 409:318–321, 2001.

[25] J.P. Van Dyke F. Herman and I.P. Ortenburger. Improved statistical exchange approximation for inhomogeneous many-electron systems. *Phys. Rev. Lett.*, 22:807, 1969.

[26] P.J. Feibelman. Partial Dissociation of Water on Ru(0001). *Science*, 295:99, 2002.

[27] E. Fermi. Un metodo statistico per la derterminazione di alcune priorieta dell atome. *Rend. Accad. Naz. Lincei*, 6:602–607, 1927.

[28] M. V. Fernandez-Serra. Melting the world's smallest raindrop. *Physics*, 2:67, 2009.

[29] M. V. Fernández-Serra and E. Artacho. Networquilibration and first principles liquid water. *J. Chem. Phys.*, 121:11136, 2004.

[30] M. V. Fernández-Serra and Emilio Artacho. Electrons and hydrogen-bond connectivity in liquid water. *Phys. Rev. Lett.*, 96(1):016404, 2006.

[31] R.P. Feynman. Forces in molecules. *Phys. Rev.*, 56:340, 1939.

[32] V. Fock. Naherunggsmethode zur Losung des quanten-mechanischen Mehrkorperprobleme. *Z. Phys*, 61:126, 1930.

[33] M.E. Gallagher, S. Haq, A. Omer, and A. Hodgson. Water Monolayer and multilayer adsorption on Ni(111). *Surf. Science*, 601:268, 2006.

[34] Sandra García-Gil, Alberto García, Nicolás Lorente, and Pablo Ordejón. Optimal strictly localized basis sets for noble metal surfaces. *Physical Review B (Condensed Matter and Materials Physics)*, 79(7):075441, 2009.

[35] N. Giovambattista, P.J. Rossky, and P.G. Debenedetti. Phase transitions induced by nanoconfinement in liquid water. *Phys. Rev. Lett.*, 102:050603, 2009.

[36] M.C. Gordillo and J. Martí. Hydrogen bond structure of liquid water confined in nanotubes. *Chem. Phys.Lett.*, 329:341, 2000.

[37] J. C. Grossman, E. Schwegler, E. W. Draeger, F. Gygi, and G. Galli. Towards an assessment of the accuracy of density functional theory for first principles simulations of water. *J. Chem. Phys.*, 120:300, 2004.

[38] B. Hammer, L. B. Hansen, and J. K. Norskov. Improved adsorption energetics within density-functional theory using revised Perdew-Burke-Ernzerhof functionals. *Phys. Rev. B*, 59:7413, 1999.

[39] W-Q. Han, Z. Liu, and H-G. Yu. Synthesis and optical properties of GaN/ZnO solid solution nanocrystals. *App. Phys. Lett.*, 96:183112, 2010.

[40] D.R. Hartree. The wave mechanics of an atom with non-coulombic central field: parts I, II, III. *Proc. Cambridge Phil. Soc.*, 54:347, 1929.

[41] H. Hellmann. *Einfuhrung in die Quantumchemie*. Franz Duetsche, Franz Duetsche, Leipzig, 1937.

[42] A. Hodgson and S. Haq. Water Adsorption and the wetting of metal surfaces. *Surf. Sci. Rep.*, 64:381, 2009.

[43] P. Hohenberg and W. Kohn. Inhomogeneous Electron Gas. *Phys. Rev.*, 136:b864, 1964.

[44] W. Hoover. Canonical dynamics : Equilibrium phase-space distributions. *Phys. Rev. A*, 31:1695–1697, 1985.

[45] P. Huang, E. Schwegler, and G. Galli. Water Confined in Carbon Nanotubes : magnetic Response and Proton Chemical Shieldings. *J. Chem. Phys*, 113:8696–8700, 2009.

[46] E.D. Isaacs, A. Shukla, P.M. Platzman, D.R. Hamann, B. Barbiellini, and C.A. Tulk. Compton scattering evidence for covalency of the hydrogen bond in ice . *J. Phys. Chem. Solids*, 61:403–406, 2000.

[47] P. Jenniskens and D.F. Blake. Structural transitions in amorphous water ice and astrophysical implications. *Science*, 265:753, 1994.

[48] W. L. Jorgensen, J. Chandrasekhar, J. D. Madura R. W. Impey, and M. L. Klein. Comparison of simple potential functions for simulating liquid water. *J. Chem. Phys.*, 79:926, 1983.

[49] William L. Jorgensen, Jayaraman Chandrasekhar, Jeffry D. Madura, Roger W. Impey, and Michael L. Klein. Comparison of simple potential functions for simulating liquid water. *The Journal of Chemical Physics*, 79(2):926–935, 1983.

[50] Rustam Khaliullin, Alexis Bell, and Martin Head-Gordon. Electron donation in the water-water hydrogen bond. *Chemistry - A European Journal*, 15(4):851–855, |2009|.

[51] C. Kittel. *Introduction to Solid State Physics*. John Wiley and Sons, John Wiley and Sons, New York, 1996.

[52] W. Kohn and L. J. Sham. Self-Consistent Equations Including Exchange and Correlation Effects. *Phys. Rev.*, 140:a1133, 1965.

[53] V.I. Korsunskii and Y.I. Naberukhin. Does the concept of ice-like structure of water agree with its radial distribution function ? *J. Struct. Chem.*, 21:624–628, 1980.

[54] P. Kumar, S. Han, and H. E. Stanley. Anomalies of water and hydrogen bond dynamics in hydrophobic confinement. *J. Phys. Cond. Matt*, 21:504108, 2009.

[55] A. Bienenstock L. Fu and S. Brennan. X-ray study of the structure of liquid water. *J. Chem. Phys*, 131:234702, 2009.

[56] C. Lee, W. Yang, and R. G. Parr. Development of the Colle-Salvetti correlation-energy formula into a functional of the electron density. *Phys. Rev. B*, 37:785, 1988.

[57] M. Lefevre-Gineau. *J. Phys. Chim. Hist. Nat. Arts*, 49:171, 1795.

[58] M. Levy. Universal variational functionals of electron densities, first-order density matrices, and natural spin-orbitals and solution of the v-representability problem. *Proc. Natl. Acad. Sci. USA*, 76:6062–6065, 1979.

[59] L. Li, J. T. Muckerman, M. S. Hybertsen, and P. B. Allen. Phase diagram, structure, and electronic properties of (Ga1-xZnx)(N1-xOx) solid solution from DFT-based simulations. *Phys. Rev. B*, 83:134202, 2011.

[60] Lindahl, E., Hess, B., and D. van der Spoel. GROMACS 3.0: A package for molecular simulation and trajectory analysis. *J. Mol. Mod.*, 7:306, 2001.

[61] B. Lindinger, R. Mettin, R. Chow, and W. Lauterborn. Ice Crystallization Induced by Optical Breakdown. *Phys. Rev. Lett.*, 99:045701, 2007.

[62] S.V. Lishchuk, N.P. Malomuzh, and P.V. Makhlaichuk. Contribution of H-bond vibrations to heat capacity of water. *Phys. Lett. A*, 375:2656, 2011.

[63] J.K.L. MacDonald. Successive approximations by the Rayleigh-Ritz variation method. *Phys. Rev*, 43:830, 1933.

[64] K. Maeda and K. Domen. Photocatalytic Water Splitting on Gallium Nitride Powder. *J. Phys. Chem. Lett.*, 1:2655, 2010.

[65] K. Maeda, K. Teramura, D. Lu, T. Takata, N. Saito, Y. Inoue, and K. Domen. Photocatalytist releasing hydrogen from water. *Nature*, 440:295, 2006.

[66] K. Maeda, K. Teramura, N. Saito, Y. Inoue, and K. Domen. Photocatalytic Overall Water Splitting on Gallium Nitride Powder. *Bull. Chem. Soc. Jpn*, 80:1004, 2007.

[67] M. W. Mahoney and W. L. Jorgensen. A five-site model for liquid water and the reproduction of the density anomaly by rigid, nonpolarizable potential functions. *J. Chem. Phys.*, 112:8910, 2000.

[68] Richard M. Martin. *Electronic Structure*. Cambridge University Press, Cambridge, UK, 2004.

[69] R. Jay Mashl, Sony Joseph, N.R. Aluru, and Eric Jacobsson. Anomalously immobilized water: A new water phase induced by confinement in nanotubes. *E nano Lett.*, 3:589, 2003.

[70] A. Michaelides, A. Alavi, and D.A. King. Insight into H_2O-ice adsorption and dissocation on metal surfaces from first principles simulations. *Phys. Rev. B*, 69:113404, 2004.

[71] A. Michaelides and K. Morgenstern. Ice nanoclusters at hydrophobic metal surfaces. *Nature Mat.*, 6:597, 2007.

[72] A. Michaelides, V.A. Ranea, P.L. de Andres, and D.A. King. General Model for Water Monomer Adsorption on Close-Packed Transition and Noble Metal Surfaces. *Phys. Rev. Lett.*, 90:216102, 2003.

[73] W.E. Knowles Middleton. *The experimenters. A Study of the Accademia del Cimento*. John Hopkins, Baltimore, 1971.

[74] O. Mishima and H.E. Stanley. The relationship between liquid, supercooled and glassy water. *Nature*, 396:329, 1998.

[75] T. Mitsui, M.K. Rose, E. Fomin, D.F. Ogletree, , and M. Salmeron. Water Diffusion and Clustering on Pd(111). *Science*, 297:1850, 2002.

[76] H.J. Monkhorst and J.D. Pack. Special points for Brillouin-zone integrations. *Phys. Rev. B*, 13:5188, 1976.

[77] E. B. Moore and V.Molinero. Ice crystallization in water's no man's land. *J. Chem. Phys.*, 132:244504, 2010.

[78] J.A. Morrone and R. Car. Nuclear Quantum effects in Water. *Phys. Rev. Lett.*, 101:017801, 2008.

[79] R. S. Mulliken. Electronic population analysis on LCAO-MO molecular wave functions I. *J. Chem. Phys.*, 23:1833, 1955.

[80] B.J. Murray and A.K. Bertram. Formation and stability of cubic ice in water droplets. *Phys. Chem. Chem. Phys.*, 8:186–192, 2006.

[81] B.J. Murray, D. A. Knopf, and A. K. Bertram. The formation of cubic ice under conditions relevant to Earth's atmosphere. *Nature*, 434:202–205, 2005.

[82] S. Nose. A unified formulation of the constant temperature molecular-dynamics methods. *J. Chem. Phys*, 81:511–519, 1984.

[83] H. Ogasawara, B. Brena, D. Nordlund, M. Nyberg, A. Pelmenschikov, L.G.M. Pettersson, and A. Nilsson. Structure and Bonding of Water on Pt(111). *Phys. Rev. Lett.*, 89:276102, 2002.

[84] P. Ordejón, E. Artacho, and J. M. Soler. Self-consistent order-N density-functional calculations for very large systems. *Phys. Rev. B*, 53:10441, 1996.

[85] M. Panhuis, P. L. A. Popelier, R. W. Munn, and J. C. Angyan. Distributed polarizability of the water dimer: Field-induced charge transfer along the hydrogen bond. *J. Chem. Phys.*, 114:7951, 2001.

[86] R. G. Parr and W. Yang. *Density-functional theory of atoms and molecules*. Oxford University Press, Oxford, UK, 1994.

[87] L. Pauling. The Structure and Entropy of Ice and of Other Crystals with Some Randomness of Atomic Arrangement. *J. Am. Chem. Soc.*, 57:2680, 1935.

[88] J. P. Perdew. Accurate Density Functional for the Energy: Real-Space Cutoff of the Gradient Expansion for the Exchange Hole. *Phys. Rev. Lett.*, 55:1665, 1985.

[89] J. P. Perdew, K. Burke, and M. Ernzerhof. Generalized Gradient Approximation Made Simple. *Phys. Rev. Lett.*, 77:3865, 1996.

[90] J.P. Perdew and Y. Wang. Accurate and simple analytic representation of the electron-gas correlation energy. *Phys. Rev. B*, 45:13244–13249, 1992.

[91] A. Poissier, S. Ganeshan, and M.V. Fernandez-Serra. The role of hydrogen bonding in water-metal interactions. *Phys. Chem. Chem. Phys.*, 13:3375–3384, 2011.

[92] P. Pulay. Convergence acceleration of iterative sequences. The case of SCF iteration. *Chem. Phys. Lett.*, 73:393–398, 1980.

[93] V.A. Ranea, A. Michaelides, R. Ramírez, P.L. de Andres, J.A. Vergés, and D.A. King. Water Dimer Diffusion on Pd(111) Assisted by an H-Bond Donor-Acceptor Tunneling Exchange. *Phys. Rev. Lett.*, 92:136104, 2004.

[94] J. Ren and S. Meng. First-principles study of water on copper and noble metal (110) surfaces. *Phys. Rev. B*, 77:054110, 2008.

[95] Guillermo Roman-Perez and Jose M. Soler. Efficient implementation of a van der waals density functional: Application to double-wall carbon nanotubes. *Phys. Rev. Lett.*, In press, 2009.

[96] J. Schmidt, J. VandeVondele, I.-F.W. Kuo, D. Sebastiani, J.I. Siepmann, J. Hutter, and C.J. Mundy. Isobaric-Isothermal Molecular Dynamics Simulations Utilizing Density Functional Theory : An Assessment of the Structure and Density of Water at Near-Ambient Conditions. *J. Phys. Chem. B*, 113:11959, 2009.

[97] Eric Schwegler, Jeffrey C. Grossman, Francois Gygi, and Giulia Galli. Towards an assessment of the accuracy of density functional theory for first principles simulations of water. ii. *J. Chem. Phys.*, 121(11):5400–5409, 2004.

[98] M. Sharma, D. Donadio, E. Schwegler, and G. Galli. Probing properties of water under confinement : infrared spectra. *Nano Lett.*, 8:2959–2962, 2008.

[99] Manu Sharma, Raffaele Resta, and Roberto Car. Intermolecular dynamical charge fluctuations in water: A signature of the h-bond network. *Phys. Rev. Lett.*, 95(18):187401, 2005.

[100] X. Shen, P.B. Allen, M.S. Hybersten, and J.T. Muckerman. Water Adsorption on the GaN (1010) Nonpolar Surface. *J. Phys. Chem. C*, 113:3365, 2009.

[101] X. Shen, Y.A. Small, J. Wang, P.B. Allen, M.V. Fernández-Serra, M.S. Hybersten, and J.T. Muckerman. Photocatalytic Water Oxida-

tion at the GaN (1010)-Water Interface. *J. Phys. Chem. C*, 114:13695, 2010.

[102] P. L. Silvestrelli and M. Parrinello. Structural, electronic, and bonding properties of liquid water from first principles. *J. Chem. Phys.*, 111:3572, 1999.

[103] J. M. Soler, E. Artacho, J. D. Gale, A. García, J. Junquera, P. Ordejón, and D. Sánchez-Portal. The Siesta method for ab initio order-N materials simulation. *J. Phys. Condens. Matter*, 14:2745, 2002.

[104] J.M. Sorenson, G. Hura, R.M. Glaeser, and T. Head-Gordon. What can x-ray scattering tell us about the radial distribution functions of water ? *J. Chem. Phys*, 113:9149, 2000.

[105] R.J. Speedy and C.A. Angell. Isothermal Compressibility of Supercooled Water and Evidence for a Thermodynamic Singularity at -45°C. *J. Chem. Phys.*, 65:851–858, 1976.

[106] R. Subbaraman, D. Tripkovic, D. Strmcnik, K.-C. Chang, M. Uchimura, A.P. Paulikas, V. Stamenkovic, and N. M. Markovic. Enhancing Hydrogen Evolution Activity in Water Splitting by Tailoring Li^+ - $Ni(OH)_2$-Pt Interfaces. *Science*, 334:1256–1260, 2011.

[107] L.H. Thomas. The calculation of atomic fields. *Proc. Cambridge Phil. Roy. Soc.*, 23:542–548, 1927.

[108] C.S. Tian and Y.R. Shen. Structure and charging of hydrophobic material/water interfaces studied by phase-sensitive sum-frequency vibrational spectroscopy. *PNAS*, 106:15148–15153, 2009.

[109] N. Troullier and J. L. Martins. Efficient pseudopotentials for plane-wave calculations. *Phys. Rev. B*, 43:1993, 1991.

[110] Hideaki Umeyama and Keiji Morokuma. The origin of hydrogen bonding. An energy decomposition study. *J. Am. Chem. Soc.*, 99:1316–1332, 1977.

[111] J. VandeVondele, F. Mohamed, M. Krack, J. Hutter, M. Sprik, and M. Parrinello. The influence of temperature and density functional models in ab initio molecular dynamics simulation of liquid water. *J. Chem. Phys*, 122:014515, 2005.

[112] L. Verlet. Computer "Experiments" on classical fluid. Thermodynamical properties of Lennard-John's molecules. *Phys. Rev*, 159:98–103, 1967.

[113] W. Wagner and A. Pruss. *J. Phys. Chem. Ref. Data*, 31:387–535, 2002.

[114] J. Wang. First-principles Study of Water: From Fundamental Properties to Photocatalytic Reactions, (Doctoral thesis) University of Stony Brook NY, USA (2010).

[115] J. Wang, G. Roman-Perez, J. M. Soler, E. Artacho, and M.V. Fernandez-Serra. Density, structure, and dynamics of water: the effect of van der Waals interactions. *J. Chem. Phys.*, 134:024516, 2011.

[116] J. Weissenrieder, A. Mikkelsen, J.N. Andersen, and P.J. Feibelman. Experimental Evidence for a Partially Dissociated Water Bilayer on Ru(0001). *Phys. Rev. Lett.*, 93:196102, 2004.

[117] Ph. Wernet, D. Nordlund, U. Bergmann, M. Cavalleri, M. Odelius, H. Ogasawara, L. A. Naslund, T. K. Hirsch, L. Ojamae, P. Glatzel, L. G. M. Pettersson, and A. Nilsson. The structure of the First Coordination shell in Liquid Water. *Science*, 304:995, 2004.

[118] Julia C. White and Ernest R. Davidson. An analysis of the hydrogen bond in ice. *The Journal of Chemical Physics*, 93(11):8029–8035, 1990.

[119] Zhigang Wu and R. E. Cohen. More accurate generalized gradient approximation for solids. *Physical Review B (Condensed Matter and Materials Physics)*, 73:235116, 2006.

[120] Y. Zhang and W. Yang. Comment on "Generalized Gradient Approximation Made Simple". *Phys. Rev. Lett.*, 80:890, 1988.

Appendix A

Polarized Molecular Orbital Dipole

While the dipole moment can be well defined and calculated for the isolated gas monomer by taking into account electronic polarization, the same quantity in condensed phases cannot be uniquely characterized, since it is not possible to partition in a unique way the electronic charge density between individual molecules (mainly because of long-range orbital delocalization and charge transfer).

Here, electronic rearrangement of charges has been taken into account in calculations of molecular dipole moments by a method that has been developed by Dr. L. Pedroza and Pr. M.V. Fernández-Serra.

In this method, electronic ground state density of the total system is obtained within a density functional theory calculation. Kohn-Sham states $|i\rangle$ that have been obtained, are a linear combination of atomic orbitals:

$$|i\rangle = \sum_{\alpha} C_{\alpha}|\nu\rangle \tag{A.1}$$

Energy levels of the system can be defined as the eigenvalues $\epsilon_i = \langle i|\mathcal{H}|i\rangle$. The Hamiltonian can then block-constructed from atomic orbitals of water molecules. New Hamiltonian, that contains already the correct ground

state electronic density is block-diagonalized. Each block represents an approximation of the electronic structure of a water molecule. This approximation neglects however the charge transfer that would occur between two molecules.

Sates of water molecule k can be written as:

$$|j^{(H_2O_{(k)})}\rangle = \sum_{\beta} C_{\beta} |\nu^{(H_2O_{(k)})}\rangle \tag{A.2}$$

By imposing localization of water states (only the atomic orbitals from a specific water molecule are considered), maximum localized Wannier functions cannot not be deduced any more from Eq. A.2.

The four first states of the blocks that have been diagonalized are chosen to represent the electronic density per water molecule and center of charge can be deduced.

The molecular dipole moment per molecule is then calculated as the sum of the center of electronic charges times the electronic charge, plus the position of nuclei times the nuclei charge.

$$\overrightarrow{\nu} = q.\overrightarrow{r} + Q.\overrightarrow{R} \tag{A.3}$$

With q the electronic charge, $\overrightarrow{r}$ the center of electronic charge, Q the charge of the nuclei and $\overrightarrow{R}$ the position of the nuclei.

Appendix B

Classical Molecular Dynamics

Classical simulations have been performed with the use of the Gromacs package [5, 60]. This appendix will briefly summarize the procedures to follow in order to be able to run an ab initio MD simulation of water.

- Box: The size of the box in principle is fixed by the density of the system. It is assumed here that all simulations will be performed at constant density (fixed volume). Gromacs can generate a box of water molecules in a "liquid-like" arrangement. It does it by repeating periodically a box of 216 water molecules (if the desired size is larger) or selecting a reduced box within this sample box (if the desired size is smaller). The command is:
  genbox -box "lattice-parameter" -cs "spce216.gro"

  where lattice parameter is the size of the cubic box and spce216.gro is the sample box (supplied by the program). There exist sample boxes for all the water potentials available in Gromacs such as SPC [7], SPCE [6], TIP4P [48] and TIP5P [67]. The program will not include in the box the exact number of molecules the user wants because the

number of molecules included are determined by the density of the sample box. Removing molecules is easy. If molecules need to be added then the command:
genbox -box "lattice-parameter" -cs "spce216.gro" -ci "insert.gro" -nmol "#MOL"
will try to insert the "#MOL" extra molecules needed. The file "insert.gro" contains the coordinates of a single molecule.

- MD parameters: Once the box is ready the molecular dynamics simulation with Gromacs can be done. All the instructions can be found in the Gromacs Manual and only a few of them are reviewed here.

  - Electrostatics: the way the electrostatic interactions (solution to the Laplace equation) are treated in Gromacs depends on the input file. Ewald algorithms are available (normal Ewald sums, fast particle-mesh Ewald (PME) where the reciprocal space sums are performed with fast-Fourier transforms, reaction field). PME has been used in this study.
  - Thermostat: given that all the classical MD have the purpose of equilibrating the system at the desired (initial) temperature for the ab initio simulations, a thermostat has to be chosen. Either a Berendsen type thermostat or Nose-Hoover type are available. Berendsen has been used in this study.
  - Constraints: the water empirical potentials here used represent all rigid molecules. Gromacs needs to know that by imposing constraints to the bonds, this is done using the shake algorithm.

- Output files: Gromacs has its own analysis tools, very well described on the manual. All the decompositions of the total energy can be monitored with the command "g energy". This author has written a

program that generates an input file "system.XV" for Siesta from the Gromacs output file with velocities and positions.

A classical MD equilibration, given that it is computationally inexpensive as compared to ab initio simulations should be as long as possible in order to ensure a proper equilibration of the system. Runs of hundreds of picoseconds for systems of less than 200 water molecules are affordable and therefore this author recommends a minimum of 300 ps for a equilibration at room temperature. This time should increase with decreasing temperatures. At the end, the energy conservation and fluctuations determine the quality of the equilibration. A good test that this author has always performed is that of removing the thermostat after the equilibration and continuing the simulation at constant energy conditions using a Verlet integrator for runs of the order of $\sim$ 100 ps. If the system maintains its temperature (always a drift exists), then the equilibration is well done.